Capacity and Interference Analysis of Multicell CDMA Systems using 3-Dimensional Smart Antennas

by

Titus Tin Hing Cheung

Bachelor of Applied Science, The University of British Columbia

A THESIS SUBMITTED IN PARTIAL FULFILLMENT OF

THE REQUIREMENTS FOR THE DEGREE OF

MASTER OF APPLIED SCIENCE

In

THE FACULTY OF GRADUATE STUDIES

DEPARTMENT OF ELECTRICAL ENGINEERING

We accept this thesis as conforming

to the required standard

THE UNIVERSITY OF BRITISH COLUMBIA

March 2003

In presenting this thesis in partial fulfilment of the requirements for an advanced degree at the University of British Columbia, I agree that the Library shall make it freely available for reference and study. I further agree that permission for extensive copying of this thesis for scholarly purposes may be granted by the head of my department or by his or her representatives. It is understood that copying or publication of this thesis for financial gain shall not be allowed without my written permission.

Department of Electrical & Computer Engineering

The University of British Columbia
Vancouver, Canada

Date 24 Apr 03

Abstract

In this thesis, we derive analytical expressions for the interference and estimate the capacity of a CDMA based wireless system for indoor mobiles in 6 groups of high riser buildings occupying 6 building blocks of a typical high density downtown city environment. The analysis compares the performances of a single element panel antenna, a 1-dimensional linear array, and a 3-dimensional vertical planar array. We further consider an appropriate 3-dimensional urban model representative for such an environment, and based upon this model, a more accurate 3-dimensional user distribution is introduced. Our work has shown that, for such an environment, the traditional assumption of uniform user distribution is not valid. It is found that by arranging smart antenna elements in specific 2- and 3-dimensional geometries, reduction of sidelobes and significant improvements in the directivity can be achieved with the same number of elements traditionally used in a 1-dimensional linear array. For a more accurate analysis, short dipoles and panel antenna elements are used instead of isotropic point sources. Surface plots for the interference and capacity from the 6 building groups for different vertical and azimuth angles are produced. The capacity with the use of a 3-dimensional smart antenna and the improvement over a linear array are then compared, taken into account of different building materials' and dimensional effects. These performance evaluation results have shown that, as compared to the 1-dimentional linear array employing the same number of antennas, significant capacity improvements are achievable.

Table of Contents

List of Tables

List of Figures

Acknowledgments

I would like to thank my supervisor, Professor Takis Mathiopoulos, who has provided the kind support to my ideas and believing in me. I'm also grateful for the funding he has provided.

Next, I would like to thank the members of the Canadian Forces. To me, they have been my second family when my parents and brothers were away. I have been able to find friends and support throughout the country. And it was my comrades who taught me how to drink and dance. My thanks also to the Armed Forces Communication and Electronics Association (AFCEA) for their kind scholarship.

I am indebted to my family, who has given so much. It is beyond words.

Finally, to my high school electronics teacher, Mr. David Wrinch. Without him, none of this would be possible. I am grateful for the personal time he had sacrificed to help me, whether it is lunch time, after school, or even holidays.

List of Abbreviations

CDMA	Code Division Multiple Access
QoS	Quality of Service
AOA	Angle of Arrival
SIR	Signal to Interference Ratio
W-PBX	Wireless Private-Branch Exchange
GBCM	Geometrically Based Single Bounce Circular Model
GBEM	Geometrically Based Single Bounce Elliptical Model
GIS	Geographical Information System
PN	Psuedo-Noise
BER	Bit Error Rate
SINR	Signal to Interference and Noise Ratio
MAI	Multiple Access Interference
LOS	Line of Sight

List of Symbols

ϕ	Azimuth Angle of Arrival
θ	Vertical Angle of Arrival
V_c	Propagating Speed of Incoming Signal
V_z	Propagating Speed of Incoming Signal along z-axis
V_x	Propagating Speed of Incoming Signal along x-axis
V_y	Propagating Speed of Incoming Signal along y-axis
Δt	Time Difference in Arrival Between Two Points for Incoming Signal
λ	Wavelength
$\psi_{z,\theta}$	Z Component of Phase for Incoming Signal from θ
$\psi_{x,\theta}$	X Component of Phase for Incoming Signal from θ
$\psi_{y,\theta}$	Y Component of Phase for Incoming Signal from θ
$\psi_{x,\phi}$	X Component of Phase for Incoming Signal from ϕ
$\psi_{y,\phi}$	Y Component of Phase for Incoming Signal from ϕ
ψ_{total}	Total Phase for Incoming Signal
M	Total Number of Elements in Array
X_m	Location of Element m on x-axis
Y_m	Location of Element m on y-axis
Z_m	Location of Element m on z-axis
s_m	Baseband Signal Received by Antenna Element m
f_{EL}	Element Factor
f_{SD}	Element Factor for Short Dipole
f_{PA}	Element Factor for Panel Antenna

f_{ϕ_0,θ_0}	Array Factor
f'_{ϕ_0,θ_0}	Array Factor with Point Source Elements
F_{ϕ_0,θ_0}	Normalized Array Factor Power
F'_{ϕ_0,θ_0}	Normalized Array Factor Power with Point Source Elements
d	Distance Between Real Element and Reflector For Panel Antenna
P_G	Power Gain
D	Directivity
Ω_A	Beam Solid Angle
E_0	Desired Signal's Energy per Bit
I_{MAI}	Multiple Access Interference
I_n	Receiver Noise
N	CDMA Processing Gain
P_t	Transmitted Power
P_c	Desired Signal Power Before De-Spreading
P_{r_i}	Received Signal Power from i-th User Before De-Spreading
P_i	Signal Power from i-th User Incident on Antenna Array
K	Number of Users per Cell
R	Cell Radius
u	User Distribution
S	Building Group Depth
$W_{building}$	Building Group Width
h	Building Group Height
W_{cross}	Width of Cross Street

X_o	Width of Main Street
c	Horizontal Distance Between Base Station Array and Point of Entry into Building Group's Front Wall
ϕ_{1max}	Maximum Azimuth Angle to Steer Beam to the Left Side Wall of Building Group D or F
ϕ_{13max}	Maximum Azimuth Angle to Steer Beam to the Right Side Wall of Building Group C or E
ϕ_{3max}	Maximum Azimuth Angle to Steer Beam to the Left Side Wall of Building Group C or E
θ_{max}	Maximum Elevation Angle to Steer Beam to Top of Building Group
ε	Permittivity
ε_0	Permittivity of Free Space
ε_r	Relative Permittivity
E_i	Incident Electric Field
E_r	Reflected Electric Field
H_i	Incident Magnetic Field
H_r	Reflected Magnetic Field
$\Gamma_{\parallel}$	Fresnel Reflection Coefficient when Incident Electric Field is Parallel to Plane of Incidence
$\Gamma_{\perp}$	Fresnel Reflection Coefficient when Incident Electric Field is Normal to Plane of Incidence
$\hat{e}$	Unit Vector of Electric Field in the Far Field Region of Array
ψ	Angle Between Horizontal Plane and Plane of Incidence
ζ	Incident and Reflected Angle
d	Distance Between User and Base Station Array
f	Carrier Frequency

β_f	Free Space Clutter Factor
I	Total Mean Interfering Power from Building Group
I'	Per User Mean Interfering Power from Building Group
h_{offset}	Vertical Separation Between Interferer and Base Station Array
$G_{element}$	Gain Due to Element Factor from Both In Cell and Out of Cell Base Station Array
G_{ch}	Total Channel Gain Due to Distance, Reflection, Diffraction, Element Factor, and Array Factor
$L_{reflection}$	Reflection Loss in dB
$L_{diffraction}$	Diffraction Loss in dB
α	Horizontal Distance Along the X Direction Between Base Station Array and Point of Entry into Adjacent Building Group's Sidewall
η	Horizontal Distance Between Base Station Array and Point of Entry into Adjacent Building Group's Side Wall
a	Sum of All Building Groups' Per User Mean Interfering Power
b	Sum of Per User Mean Interfering Power from Adjacent Building Groups

Chapter 1 INTRODUCTION

As cellular systems evolve, there has always been a need to improve on capacity and coverage. Some of the driving forces behind this need include more subscribers, newer services that demand better and more reliable call connections, and better coverage. For the 1st and 2nd generation standards, these have been achieved by using additional base stations. Small macro cells in the size of 1 – 10 km in radii were deployed and sectorization was also used to provide higher capacity and channel reuse for smaller areas. Since it is anticipated that in building wireless access to be one of the most likely places for mobiles [1], micro cells in the order of street level service and in building per floor pico cells have also been studied and implemented for both outdoor and indoor users with the 3rd generation standard. For example, W-PBX (Wireless Private Branch Exchange) and parasitic systems, which uses conventional cellular handsets and spectrum, provides coverage inside buildings by relying on the building penetration loss to provide isolation from outdoor cellular systems.

As the demand on capacity and coverage continues to grow, it is becoming increasingly difficult and expensive to install additional base stations. Further sectorization would also increase hand over rates, placing a higher demand on network resources. Also, as outdoor base station antennas are brought closer to the buildings and street level in newer cellular systems, the performance of indoor systems may degrade because less cellular channels can be re-used inside the buildings. At the same time, performance degradation may also be experienced by the outdoor systems [2]. Alternatively, antenna arrays allow the selective gain and attenuation of desired and interfering signals from different Angle of Arrivals (AOAs); therefore providing a solution to the higher demand of both coverage

and capacity. With smart antennas, the antenna pattern can be changed by steering beams and nulls dynamically to improve or maintain the Signal to Interference and Noise Ratio (SINR), depending on the AOAs of the incoming signals [3]. As for indoor systems, recent researches have suggested for the use of outdoor micro cell base stations to serve indoor users over the deployment of pico cells inside buildings [4], [5], and in [6], [7], 3-dimensional propagation was investigated.

In spite of the number of publications on smart antennas, the vast majority of past studies and implementations have considered the use of 1-dimensional linear arrays. Further, simplifying assumptions were common practice in the modelling and analysis of arrays for cellular systems. For example, the use of an ideal isotropic antenna point source, which radiates energy equally to all directions, was used for calculating the array's radiation pattern [8], [9], [10]-[13]. Also, piecewise discontinuous radiation pattern was assumed for cell sectorization [9], [13]. For system capacity analysis, a uniform user distribution [3] was used, which is only true for larger macro cell sizes. For the much smaller street level micro cell sizes, where a city block is about 150 m long [14], such assumption would lead to highly inaccurate results. Also, initial analysis was based on horizontal propagation [15], [16], with subsequent studies primarily on varying channel effects and statistics [8], [13], [17]-[23], and coverage [22], [24]. Further, simple models, such as the Geometrically Based Single Bounce Circular Model (GBCM) and Geometrically Based Single Bounce Elliptical Model (GBEM) [25], were used to analyse horizontal propagation and reflection. We are not aware of any published analytical results on a cellular system taking into consideration of a full 3-dimensional signal

propagation, user distribution, environmental modelling, and incorporating real antenna element factor, which describes the gain provided by a single antenna element over all vertical and azimuth angles.

Motivated by the above, this thesis presents a comprehensive study into the analysis, estimation, and improvement of system capacity in a downtown environment for in building users with outdoor base stations. Because in a downtown environment, high risers can house a large number of subscribers, there is a need to service mobiles from different vertical directions. As such, the use of a 3-dimensional array is proposed and performance will be compared to the simpler linear array. In order to facilitate capacity analysis and estimation, a 3-dimensional model representative of a typical downtown and user distribution are derived and used. Coupled along with 3-dimensional propagation and 3-dimensional antenna array model, an analytical solution to the mean, or steady state, system capacity is derived first in a single cell system, and extended into a multi cell environment.

The major research contributions of this thesis are as follows:

- The performances and steering abilities of antenna arrays of improved design are presented. By using an array of different geometry and similar number of elements, it is shown that the beamwidth, directivity, and gain can be improved significantly.
- The use of realistic modelling of antenna elements. For sectorized panel antennas, the radiation pattern is computed by placing a short dipole in front of a

reflector. The vertical radiation pattern of short dipole is also taken into account. This method is more accurate than the assumption of perfect sectorization and the use of point source elements.

- An accurate 3-dimensional model of user distribution in buildings is introduced. This is an important step in computing capacity and interference in smaller micro cell environments, and provides better results than the assumption of uniform user distribution.
- The use of a typical downtown model with building dimensions and locations were taken from the Vancouver Geographical Information System. Based on this urban model, a modified 3-dimensional single bounce model is proposed. This is more accurate than the use of the GBCM and GBEM models.
- 3-dimensional capacity and interference surface plots with the use of panel antenna, 1x5 linear array, and 5x5 vertical planar array are compared in a multi cell scenario.

The organization of the thesis is as follows.

Chapter 2 provides the fundamental background on array radiation pattern derivation and analysis. For realistic modelling, short dipole and panel antenna are used. Then, higher dimensional array structures are introduced and a suitable design with similar hardware complexities to existing arrays is proposed. A comparison is then made to the simpler 1-dimensional linear arrays by both analytical and calculated results. Radiation patterns are

shown in both planar and 3-dimensional views throughout the chapter. Then, CDMA and the derivation of a single cell CDMA capacity are presented.

Chapter 3 presents the 3-dimensional downtown model used in our subsequent analysis. In order to provide a realistic model, dimensions representative of a real downtown is taken from a Geographical Information System (GIS). The resulting user distribution is then derived.

In Chapter 4, a system model of the multi cell system is introduced. This is accomplished by taking into consideration the effects of reflection, diffraction, building penetration, propagation, and element factor on power control. In addition, a model for reflection in 3-dimension is presented and a modified single bounce model is proposed based on the urban model. Then, interference from adjacent cells are modelled for system capacity analysis.

In Chapter 5, capacity results are presented. 3-dimensional and linear arrays will be compared, and the effects of building materials on interference and capacity will be shown. Surface plots of interference from individual cells are shown, in addition to the capacity plot. The improvement from the use of a 3-dimensional smart antenna is illustrated and discussed.

Finally, Chapter 6 concludes the thesis and provides suggestions to future research.

Chapter 2 SMART ANTENNA ARRAYS AND CDMA CAPACITY

2.1 Introduction

One of the keys to improve system capacity of a cellular network is to study and exploit the performances of different types of antenna arrays and elements. With the use of an array of antenna elements, it is possible to distinguish signals arriving from different directions by detecting and exploiting the phase differences of a received signal between each individual element. As such, it is possible to nullify or amplify interference and desired signal in order to enhance SINR. In this chapter, we illustrate the different element types and array structures, along with their corresponding behaviour and performances. The organization of this chapter is as follows. After this introduction, the derivation of array factor, and directivity are provided in Section 2.2. This is followed by the introduction of 1-dimensional linear array in Section 2.3. Then, higher dimensional antenna arrays are shown to provide better gain, directivity, and steering ability with similar hardware complexities to linear array in Section 2.4. In Section 2.5, we show improvement to CDMA system capacity with the use of antenna arrays. Section 2.6 presents the conclusion of this chapter.

2.2 Radiation Pattern and Directivity

The most basic type of antenna element is of the dipole type. For the direction (ϕ, θ) shown in Fig. 2.1, the gain provided by an antenna element at the origin is described by the element factor $f_{EL}(\phi, \theta)$. The dipole element exhibits an omni-directional horizontal

pattern, where an equal gain is applied to all azimuth angles (horizontal plane). The specific vertical radiation pattern is depended on the length of the element.

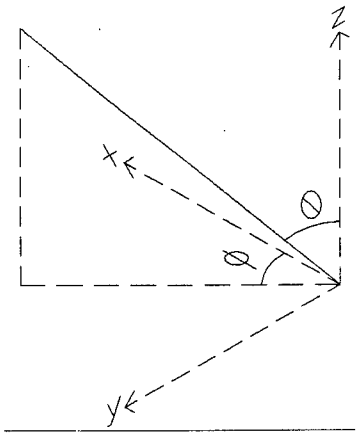

Fig. 2.1 Polar Coordinates for Antennas

When the length of the element is about a tenth of a wavelength [26], the short dipole element factor is

$$f_{SD}(\theta) = \sin\theta \tag{2.1}$$

and the complete element response, shown in Fig. 2.2, resembles the shape of a donut.

However, if an array of M antenna elements is used, the radiation pattern needs to be modelled by taking into account the specific location of each element in the x-, y-, and z-axis, which determines the relative time of reception for an incoming signal's wavefront. For our analysis, we will assume that an element is centred at the origin, and is parallel with the z-axis. Let V_c denotes the propagating speed of an incoming signal, and referring to Fig. 2.3, the speed component along the z-axis, V_z, for a wavefront arriving at a vertical angle θ is

$$V_z = \frac{V_c}{\cos\theta}. \tag{2.2}$$

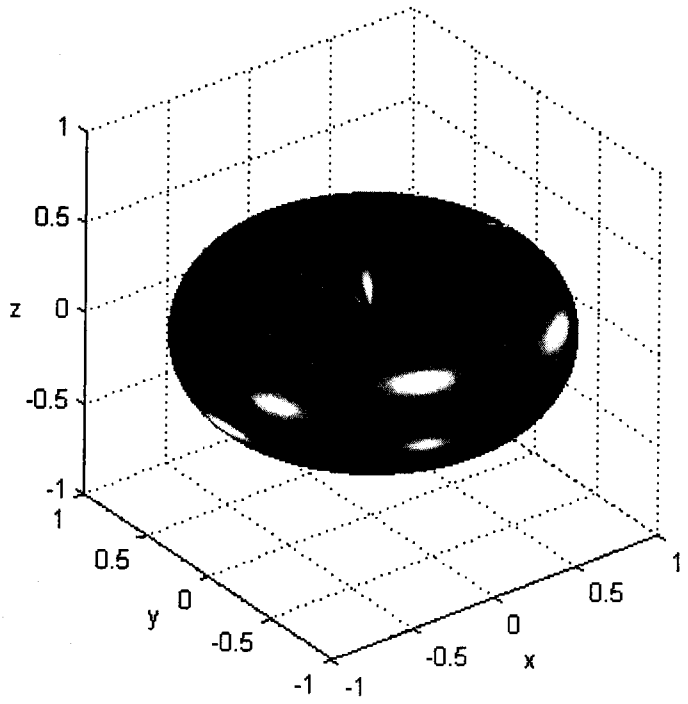

Fig. 2.2 Radiation Pattern of a Short Dipole

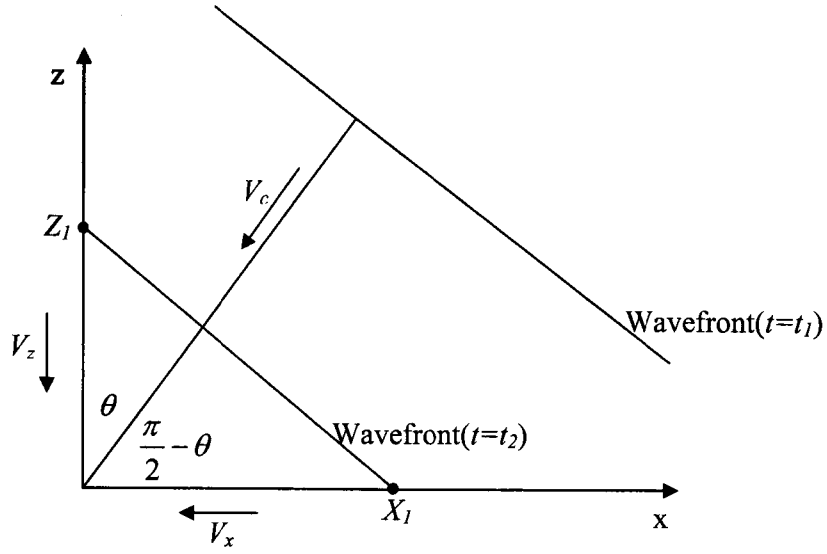

Fig. 2.3 Speed Components for a Signal Arriving from Vertical Angle θ

Referenced to the time, t, when the wavefront will arrive at the origin, the signal arrives at a point on the z-axis Δt earlier, where Δt is

$$\Delta t = \frac{Z_1}{V_z} = \frac{Z_1}{V_c}\cos\theta \tag{2.3}$$

and Z_1 denotes the location of the point on the z-axis. The corresponding phase at the point is

$$\psi_{z,\theta} = \frac{-\Delta t}{T} = \frac{-\Delta t V_c}{\lambda} = \frac{-Z_1}{\lambda}\cos\theta. \tag{2.4}$$

Similarly, for points located at X_1 and Y_1 along the x- and y-axis, the phases detected of the incoming signal are

$$\begin{aligned} \psi_{x,\theta} &= \frac{-X_1}{\lambda}\cos(\frac{\pi}{2}-\theta) = \frac{-X_1}{\lambda}\sin\theta \\ \psi_{y,\theta} &= \frac{-Y_1}{\lambda}\sin\theta. \end{aligned} \tag{2.5}$$

In addition, for a wavefront arriving from an azimuth angle ϕ, as illustrated in Fig. 2.4, the phases contributed by the azimuth angle are

$$\begin{aligned} \psi_{x,\phi} &= \frac{-X_1}{\lambda}\cos\phi \\ \psi_{y,\phi} &= \frac{-Y_1}{\lambda}\sin\phi. \end{aligned} \tag{2.6}$$

In more general terms, the combined phase of the incoming signal arriving at the m-th antenna element located at (X_m, Y_m, Z_m) is then

$$\begin{aligned}\psi_{Total} &= \psi_{x,\theta} + \psi_{y,\theta} + \psi_{z,\theta} + \psi_{x,\phi} + \psi_{y,\phi} \\ &= \frac{-1}{\lambda}\left[X_m \cos\phi\sin\theta + Y_m \sin\phi\sin\theta + Z_m \cos\theta\right]\end{aligned} \tag{2.7}$$

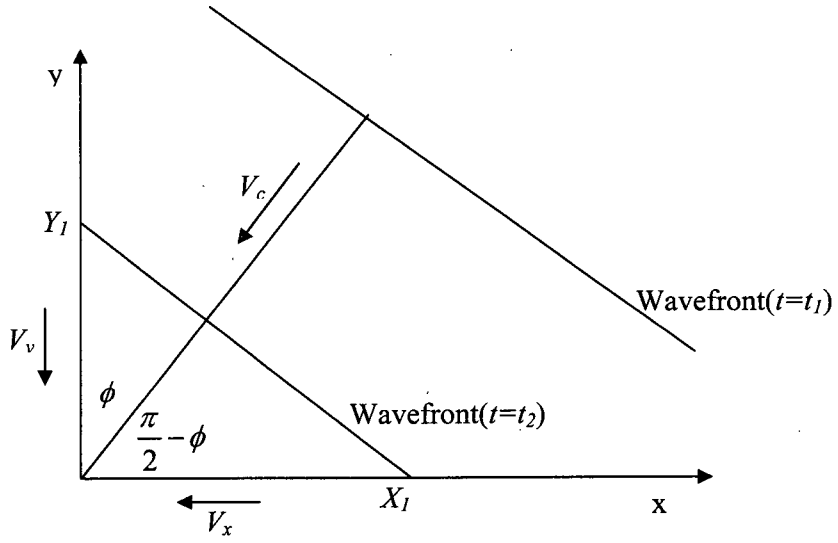

Fig. 2.4 Speed Components for a Signal Arriving from Azimuth Angle ϕ

The signal received by the m-th antenna element is

$$\begin{aligned}s_m &= f_{EL}(\phi,\theta) I_m \exp(j2\pi\psi_{total}) \\ &= f_{EL}(\phi,\theta) I_m \exp\left\{\frac{-j2\pi}{\lambda}\left[X_m \cos\phi\sin\theta + Y_m \sin\phi\sin\theta + Z_m \cos\theta\right]\right\}\end{aligned} \tag{2.8}$$

where I_m is the gain of each antenna element. Furthermore, the array response of an antenna array with M elements is

$$\begin{aligned}f(\phi,\theta) &= \sum_{m=0}^{M-1} s_m \\ &= f_{EL}(\phi,\theta) f'(\phi,\theta)\end{aligned} \tag{2.9}$$

where

$$f'(\phi,\theta) = \sum_{m=0}^{M-1} I_m \exp\{-j\beta\left[X_m \cos\phi\sin\theta + Y_m \sin\phi\sin\theta + Z_m \cos\theta\right]\} \tag{2.10}$$

is the array response with point source elements, and

$$\beta = \frac{2\pi}{\lambda}. \tag{2.11}$$

Recognizing that Eq. 2.10 is maximum when the argument of all exponentials is zero, the array is able to be steered to the direction (ϕ_0, θ_0) by subjecting each m-th antenna element's signal to a phase shift, or weight, of

$$W_m(\phi_0,\theta_0) = \exp\{j\beta[X_m \cos\phi_0 \sin\theta_0 + Y_m \sin\phi_0 \sin\theta_0 + Z_m \cos\theta_0]\}. \tag{2.12}$$

The complete array factor can then be expressed as

$$f_{\phi_0,\theta_0}(\phi,\theta) = f_{EL}(\phi,\theta) f'_{\phi_0,\theta_0}(\phi,\theta) \tag{2.13}$$

where

$$\begin{aligned} f'_{\phi_0,\theta_0}(\phi,\theta) = \sum_{m=0}^{M-1} I_m \exp\{-j\beta\,[&X_m(\cos\phi\sin\theta - \cos\phi_o \sin\theta_o) \\ &+ Y_m(\sin\phi\sin\theta - \sin\phi_o \sin\theta_o) \\ &+ Z_m(\cos\theta - \cos\theta_o)]\}. \end{aligned} \tag{2.14}$$

To enable the direct comparison of beamwidth, defined as the number of degrees within which the beam has its power greater than one half the maximum, and directivity of arrays with different number of elements, the normalized array factor's magnitude squared (power response) is used and is defined as

$$F_{\phi_o,\theta_0}(\phi,\theta) = \frac{\left|f_{\phi_o,\theta_0}(\phi,\theta)\right|^2}{\max\left(\left|f_{\phi_o,\theta_0}(\phi,\theta)\right|^2\right)} \tag{2.15}$$

where $|\cdot|$ denotes absolute value of $\cdot$, and the directivity [26] of an array is

$$D(\phi,\theta) = \frac{4\pi}{|\Omega_A|}\left|F_{\phi_o,\theta_0}(\phi,\theta)\right|^2 \tag{2.16}$$

where

$$\Omega_A = \int_0^{2\pi}\int_0^{\pi}\left|F_{\phi_o,\theta_0}(\phi,\theta)\right|^2 \sin(\theta)d\theta d\phi. \tag{2.17}$$

The directivity shows the effective gain in power in the specified direction relative to an isotropic point source, which radiates energy equally to all directions.

2.3 1-Dimensional Linear Array

In the past it appears that most, if not all, studies of smart antennas have been limited to an array of elements equally spaced along a single axis of the coordinate system, as shown in Fig. 2.5. Such an array has virtually no vertical steering capability, and regardless of the spacing in between elements, is not able to distinguish signals from either side of the array, or the x-axis. Further, the beamwidth is widened when the array is steered to its endfire direction, or along the x-axis. These effects are illustrated in Fig. 2.6 for an 8 element 1-dimensional linear array with elements spaced 0.5λ apart when steered to various azimuth directions in Fig. 2.6. As shown by these computer simulated results, a linear array has a limitation to single out a specific azimuth direction and is subjected to any interference that may originate from either side of the array.

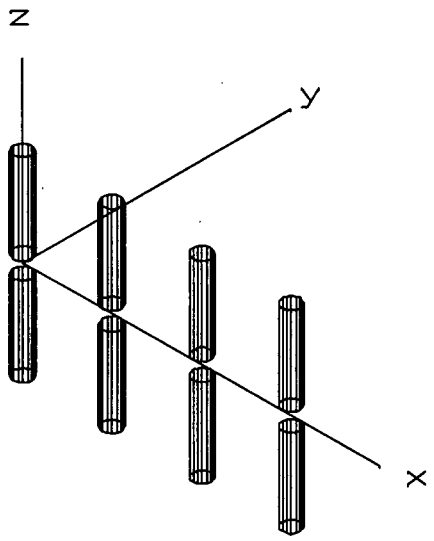

Fig. 2.5 A Linear Array of 4 Dipoles Spaced Along the X-Axis

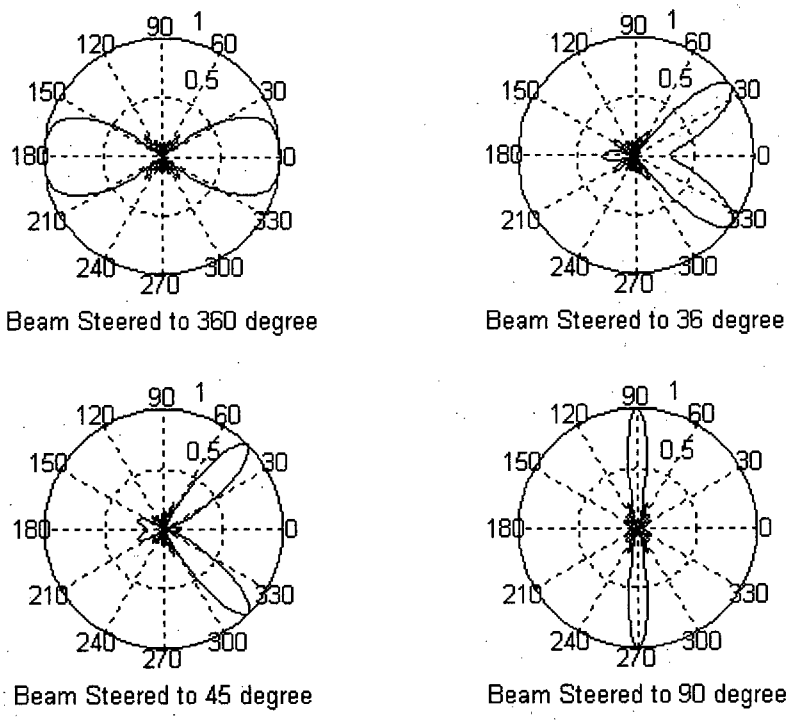

Fig. 2.6 Azimuth Radiation Pattern for 8 Dipoles 0.5λ Spaced

A method to eliminate one of the two main lobes of a linear array, thus providing a high front-to-back gain, and a reduction of the beamwidth when steered towards the endfire directions, is to employ panel antenna elements, which have been used traditionally to provide cell sectorization. Instead of assuming perfect sectorization, where the element has uniform gain over a subset of the azimuth angles, and zero gain elsewhere, the array factor of a panel antenna can be simulated by placing a reflector at a distance $d\lambda$ behind the radiating element. As such, an image is located at a distance $2d\lambda$ behind the radiating omni-directional antenna, as illustrated in Fig. 2.7.

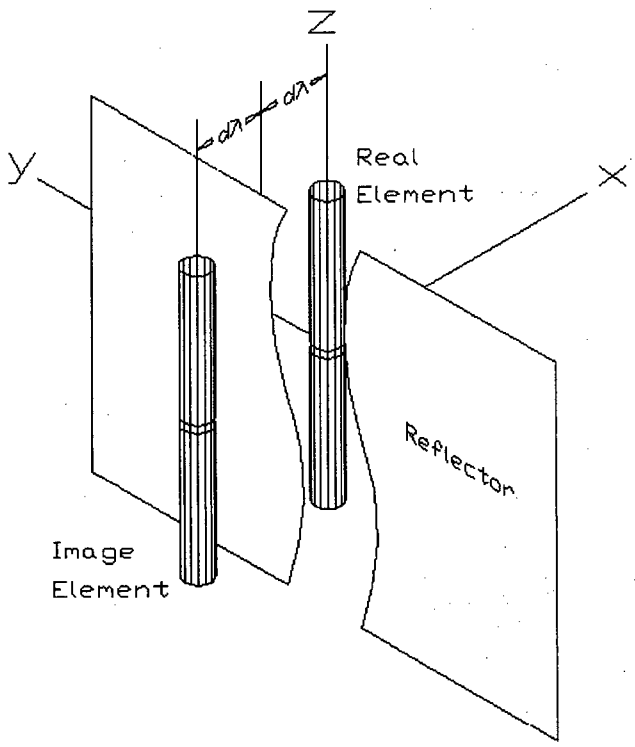

Fig. 2.7 Simulation of Panel Antenna Element Factor

From Eqs. 2.9 and 2.10, where $I_1 = 1$ and $(X_1, Y_1, Z_1) = (0,0,0)$ for the real element and $I_2 = -1$ and $(X_2, Y_2, Z_2) = (-2d\lambda, 0, 0)$ for the image element, the element factor for a panel antenna element is

$$f_{PA}(\phi,\theta) = f_{SD}(\theta)\{1 - \exp[-j\beta(-2d\lambda\cos\phi\sin\theta)]\} \tag{2.18}$$

and the azimuth radiation pattern is plotted in Fig 2.8 for $2d\lambda = 0.5\lambda$. As illustrated, due to cancellation by the image elements, panel antenna elements have a half power beamwidth of 120^0. In other words, the gain is less than 0.5 for angles between $0^0 - 30^0$ and $150^0 - 180^0$. If coverage is needed for all azimuth angles, two additional antennas are needed.

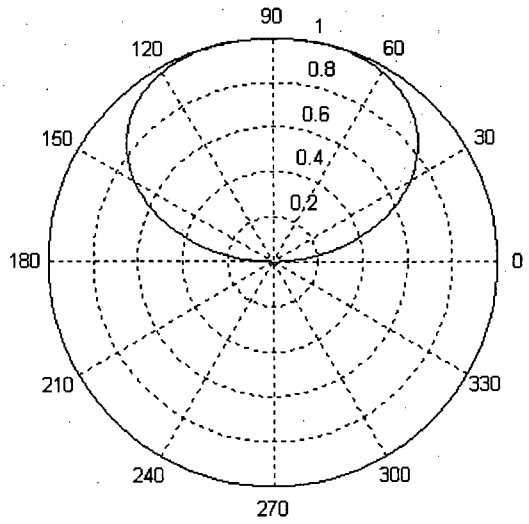

Fig. 2.8 Azimuth Radiation Pattern of a Panel Antenna Element

To calculate the array factor for an array of panel antenna elements, we let

$$f_{EL}(\phi,\theta) = f_{PA}(\phi,\theta) \tag{2.19}$$

in Eq. 2.13 and the computed azimuth radiation patterns for 8 panel antenna elements spaced 0.5λ are plotted in Fig. 2.9. Compared to Fig. 2.6, such an array is not susceptible to interference from one side of the array thus providing a high front-to-back ratio. Note also that the array is unable to steer to the angle 360^0 due to the cancellation effect mentioned previously.

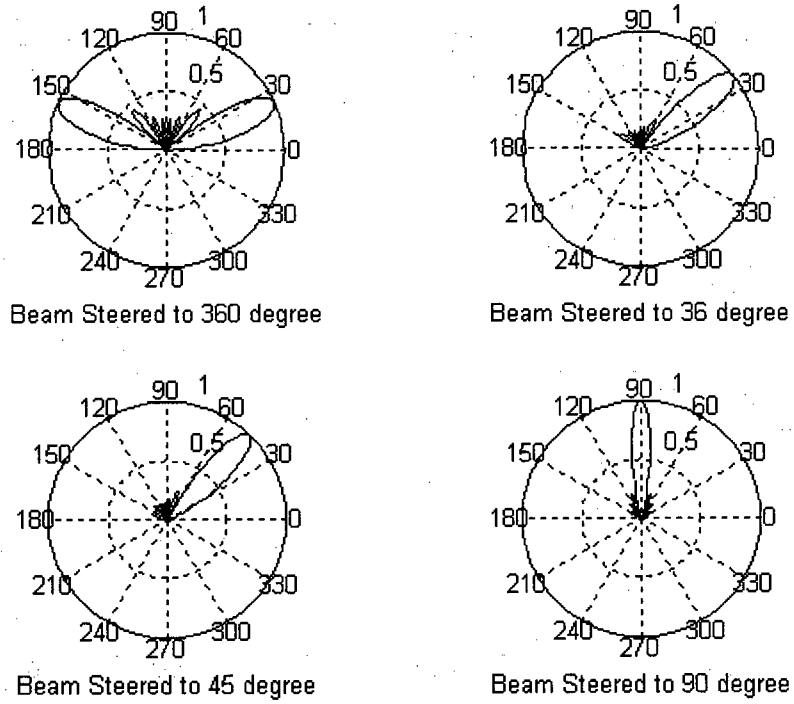

Fig. 2.9 Azimuth Radiation Pattern for 8 Panel Antenna Elements 0.5λ Spaced

2.4 Higher Dimensional Antenna Arrays

By extending the locations of the antenna elements into the 2nd and 3rd dimensions, we are providing additional degrees of freedom for an antenna array to steer its beam. In this

section, we will compare the performance gain of these higher dimensional array structures to the linear arrays described in the previous section.

2.4.1 2-Dimensional Antenna Array

As discussed in the previous section, the use of panel antennas eliminates the problem of having a double main lobe in a linear array but requires the use of at least two additional linear arrays to provide coverage to all azimuth angles. If each array employs 8 panel antennas, the total number of elements used is 24. Alternatively, a 5x5 planar array, where $M = 25$, of similar complexity and shown in Fig. 2.10 can be used.

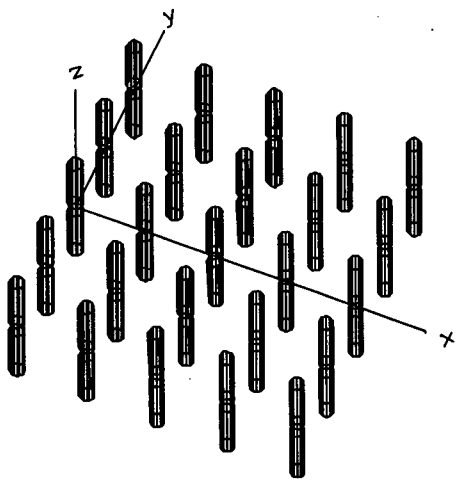

Fig. 2.10 5x5 Planar Antenna Array

With a total of M omni-directional antenna elements providing coverage to the entire cell, and because of its 2-dimensional arrangement, a $\sqrt{M}x\sqrt{M}$ planar array provides a high front-to-back ratio and allows its main beam to be steered to any azimuth direction. The computer simulated radiation patterns for a 5x5 planar array are plotted in Fig. 2.11.

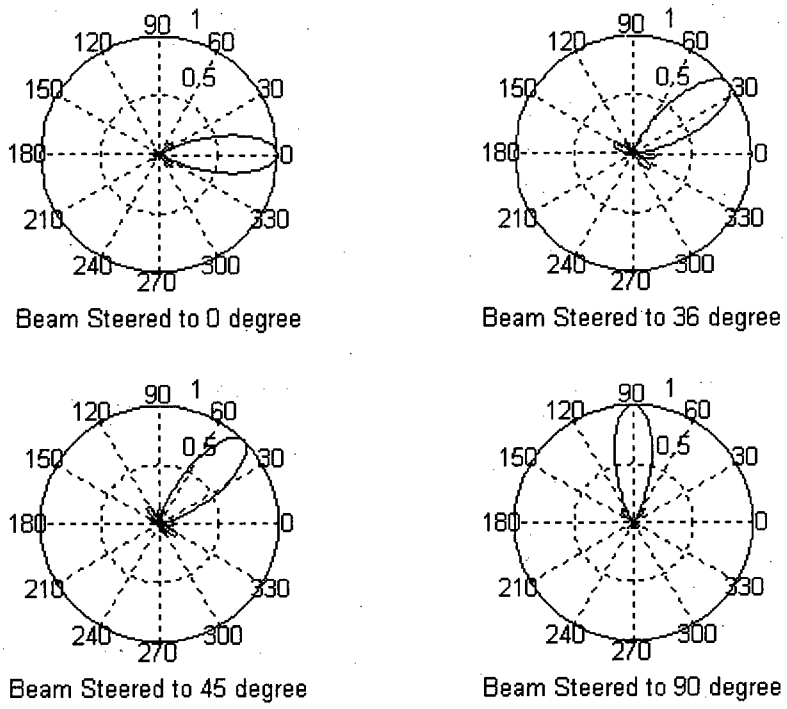

Fig. 2.11 Azimuth Radiation Pattern for a 5x5 Planar Array with 0.4λ Spaced Elements

Referring to Eqs. 2.13 and 2.14, the gain provided by a 5x5 planar array to its steered direction is

$$\begin{aligned} \left| f_{planar,\phi_0,\theta_0}(\phi_0,\theta_0) \right| &= \left| f_{SD}(\theta_0) \sum_{m=0}^{24} \exp[-j\beta(0)] \right| \\ &= \left| 25 f_{SD}(\theta_0) \right|. \end{aligned} \tag{2.20}$$

In comparison, the gain provided by a linear array of eight panel antennas to the steered direction is

$$\begin{aligned} \left| f_{linear,\phi_0,\theta_0}(\phi_0,\theta_0) \right| &= \left| f_{PA}(\phi_0,\theta_0) \sum_{m=0}^{7} \exp[-j\beta(0)] \right| \\ &= \left| 8 f_{SD}(\theta_0) \{1 - \exp[-j\beta(-2d\lambda \cos\phi_0 \sin\theta_0)]\} \right| \\ &\le \left| 8 f_{SD}(\theta_0) \right|. \end{aligned} \tag{2.21}$$

Therefore, with the use of 25 omni-directional antennas instead of 24 panel antennas, a 5x5 planar array provides an effective gain, or an improvement, of

$$P_G \geq 10\log_{10}\frac{[25 f_{SD}(\theta_0)]^2}{[8 f_{SD}(\theta_0)]^2} \geq 9.9\text{dB}. \tag{2.22}$$

In addition to this significant power gain, the 5x5 planar array eliminates inter-sector softer handover and when coupled to dynamic null-steering algorithms [12], provides effectively over three times the number of nulls to reject interferers.

2.4.2 3-Dimensional Antenna Array

Since wireless services are planned for smaller cell sizes, the vertical heights of buildings relative to the cell radius become more significant. In addition to a distribution of users in different azimuth directions, there is also a distribution of users from different floors of buildings. As such, there is a need for antennas to differentiate and selectively steer to different elevation angles, in additional to the different azimuth angles. In order to achieve this, an array must have its antenna elements positioned along the z-axis to sense phase differences of signals arriving from different elevation angles.

Because the array is able to steer its beam to users on different floors of a building, it is advantageous to position the array at half the height of the building being served, as shown in Fig. 2.12, where Array 1 serves building D and Array 2 serves building F. Depending upon the application, the array may be required to also serve users from all azimuth angles, or only from a subset of azimuth angles. For example, it is quite

common for some residential areas to have a central courtyard, completely surrounded by buildings. Therefore, the array can be mounted on a tower in the centre of the courtyard, serving users from all azimuth and elevation angles. In other areas, such as in downtown, where buildings are separated by streets, it might be necessary for the array to be mounted on the side of a building, serving only buildings on the opposite side and as such, require the use of panel antenna elements.

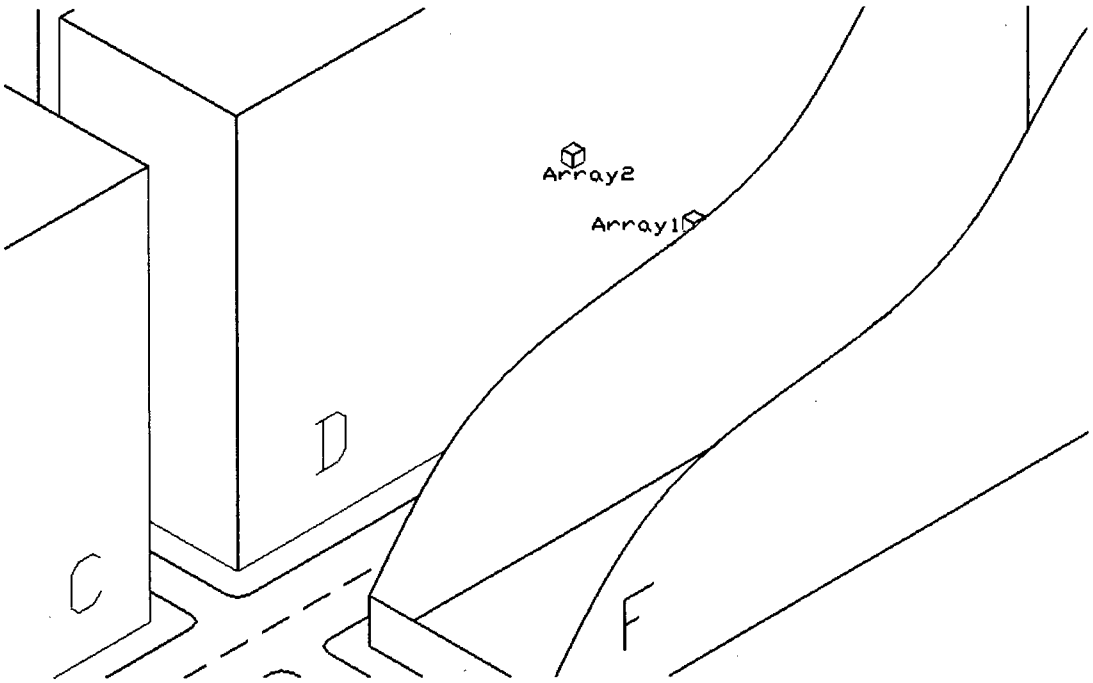

Fig. 2.12 Ideal Position of 3-Dimensional Array

Since it is anticipated that there will be a higher demand for wireless access in buildings in downtown environments, it is important to investigate the use of higher dimensional panel antenna arrays. Because of the advantages of using a 5x5 planar array, a vertical

planar array, as illustrated in Fig. 2.13, consisting of panel antenna elements, will be used.

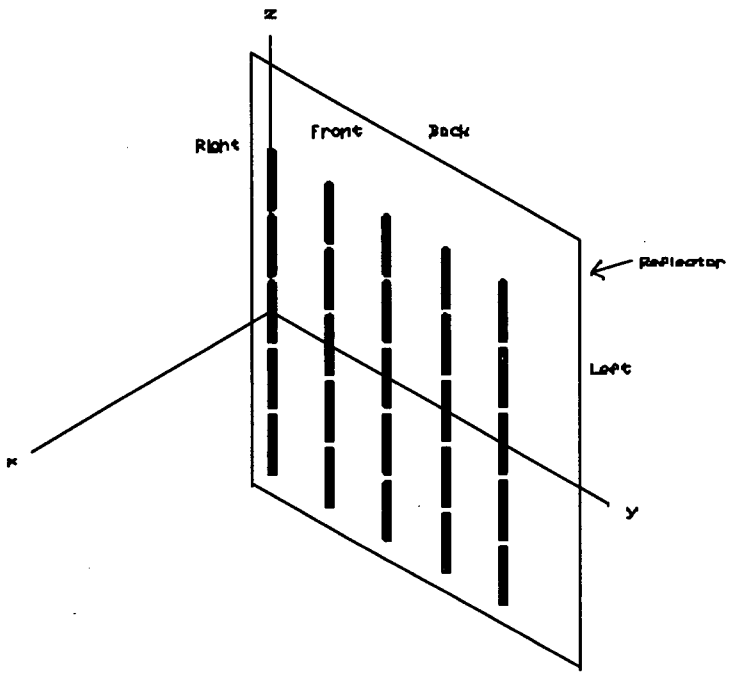

Fig. 2.13 5x5 Vertical Planar Array with Reflector

Due to the reflector, or the use of panel antenna elements, the 5x5 vertical planar array will have a limit on both the azimuth and elevation angles the array can steer to. In addition to only able to receive signals from one side of the array, there is a constraint on the span of both azimuth and elevation angles similar to that shown in Fig. 2.8 for an individual panel antenna element. However, as will be shown in Chapter 4, this limit helps reduce interference from adjacent cells on the left and right side of the array because interference from either side of the array is subjected to a lesser gain.

The vertical arrangement of the array elements allows the beam to be steered to different vertical directions. It also allows a significant reduction in the vertical beamwidth. Figs. 2.14 and 2.15 show the 3-dimensional radiation pattern of a 1x5 linear array and a 5x5 vertical planar array when steered to the $(\phi_0, \theta_0) = (0,150)$ direction, with the use of panel antenna elements and taking into account also the short dipole's inherent vertical pattern. As indicated, the 5x5 vertical planar array is able to select a specific vertical elevation angle, in addition to reducing the vertical half power beamwidth.

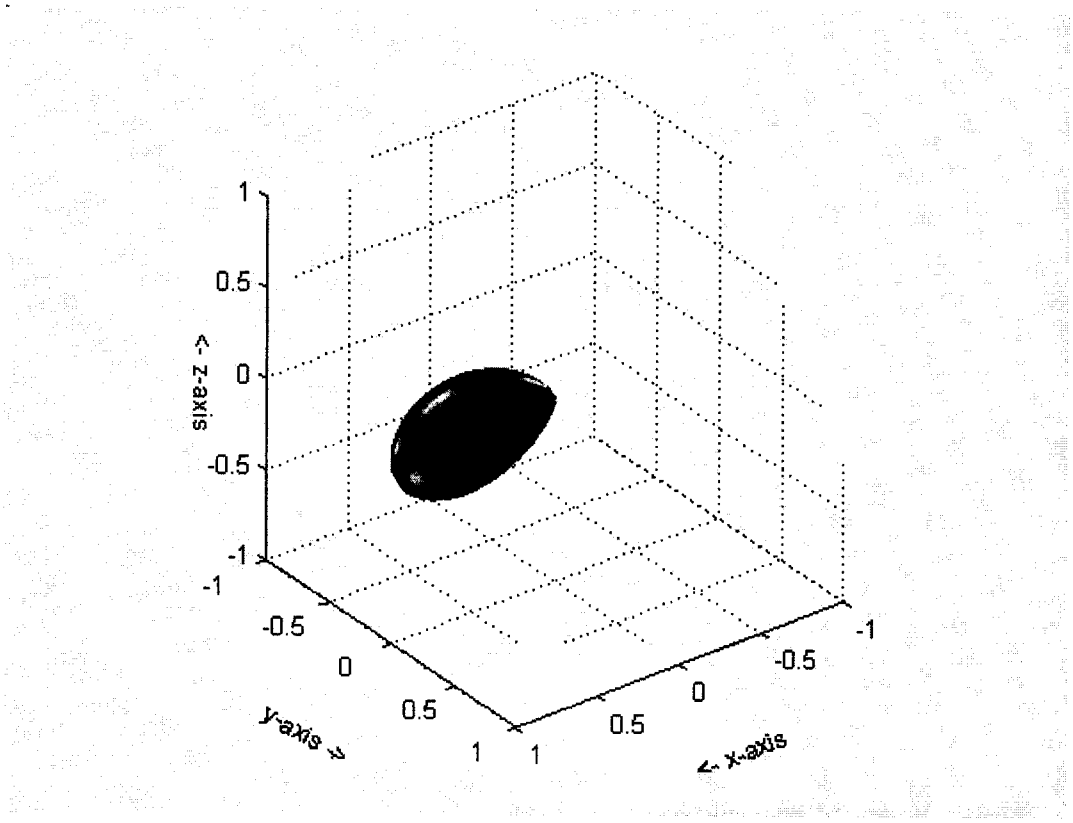

Fig. 2.14 Radiation Pattern of a 1x5 Linear Array with Panel Antenna Elements Directivity(ϕ_0, θ_0) = 2.1505 Vertical Beamwidth = 56^0

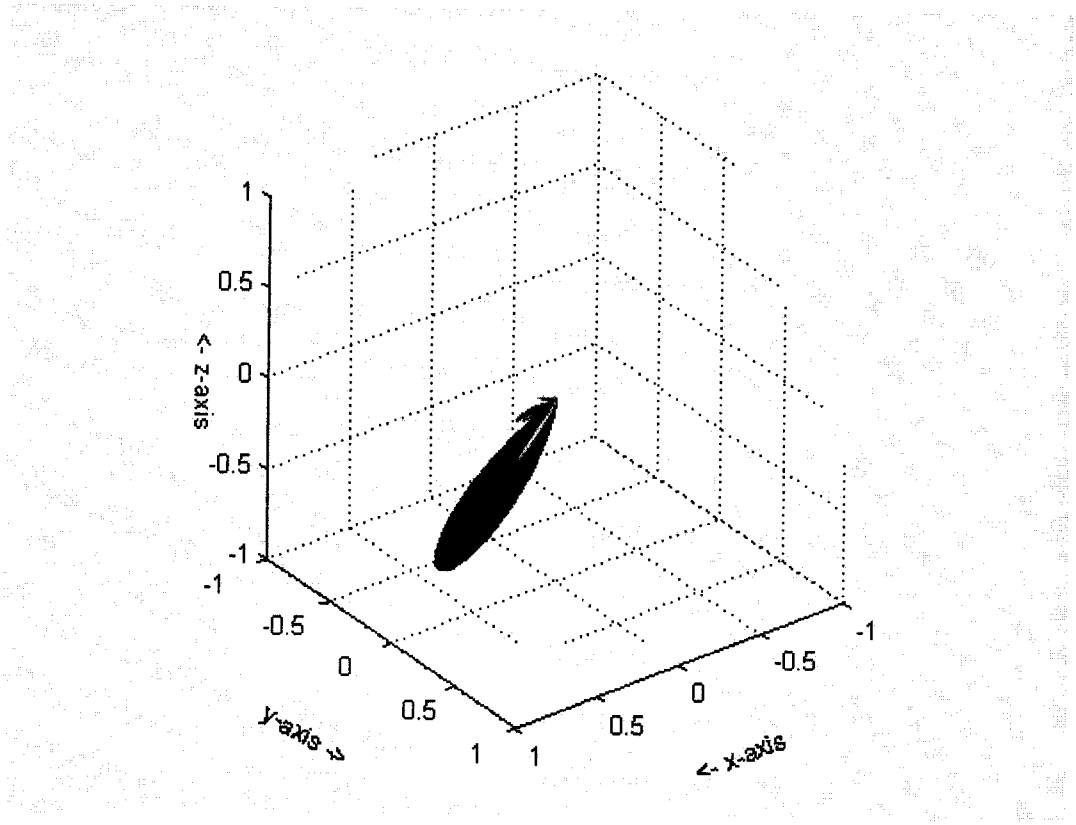

Fig. 2.15 Radiation Pattern of a 5x5 Vertical Planar Array with Panel Antenna Elements Directivity(ϕ_0, θ_0) = 21.624 Vertical Beamwidth = 19^0

Shown also in Figs. 2.14 and 2.15 are the arrays' directivity values. The power gain provided by a 5x5 vertical planar array, effectively five times the number of elements of a 1x5 linear array, is

$$P_G = 10\log_{10}\left(\frac{21.624}{2.1505}\right) \qquad (2.23)$$
$$= 10.024\text{dB}$$

Clearly from the above equation, a five times increase in the number of elements provides an additional degree of freedom for beam steering, and increases the array gain ten times.

2.5 CDMA Capacity

In the previous section, we have described how antenna arrays can be used to provide better performances by reducing beamwidth, and providing higher gain. These allow the increase of the capacity of a cellular system. In a CDMA system, spectrum is shared among multiple users. To distinguish and separate the different signals, each user transmits with a unique psuedo-noise (PN) code that is orthogonal to all other users in the system, where the coding operation is performed by multiplying the user data with the PN code. This allows multiple access by different users during the same time within the same bandwidth. Since the PN code has a shorter bit period than the data symbols, the requirement for transmission bandwidth is increased by [9]

$$PG = \frac{T_b}{T_{PN}} \tag{2.24}$$

where PG, T_b, and T_{PN} are the processing gain, user data bit period, and PN code bit period, respectively. Because of conservation of energy and the increase in bandwidth, the transmitted amplitude is reduced by the processing gain. In order to recover the original data symbols at the receiver, the same PN code is used to multiply with the received signal for de-spreading, during which the original data symbols are recovered prior to matched filter detection. Meanwhile, any received interference or noise is spread with the amplitude suppressed. Because the Bit Error Rate (BER) during matched filter detection is determined by the SINR after de-spreading, the number of users, or capacity, is therefore interference limited [27]. As a result, it is common to use the SINR as a performance measure to determine capacity limits. In the receiver, after de-spreading, the SINR parameter for a given call connection is

$$\text{SINR} = \frac{E_0}{N_o} = \frac{E_0}{I_{MAI} + I_n} \tag{2.25}$$

where we will assume SINR = 9 dB [3], E_0 is the desired mobile's energy per bit, and I_{MAI}, I_n are the power spectral density for the Multiple Access Interference (MAI) and receiver noise, respectively. Assuming a system with K users is limited by MAI, with non-continuous voice activity, which reduces the average MAI [9], Eq. 2.25 can be expressed as

$$\text{SINR} = \frac{E_0}{\nu I_{MAI}} = \frac{P_{r_0}}{\frac{\nu}{N}\sum_{i=1}^{K-1} P_{r_i}} \tag{2.26}$$

where P_{r_0} and P_{r_i} are the received power from the desired user and i-th interferer prior to de-spreading, and for the IS-95 standard [9], ν is the voice activity factor, which typically has the value of 0.6, and $N = 128$ is the processing gain.

If an antenna array is used, the signals incident on the array will experience a different gain depending on its AOA, and Eq. 2.26 needs to factor this into account. Assuming perfect power control by each cell, the required received power per user is P_c, and the array is steered to the AOA for each user, the power incident on the array is

$$\begin{aligned} P_i &= \frac{P_c}{\left|f_{\phi,\theta}(\phi,\theta)\right|^2} \\ &= \frac{P_c}{\left|f_{EL}(\phi,\theta)\right|^2 M^2}. \end{aligned} \tag{2.27}$$

If the desired user's AOA is (ϕ_0,θ_0), and the i-th user's AOA is (ϕ,θ), the received interfering power from the i-th user is

$$\begin{aligned} P_{r_i} &= \left| f_{\phi_o,\theta_0}(\phi,\theta) \right|^2 P_i \\ &= \left| f_{EL}(\phi,\theta) f'_{\phi_o,\theta_0}(\phi,\theta) \right|^2 P_i \\ &= \left| f_{EL}(\phi,\theta) f'_{\phi_o,\theta_0}(\phi,\theta) \right|^2 \frac{P_c}{\left| f_{EL}(\phi,\theta) \right|^2 M^2} \\ &= P_c F'_{\phi_o,\theta_0}(\phi,\theta) \end{aligned} \tag{2.28}$$

where

$$F'_{\phi_o,\theta_0}(\phi,\theta) = \frac{\left| f'_{\phi_o,\theta_0}(\phi,\theta) \right|^2}{M^2}. \tag{2.29}$$

Substituting Eq. 2.28 into Eq. 2.26, the SINR for the desired user with the use of antenna array becomes

$$\text{SINR} = \frac{P_c}{\frac{\nu}{N} \sum_{i=1}^{K-1} P_c F'_{\phi_o,\theta_0}(\phi,\theta)} \tag{2.30}$$

and the mean SINR for each connection, if K users are in the system, is

$$\begin{aligned} \text{SINR} &= \frac{P_c}{\frac{\nu}{N} E\left[\sum_{i=1}^{K-1} P_c F'_{\phi_o,\theta_0}(\phi,\theta) \right]} \\ &= \frac{P_c}{\frac{\nu}{N} P_c (K-1) E\left[F'_{\phi_o,\theta_0}(\phi,\theta) \right]} \\ &= \frac{1}{\frac{\nu}{N}(K-1) \int_{x_1}^{x_2} \int_{\phi_1}^{\phi_2} \int_{\theta_1}^{\theta_2} u(x,\phi,\theta) F'_{\phi_o,\theta_0}(\phi,\theta) d\theta d\phi dx} \end{aligned} \tag{2.31}$$

where $E[]$ is the expectation operator, $u(x,\phi,\theta)$ is the probability distribution function of users around the antenna array. The integral limits of the above equation are as illustrated in Fig. 2.16, which shows an antenna array can steer its beam to any location

in a building group throughout the vertical angles $[\theta_1,\theta_2]$, azimuth angles $[\phi_1,\phi_2]$, and front to back $[X_1,X_2]$ of the building group under investigation.

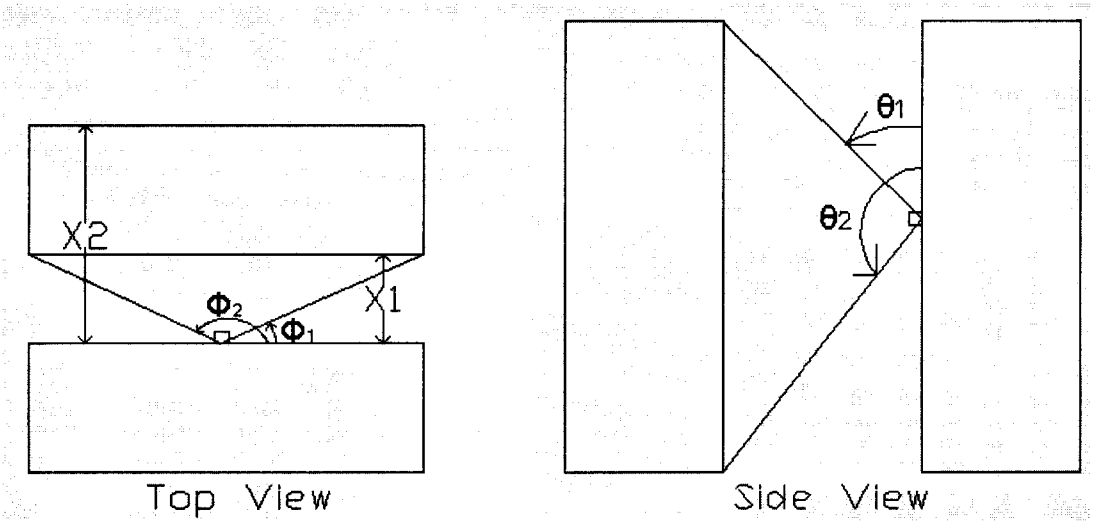

Fig. 2.16 Integral Limits for User Probability Distribution Function

From Eq. 2.31, the mean system capacity[1] is

$$K = \frac{1}{\frac{\nu}{N}\mathrm{SINR}\int_{x_1}^{x_2}\int_{\phi_1}^{\phi_2}\int_{\theta_1}^{\theta_2} u(x,\phi,\theta)F'_{\phi_0,\theta_0}(\phi,\theta)\,d\theta\,d\phi\,dx} + 1. \qquad (2.32)$$

Note the performance evaluation results presented in Chapter 5 show that the total number of users supported by our proposed 3-dimensional vertical planar array exceeds the number of orthogonal codes, N, available in the IS-95 system given SINR = 9 dB. However, the purpose of our work is to show the effects of capacity at different angles

[1] In this thesis, the mean system capacity is the average capacity for a given (ϕ_0,θ_0) that the array is steered to. Note that this capacity changes at different steered angles and the minimum capacity for all possible angles will be denoted as the capacity for the system.

for different array structures and therefore, this point will be ignored. A solution to this problem is to increase the SINR threshold (> 9 dB), which will reduce the number of users.

2.6 Conclusions

In this chapter, we have presented the different antenna structures from simple 1-dimensional linear array to 3-dimensional array. Linear array is the most basic type and is the easiest to model. However, linear array does not provide the gain available with higher dimensional arrays. Further, problems with two main lobes and the in-ability to steer to different vertical directions limit the potential performance available in smart antenna systems. We showed by using a 2-dimensional planar array, we can achieve up to ten times in power gain, and a reduction of inter-sector handover. We have also demonstrated that the use of panel antenna elements eliminates one of the main lobes and arranging elements in a 3-dimensional fashion allows the control of vertical steering and beamwidth. These further increase the gain and directivity of the main beam. Further, realistic antenna elements were modelled and incorporated into the array factor for accurate antenna arrays' representations. In a CDMA system, the SINR has an inverse relationship with the user capacity and the use of an antenna array allows the improvement of SINR by reducing gain to unwanted users. This is shown by the application of a vertical planar array in an urban environment, which allows the array to differentiate users' signals from different floors of a building and thus increase the overall user capacity in the mean sense.

Chapter 3 USER DISTRIBUTION

3.1 Introduction

In order to study and predict the capacity with the use of different antenna array configurations, the scenario in which the arrays will be applied must be modelled. This chapter will present a 3-dimensional model of a typical downtown environment that applies equally well to the downtown core of large metropolitan cities, such as for example Manhattan, NY, USA, or Vancouver, BC, Canada. Its organization is as follows. After this introduction, Section 3.2 will present the proposed layout and arrangement of the downtown model, along with the corresponding cell outline and dimensions. Section 3.3 introduces an improved user distribution model, over the ubiquitous uniform user distribution as used in previous studies. Section 3.4 presents the conclusion of this chapter.

3.2 Downtown Model

The typical downtown resembles that of a rectangular grid, which our model in Fig. 3.1 is based upon. The dimensions and separations of each city block are taken from the Vancouver Geographic Information System (GIS) Database [14], and correspond well also to measurements from the upper west side of Manhattan [28]. Each city block is approximately of size 150 m long and 80 m wide, and contains two building groups, each identified with an alphabet letter and separated by a 5 m spacing. The buildings are assumed to be of 30 floors high at 3 m per floor, and are modelled by a continuous building group with a flat surface [28], [29].

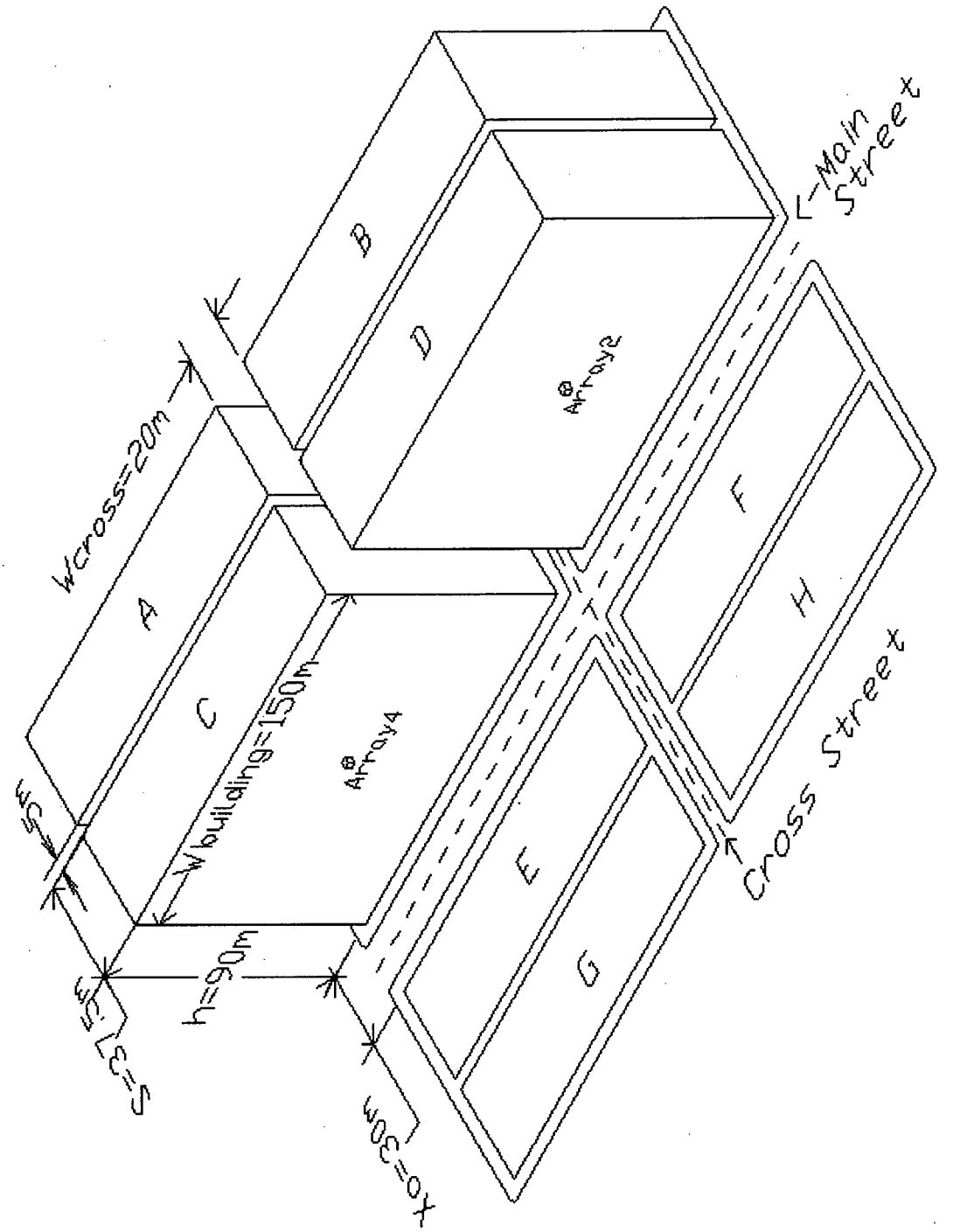

Fig. 3.1 Downtown Model (1:50 Scale)

For example, building group C is 150 (w) by 37.5 (d) and 90 (h) tall, separated from building group A by 5 m. Each building group is proposed to be a single cell of service, served by an antenna array mounted on a building on the opposite side of the street. This is depicted in Fig. 3.1 with two antenna arrays mounted on the side of building groups C and D, serving building groups E and F respectively. Further, the main street traversing the long side of each building group has a width of 30 m, while the cross street has a width of 20 m.

3.3 Modified User Distribution Model

Because the performance of an antenna array depends on the accuracy and capability for beam steering, the location and distribution of the intended users must be modelled accurately in order to provide meaningful results. In the past, typically users were assumed to be uniformly distributed around the base station antenna [3]. However, in general, this is only valid in the case of macro cell where users are spread over a large cell area with radius of up to 10 km [15], serviced by omni-directional antenna elements. In our study, we consider users who are inside buildings and the proposed array elements are non omni-directional. Even if users have a uniform spatial distribution, the perceived user density is different from the antenna's point of view. As such, a new user distribution model is needed.

As illustrated in Fig. 3.2, the antenna beam covers a larger area as it is steered off centred, or towards the ends of the building, even while maintaining a constant beamwidth. This effectively causes the perceived user density to increase exponentially

as the array is steered further towards the ends of the building and reduces the actual realizable capacity. We will assume that the signal attenuation through buildings is high enough that signals originating from an adjacent building facing a parallel street will not change our results. Therefore, the array on building group F will not receive interfering signals from building group B.

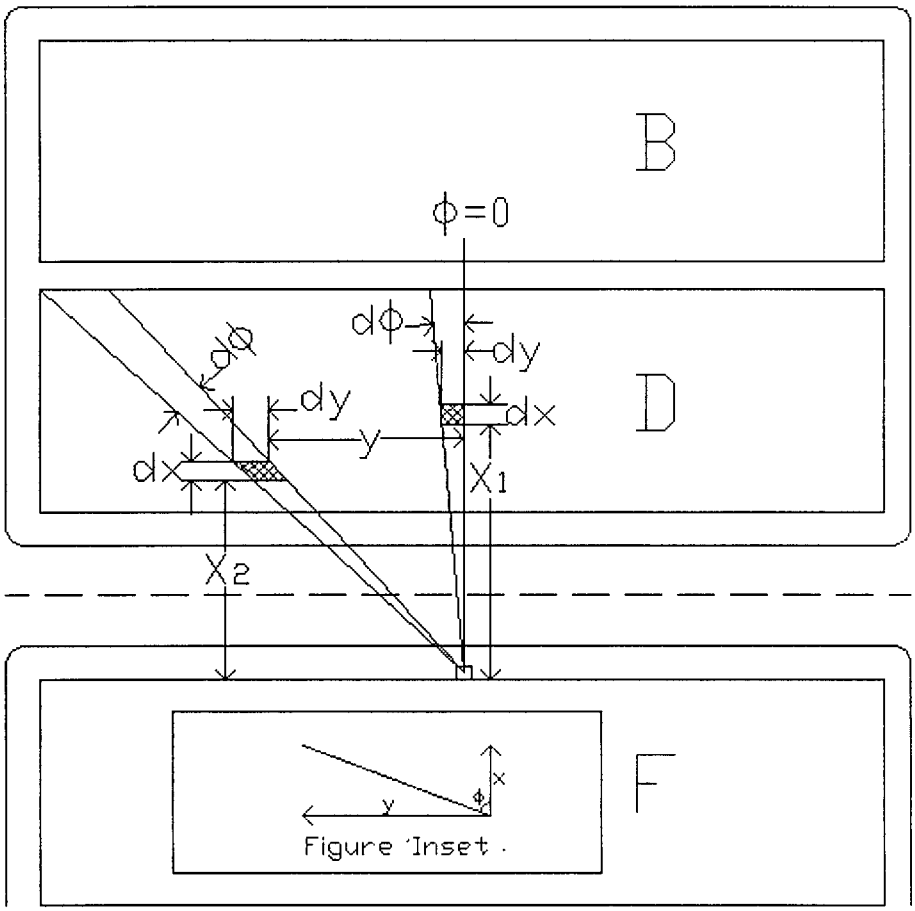

Fig. 3.2 Modified User Density (Horizontal)

The more accurate user distribution can be modelled by the area of floor space covered per degree of beamwidth, for the different azimuth angles the antenna is steered to. From Fig. 3.2, we can see that X_1 and X_2 are the distances between the hashed area elements and the antenna array in the x direction, and y is the distance between the elemental area and the $\phi = 0$ line. Using the geometry from the inset of Fig. 3.2, and assuming the antenna is placed at middle of the block, we have

$$y = x\tan(\phi). \tag{3.1}$$

Accordingly, the area of coverage per degree increases as the steered azimuth angle, ϕ in Eq. 3.1, increases. The increase can be found by taking the derivative of y with respect to ϕ, i.e.

$$\frac{dy}{d\phi} = x\left[1 + \tan^2(\phi)\right] \tag{3.2}$$

and therefore, the hashed area element is

$$\begin{aligned} dA &= dydx \\ &= x\left[1 + \tan^2(\phi)\right]d\phi dx. \end{aligned} \tag{3.3}$$

As indicated by Eq. 3.3, the area is dependent on the steered azimuth angle, ϕ, as well as the distance away from the antenna array along the x-axis. Assuming the number of users is proportional to the floor area, the effective user distribution for a single floor in a downtown building is

$$u_{floor}(x,\phi) = \frac{x\left[1+\tan^2(\phi)\right]}{\int_{X_0}^{X_0+S}\int_{\phi_{\max 1}(x)}^{\phi_{\max 1}(x)} dA} = \frac{x\left[1+\tan^2(\phi)\right]}{\int_{X_0}^{X_0+S}\int_{\phi_{\max 1}(x)}^{\phi_{\max 1}(x)} x\left[1+\tan^2(\phi)\right]d\phi dx} = \frac{x\left[1+\tan^2(\phi)\right]}{SW_{building}} \tag{3.4}$$

where

$$\phi_{\max 1}(x) = \tan^{-1}\left(\frac{W_{building}}{2x}\right) \tag{3.5}$$

is the maximum ϕ bounded by the size of the building group, and S, $W_{building}$, and X_0, are the building group's depth, width, and main street width as illustrated in Fig. 3.1.

Since we will examine the capacity gain by employing arrays that have vertical steering ability also, the complete user distribution must take into account the effects of the vertical elevation angle, θ, as well. Shown in Fig. 3.3 is an antenna array mounted on the side of building group F, which only its footprint is shown, at a fixed distance X_0 away from building group D. As shown, the vertical coverage spanned by each vertical degree is not constant and is completely dependent on both the azimuth, ϕ, and vertical, θ, steered angle.

The height of the building group covered by each degree of vertical angle, θ, determines the amount of interference received by the antenna array. Referring to Fig. 3.3, we have

$$c(\phi,x) = \frac{x}{\cos(\phi)} \tag{3.6}$$

where $x = X_0$ is the width of the main street. If the location of the antenna array in Fig. 3.3 is at $(x,y,z) = (0,0,0)$,

$$z = c(\phi, X_0)\tan\left(\frac{\pi}{2} - \theta\right) \tag{3.7}$$

and the change in height per degree change of vertical elevation is

$$\frac{dz}{d\theta} = c(\phi, X_0)\left[1 + \tan^2\left(\frac{\pi}{2} - \theta\right)\right]. \tag{3.8}$$

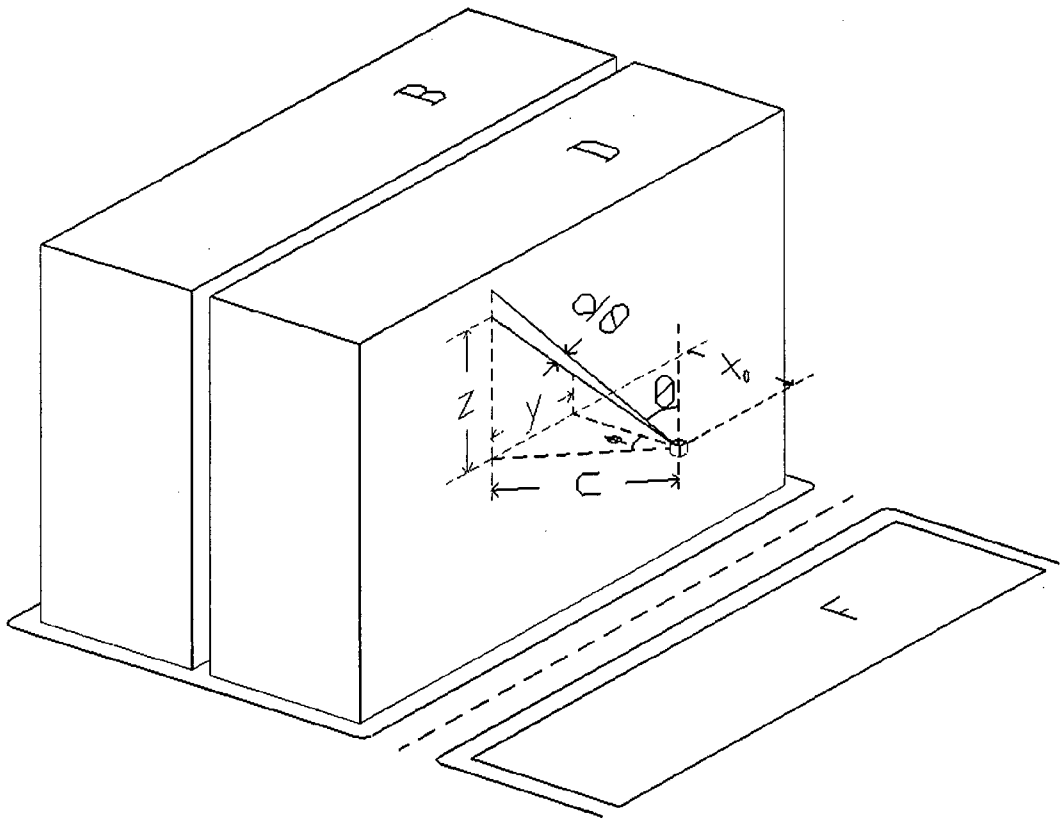

Fig. 3.3 Modified User Density (Vertical)

Since in the vertical direction the building is hard-partitioned into different floors, it is fair to assume that the vertical height element *dz* is constant from the front of the building

to the back. For example in the case of Fig. 3.4, if the antenna beam is steered to a user on the 25th floor, it is not susceptible to an interferer from the 28th floor. This allows separating a building into different vertical sectors, or service areas.

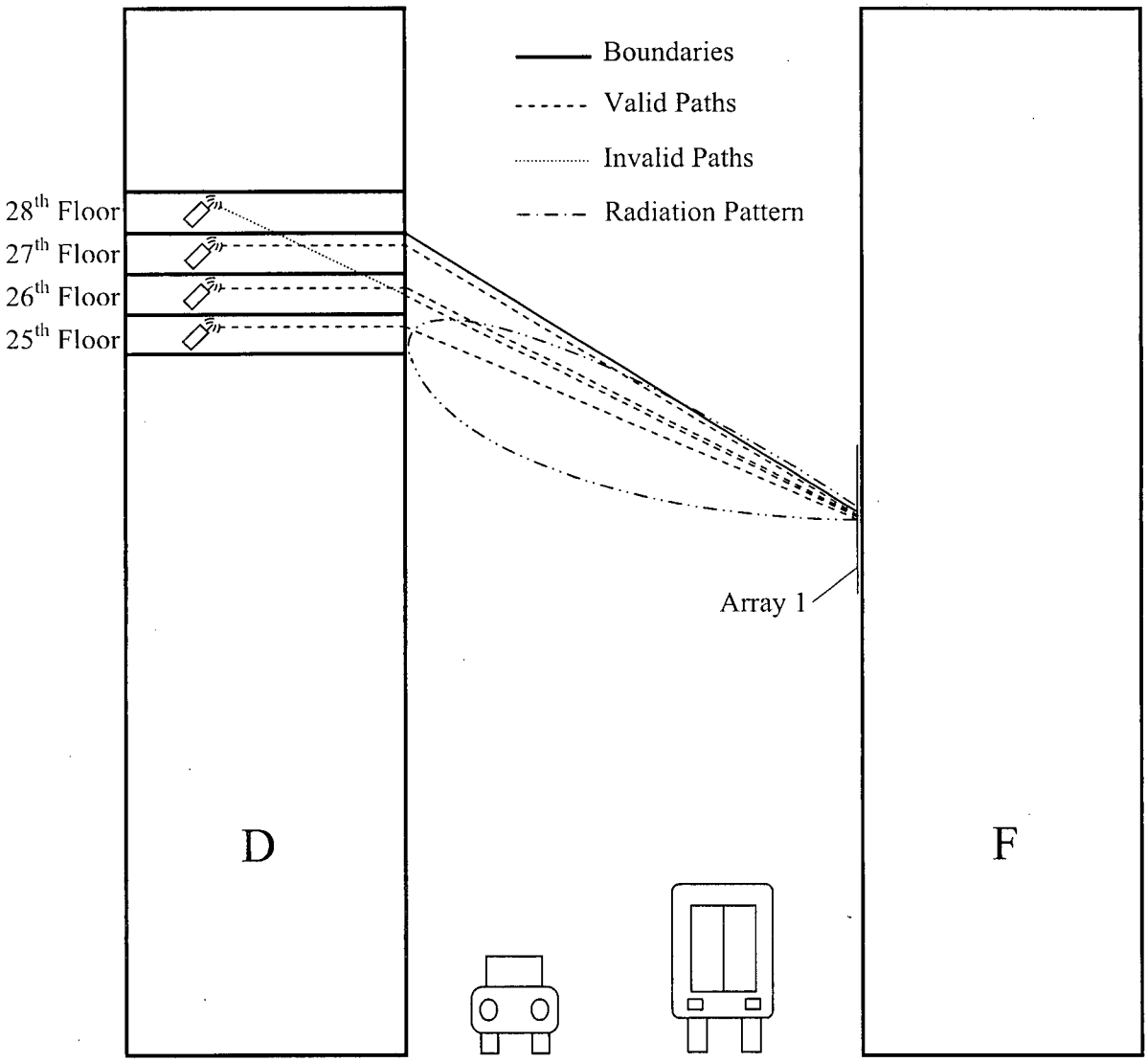

Fig. 3.4 Separation of Building Floors

By combining Eqs. 3.3 & 3.8 to include a 3-dimensional space, we have a volume element within a building, i.e.

$$\begin{aligned} dV &= dzdydx \\ &= c(\phi, X_0)\left[1+\tan^2(\frac{\pi}{2}-\theta)\right]x\left[1+\tan^2(\phi)\right]d\theta d\phi dx. \end{aligned} \tag{3.9}$$

As indicated by Eq. 3.9, the volume element in a building covered by an antenna array is dependent on its location, relative to the array itself. In other words, as the antenna beam is steered to different azimuth and/or vertical angles, (ϕ_0, θ_0), it is subjected to different level of interference. Assuming the probability of finding a user at (x, ϕ_0, θ_0) is proportional to the size of volume element covered when the array is steered to (ϕ_0, θ_0), the effective user probability distribution function for a 3-dimensional building is

$$\begin{aligned} u_{building}(x,\phi,\theta) &= \frac{c(\phi, X_0)\left[1+\tan^2(\frac{\pi}{2}-\theta)\right]x\left[1+\tan^2(\phi)\right]}{\int_{X_0}^{X_0+S}\int_{-\phi_{max1}(x)}^{\phi_{max1}(x)}\int_{\theta_{max}(\phi)}^{\pi-\theta_{max}(\phi)} dxdydz} \\ &= \frac{c(\phi, X_0)\left[1+\tan^2(\frac{\pi}{2}-\theta)\right]x\left[1+\tan^2(\phi)\right]}{SW_{building}h} \end{aligned} \tag{3.10}$$

where

$$\theta_{max}(\phi) = \frac{\pi}{2} - \tan^{-1}\left(\frac{h}{2c(\phi, X_0)}\right). \tag{3.11}$$

3.4 Conclusions

In this chapter, a downtown model representative of typical large metropolitan cities, such as for example Manhattan, NY, USA or Vancouver, BC, Canada was presented with

city blocks and buildings dimensions taken from the Vancouver GIS system. We have also introduced a more accurate user distribution in buildings when served by an external antenna array mounted on a building group across the main street. We will use this model and user distribution for our interference analysis and capacity estimation in the next chapter.

Chapter 4 MULTICELL INTERFERENCE

4.1 Introduction

In addition to local in-cell interferers, the capacity for CDMA systems is also limited by out-of-cell interference. Because of the antenna height, sources of interference are limited to areas deduced from single bounce ray tracing based on reflection off surrounding buildings, in addition to the direct LOS paths. Previous studies have considered the general case of ray propagation in mainly the horizontal plane for capacity analysis [17], [30]. This chapter introduces a new 3-dimensional single bounce model for a multicell system, taking into account the structures and locations of the arrays, surrounding buildings, and the reflection properties of the buildings. Because exact shape and dimensions are not considered, it is not as accurate as site specific ray-tracing models. However, this method offers a generic approach that is analytically tractable and still takes into account of a site geometry that is representative of most typical downtown environments. As such, for the purpose of visualizing system level changes such as the introduction of additional arrays, or changes in array locations and site geometries, this provides a faster and more efficient method without limiting the results to a specific site layout. Because of the height of the antenna array, and the intended users are in buildings, rays are reflected by buildings rather than scattered by ground level moving objects. The model will incorporate the building wall's permittivity into the reflection co-efficient, and measured values of diffraction loss for shadowed regions. It is assumed in our model that building floors will provide sufficient partition between different floors of a building, and that penetration loss on the building wall's surface is compensated by power control. The chapter is organized as follows. After this introduction, Section 4.2

presents the considered system model, including its main assumptions. Then, the effects of diffraction, building penetration loss, path loss, and element factor on power control are presented in Section 4.3. Section 4.4 discusses some of the geometrically based single bounce models used in previous studies, and Section 4.5 introduces our modified single bounce model to analyse interference generated from buildings that are adjacent to the intended cell of service. Section 4.6 presents the conclusions of this chapter.

4.2 System Model

In order to determine the capacity supported in a cell, interference from adjacent cells must also be taken into account. Consequently, Eqs. 2.31 and 2.32 needs to be modified to include the effects from other cells. To achieve this, propagation effects such as reflection, diffraction, attenuation, penetration loss, and the gain provided by the element factor need to be taken into account to determine the direction and power of received signals from other mobile users in adjacent cells. It should be noted that mutual coupling effects will be ignored since recent researches have shown that it does not have any [31] or have minimal [32] effect on capacity. Because of the assumption of perfect power control, the dynamics and actual operation of power control need not be considered, and steady state is assumed. For our model presented in the previous chapter, we have considered that the base station antennas are placed at half the height of the building groups, i.e. well below the surrounding buildings' height, thus we have assumed a direct LOS path to the buildings that it serves. In [33], measurements for a roof mounted antenna have shown that incoming signal propagate along the streets. Therefore, propagation via diffraction over the top of each building group can be neglected [28],

[34]. We will also assume propagation via ground rays to be negligible due to the controlled vertical radiation. Because of the close proximity of the mobile users to the antenna array, little power is required to be transmitted by each terminal and the penetration loss is assumed to be compensated by power control. Furthermore, because signals only propagate from one side of the street to the other without being attenuated or scattered by moving objects on the ground, in addition to the relatively fixed position of the wireless terminals in the buildings, the channel is assumed to be static [35] and primarily LOS based. As a result of the penetration loss, waves originated from a wireless terminal scattered inside buildings will be ignored. Suppose we wish to serve users in building group D in Fig. 4.1, interference from the adjacent building groups, i.e. F, C, E, I, and J, must be considered, and by extending Eq. 2.30 for our multicell case

$$\text{SINR} = \frac{P_c}{\frac{\nu}{N} I_{total}(\phi_0, \theta_0)} \tag{4.1}$$

where I_{total} is the total interference received when Array 1 is steered towards (ϕ_0,θ_0) and can be expressed as

$$I_{total}(\phi_0,\theta_0) = I_D(\phi_0,\theta_0) + I_F(\phi_0,\theta_0) + I_C(\phi_0,\theta_0) + I_E(\phi_0,\theta_0) + I_I(\phi_0,\theta_0) + I_J(\phi_0,\theta_0). \tag{4.2}$$

In the above equation,

$$\begin{aligned} I_D(\phi_0,\theta_0) &= E\left[\sum_{i=1}^{K-1} P_{r_i}^D\right] & I_F(\phi_0,\theta_0) &= E\left[\sum_{i=0}^{K-1} P_{r_i}^F\right] \\ I_C(\phi_0,\theta_0) &= E\left[\sum_{i=0}^{K-1} P_{r_i}^C\right] & I_E(\phi_0,\theta_0) &= E\left[\sum_{i=0}^{K-1} P_{r_i}^E\right] \\ I_I(\phi_0,\theta_0) &= E\left[\sum_{i=0}^{K-1} P_{r_i}^I\right] & I_J(\phi_0,\theta_0) &= E\left[\sum_{i=0}^{K-1} P_{r_i}^J\right] \end{aligned} \tag{4.3}$$

where the superscript for P_{r_i} indicates the origin of the received i-th user interfering power. The resulting interference and capacity applies to other adjacent building groups as well, assuming there are further building groups beyond those depicted in Fig. 4.1.

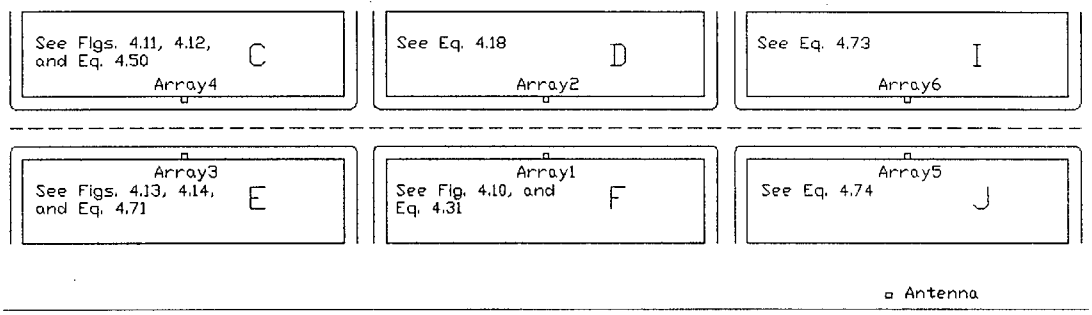

Fig. 4.1 Multicell Interference System Model

4.3 Power Control

Despite the assumption of perfect power control, each mobile produces a different level of interference to adjacent cells as a function of the channel loss to the serving base station. This is because depending on the location of a mobile user, the channel loss to the serving base station's antenna array is different than if the mobile is at another location, and with power control, the base station instructs the mobile to adjust its transmitted power such that the same power is received. Therefore, interference from mobiles in adjacent cells is location dependent. Given the ability of an antenna array to steer to different directions, the mean interference received is also a function of the beam's steered direction. Therefore, all factors associated with power loss must be considered. Sections 4.3.1-4.3.5 will discuss the loss from reflection, diffraction, penetration, distance, and element factor, respectively, for use in our system model.

4.3.1 Reflection Loss

When a radio wave impinges on an object, part of the energy is reflected. The electric field intensities of the reflected and incident waves are related by the Fresnel reflection coefficient, Γ, which is a function of the wave polarization, angle of incidence, and the relative permittivity, ε_r, of the obstacle. If the plane of incidence is defined as the plane containing both the incident and reflected waves, Figs. 4.2 and 4.3 show the two cases when the electric field is parallel and perpendicular to the plane of incidence, where E_i and E_r are the incident and reflected waves respectively.

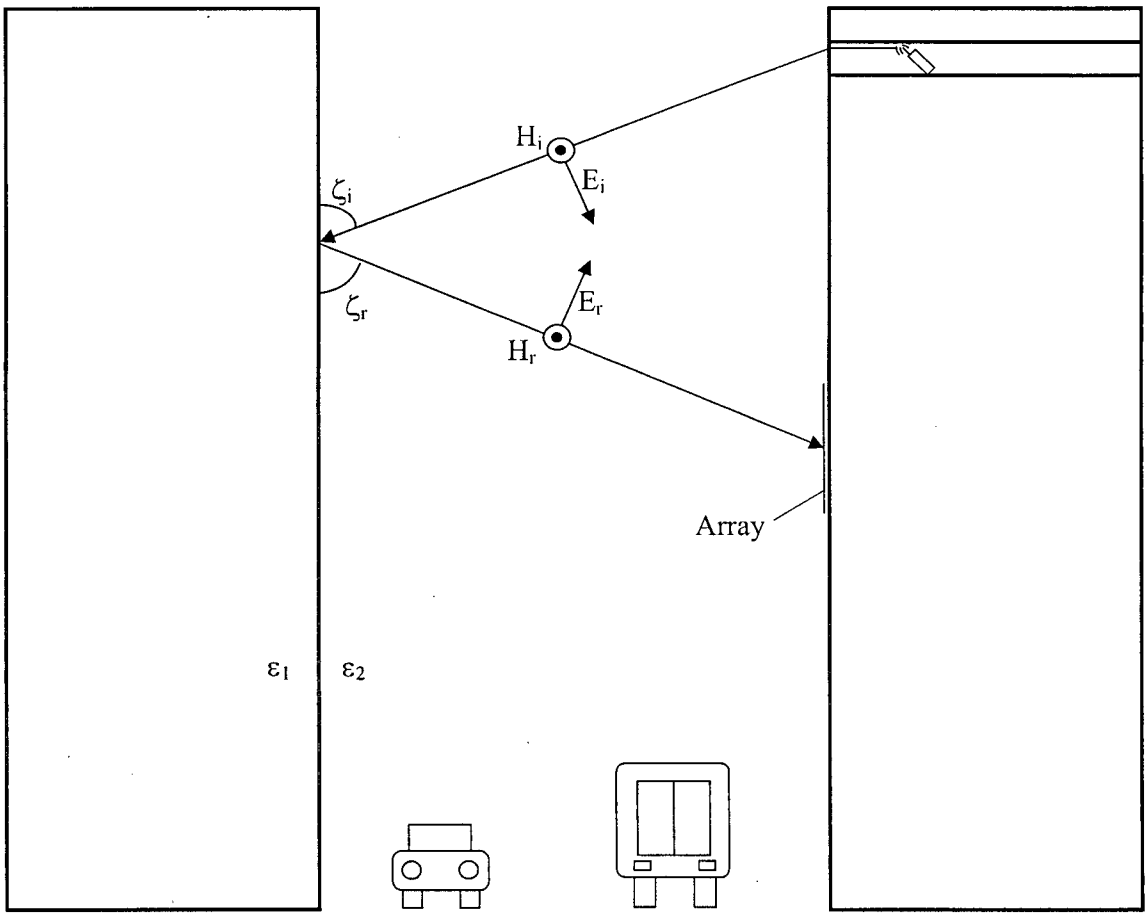

Fig. 4.2 Electric Field Parallel to Plane of Incidence
Side View of City Block

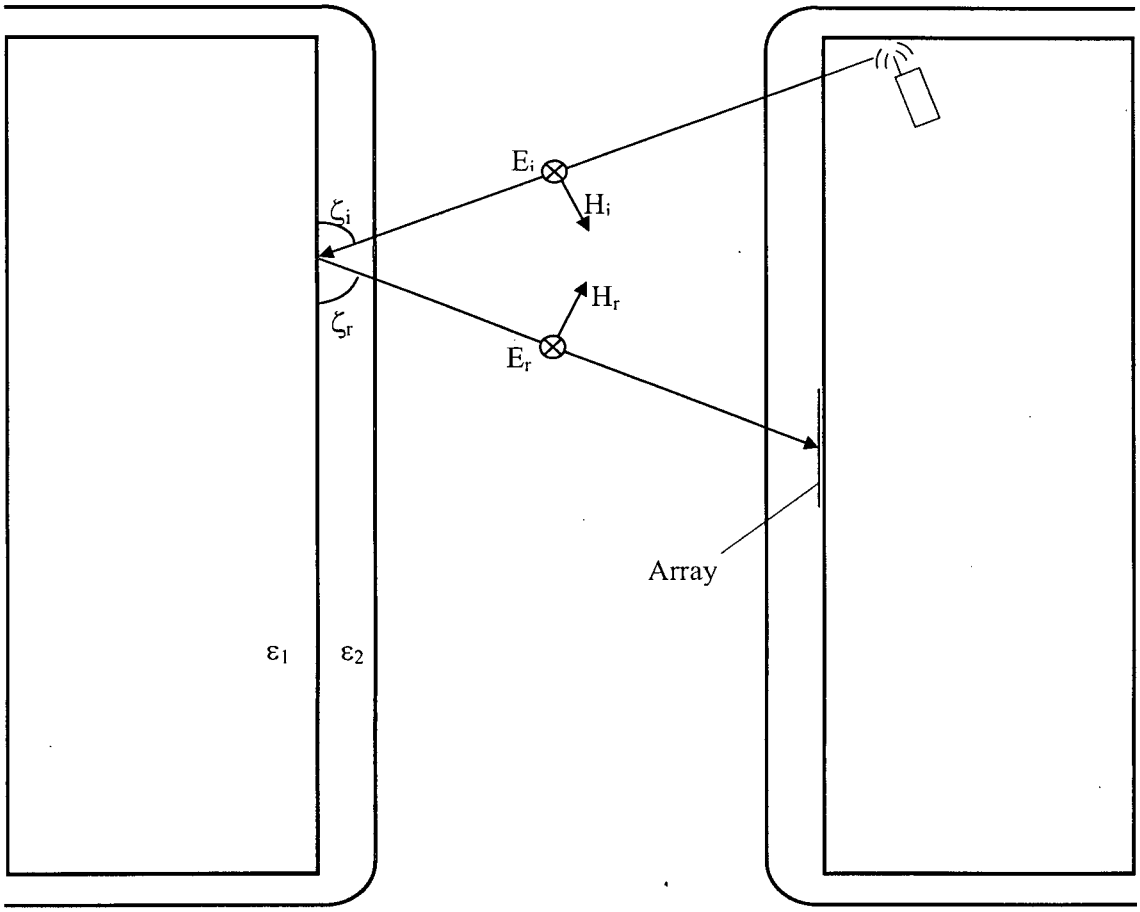

Fig. 4.3 Electric Field Normal to Plane of Incidence
Top View of City Block

As shown in both figures, even if the intended cell of service are the buildings across the street (left side on Figs. 4.2 and 4.3), the array is still susceptible to interference generated from buildings on its side of the street (right side on Figs. 4.2 and 4.3). Also shown is that the electric field components are vertically polarized, which is the orientation that the base station array able to receive. Because the interfering signal propagates both vertically and horizontally to the receiving antenna array, by bouncing

off the buildings being served, the reflection coefficient must take into account both cases shown.

Assuming that the medium defined by ε_2 is free space, we have

$$\begin{aligned} \varepsilon_1 &= \varepsilon_{1r}\varepsilon_0 \\ \varepsilon_2 &= \varepsilon_0 \end{aligned} \tag{4.4}$$

where ε_0 is the permittivity of free space and ε_{1r} is the relative permittivity of the building material, tabulated in Table 4.1 for common materials..

	Material			
	Glass	Plexiglass	Brick	Limestone
Permittivity (ε_{1r})	4-7	3.45	4.44	7.51

Table 4.1 Permittivity of Common Building Materials

From Figs. 4.2 and 4.3, assuming the front of buildings is reasonably smooth, we have

$$\begin{aligned} \zeta_r &= \zeta_i \\ E_r &= \Gamma E_i \end{aligned} \tag{4.5}$$

where $\Gamma = \Gamma_{\parallel}$ when E_r and E_i are parallel to the plane of incidence, and $\Gamma = \Gamma_{\perp}$ when E_r and E_i are perpendicular to the plane of incidence as illustrated in Figs. 4.1 and 4.2 respectively, and are defined as [26]

$$\Gamma_{\parallel} = \frac{-\varepsilon_r \sin\zeta_i + \sqrt{\varepsilon_r - \cos^2\zeta_i}}{\varepsilon_r \sin\zeta_i + \sqrt{\varepsilon_r - \cos^2\zeta_i}} \tag{4.6}$$

and

$$\Gamma_{\perp} = \frac{\sin\zeta_i - \sqrt{\varepsilon_r - \cos^2\zeta_i}}{\sin\zeta_i + \sqrt{\varepsilon_r - \cos^2\zeta_i}}. \tag{4.7}$$

In addition to strictly horizontal or vertical propagation, Fig. 4.4 shows the case when a signal from an interfering user in building group F is reflected off building group D at an angle to Array 1. It shows that the normal and parallel axes of the propagating wave do not coincide with the horizontal and vertical spatial axes, and that the vertically polarized wave received by the array has components both normal and parallel to the plane of incidence. As such, both reflection coefficients of Eqs. 4.6 and 4.7 must be taken into account and superposition is applied to determine the amplitude of the reflected waves. For this, we need to determine the vector of the incident electric field, and decompose it into components that are perpendicular and parallel to the plane of incidence. For a vertically oriented antenna, the electric field unit vector in the far field is [26]

$$\hat{E}(\theta) = \hat{\theta} \tag{4.8}$$

where $\hat{}$ denotes the unit vector and θ is the vertical angle in Fig. 4.4. Illustrated in Fig. 4.5, the direction of the incident electric field vector, E_i, is therefore perpendicular to the direction of propagation, where $E_{\perp}$ and $E_{\parallel}$ are the components that are perpendicular and parallel to the plane of incidence.

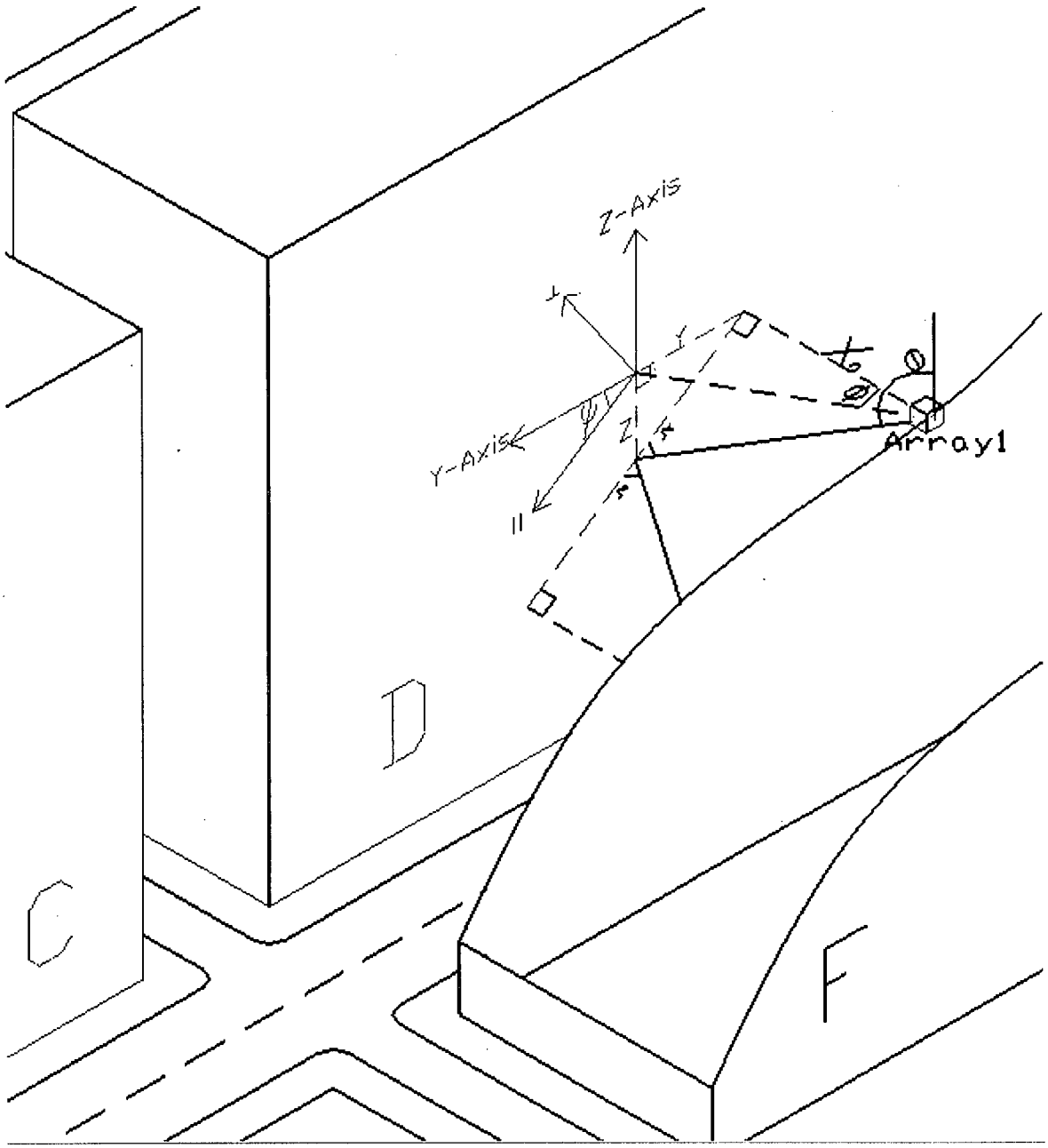

Fig. 4.4 3-D Reflection

Suppose $Z' = 1 + |Z|$, we can relate the electric field components geometrically in Fig. 4.5, and the incident electric field have intensity of

$$E_i = Z' \sin(\alpha) \tag{4.9}$$

where

$$\begin{aligned} Z &= \frac{c(\phi, X_0)}{\tan(\alpha)} \\ \alpha &= \pi - \theta. \end{aligned} \tag{4.10}$$

The electric field components that incident on the building's wall are therefore

$$\begin{aligned} E_\perp &= Z' \sin(\nu) \\ E_\parallel &= \sqrt{E_i^{\,2} - E_\perp^{\,2}} \end{aligned} \tag{4.11}$$

where

$$\begin{aligned} \nu &= \frac{\pi}{2} - \psi \\ \psi &= \tan^{-1}\left(\frac{Z}{Y}\right) \\ Y &= X_0 \tan(\phi) \end{aligned} \tag{4.12}$$

and the reflected electric field intensities can be obtained using Eqs. 4.5 – 4.7 where the incident angle is

$$\zeta = \tan^{-1}\left(\frac{X_0}{\sqrt{Y^2 + Z^2}}\right). \tag{4.13}$$

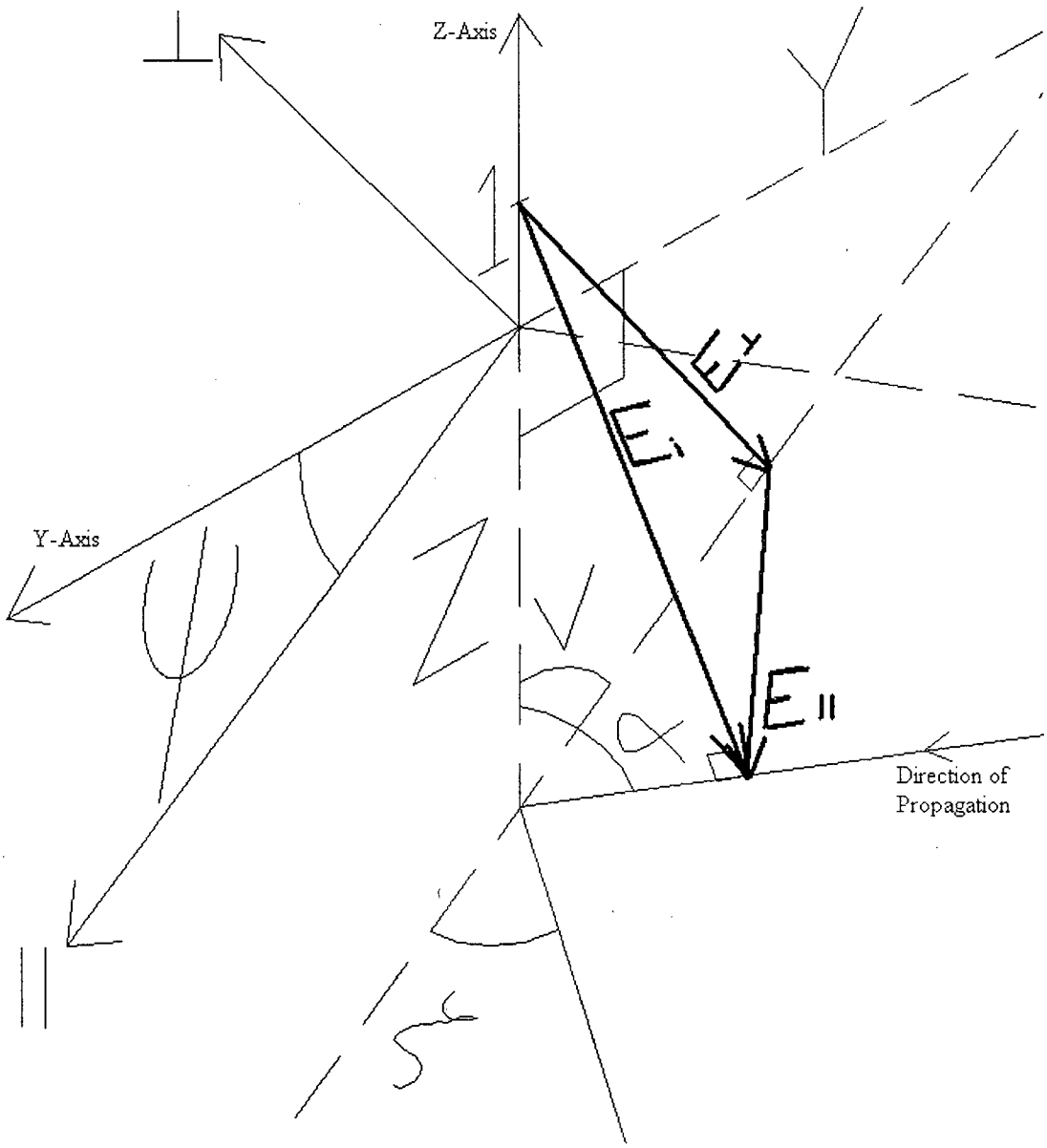

Fig. 4.5 Electric Field Components

The electric field amplitude loss associated with a reflection is

$$L_{reflection} = \left[\frac{E_i}{E_r}\right] = \left[\frac{E_i}{\sqrt{(\Gamma_\perp E_\perp)^2 + (\Gamma_\parallel E_\parallel)^2}}\right] \tag{4.14}$$

and allow us to find the power of an interfering signal after a reflection in our model.

4.3.2 Diffraction Loss

Diffraction occurs whenever a radio wave impinges upon a discontinuous surface such as a building corner, and provides coverage to shadowed regions where there is no LOS to the base station array. Unlike the macro cell scenario, where the base station antenna is raised many times higher than surrounding buildings and diffraction over roof tops is common, diffraction in a micro cell environment is primarily limited to building corners to provide coverage to perpendicular cross streets [28]. Niu and Bertoni [28] have performed a series of measurements in Manhattan and concluded that in an urban area with rectangular street grid and high rise buildings, diffraction accounts for 15 to 20 dB of power loss. Measurements in Stockholm [36] and Tampa [37] indicated that loss is in the range of 20 – 25 dB and concluded that 20 dB of loss is seen around a corner. Fig. 4.6 illustrates the shadowed regions in our urban model where interference to Array 1 is by means of diffraction. The value of 20 dB will be used as diffraction loss in our model.

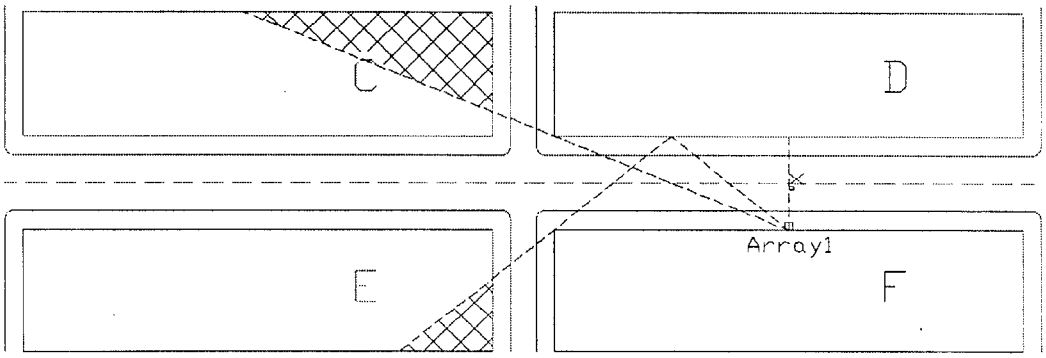

Fig. 4.6 Shadowed Regions

4.3.3 Distance Path Loss

In [1] and [39], the use of a free space propagation path loss model was suggested between an external antenna and a user located within a building, without the use of an outdoor reference value. Regression analysis was also performed in [1] to compute various building parameters that best fits measurements made inside buildings and the following was suggested as a suitable path loss model

$$PL(\text{dB}) = 32.44 + 20\log d + 20\log f + \beta_f \qquad (4.15)$$

where d, f, and β_f are the distance between the user and the serving base station array, frequency of signal, and free space clutter factor with a mean value of 18.3 dB, respectively. Eq. 4.15 will therefore be used to model propagation loss in our model.

4.3.4 Building Penetration Loss

Since our intended users are located in buildings, served by an external antenna array, the power loss associated with signals propagating through the external walls of a building must be taken into account. In [38], a series of measurements at 900 MHz, 1800 MHz,

and 2300 MHz were conducted and the average penetration loss was concluded to be 17 dB. Because all mobiles are subjected to a similar penetration loss of 17 dB, we can assume that the power control is able to compensate for this loss. Further, since measurements were made directly inside buildings in [1] of signal from an external transmitter, and β_f in Eq. 4.15 is very close to the average penetration loss reported in [38], it is assumed that β_f is representative of the building penetration loss.

4.3.5 Element Factor

From Eq. 2.28, it can be observed that the elemental factor need not be considered because perfect power control is assumed to be able to compensate for this in a single cell system. However, in a multi cell system, each base station has no power control ability on adjacent cells, and interfering signals from adjacent cell users arrive at different AOAs to both the adjacent and in cell antenna arrays as illustrated in Fig. 4.10. If panel antenna elements are used, for an interfering user in building group F, served by Array 2, we let (ϕ_F, θ_F) and (ϕ, θ) be the AOAs for the interfering user's signal to Array 2 and 1. The required power to be transmitted by the user due to the element factor is

$$P_{t\_element} = \frac{P_c}{\left|f_{PA}(\phi_F, \theta_F)\right|^2} \tag{4.16}$$

and the power received by Array 1 due solely from the effects of element factor is

$$\begin{aligned} P_{r\_element} &= P_{t\_element}\left|f_{PA}(\phi,\theta)\right|^2 \\ &= P_c\left|\frac{f_{PA}(\phi,\theta)}{f_{PA}(\phi_F,\theta_F)}\right|^2 \\ &= P_c G_{element} \end{aligned} \tag{4.17}$$

where $G_{element}$ will be used as the element factor gain in our model.

4.4 Single Bounce Models

In the past, single bounce models have been used to study the effects of AOA in cellular systems. In our system model, the height of the building groups limit propagation from other buildings on parallel streets, but serves to contain interferences from buildings that are facing the same street by reflection. As indicated by previous studies [32], [40]-[43], the street where the antenna faces acts as a channel providing a wave guiding effect. Typically in the past, unless specific site layout is used, geometrically based single bounce models were used to study propagation and AOA of signals in an urban environment. For example, the Geometrically Based Single Bounce Circular Model (GBCM), shown in Fig. 4.7, was originally proposed for use in the analysis of a macro cellular scenario where scatterers are assumed to lie within a pre-determined radius about a mobile terminal [3]. This is because the model assumes that the base station antenna is relatively high, compared to its surroundings. The multi-path generated by this model requires the generation of the location of scatterers based on a distribution model within the circular region, and that the individual signal paths are subjected to a single reflection off each scatterer reaching the base station antenna. The determination of the radius used in the model, however, requires the use of measured results [3].

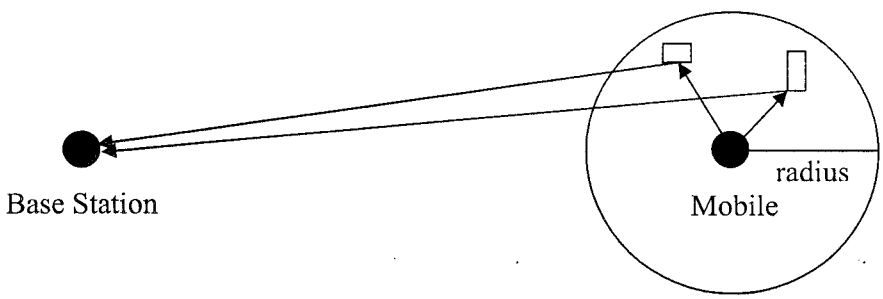

Fig. 4.7 GBCM Model

Another popular model applied for smaller micro cellular service, or street level service, is the Geometrically Based Single Bounce Elliptical Model (GBEM). Instead of assuming that scatterers are surrounding only the mobile, the GBEM model, shown in Fig. 4.8, is applicable to situations where the base station antenna height is relatively low to the ground and is surrounded by nearby objects [25]. It is assumed in this model that scatterers are distributed within an ellipse, where the base station and the mobile are located at the foci. As such, back propagation is allowed to reflect off objects behind the base station antenna.

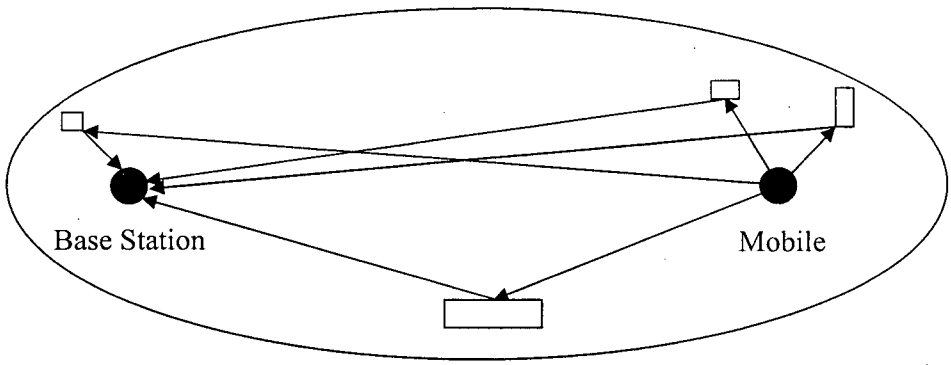

Fig. 4.8 GBEM Model

4.5 Modified 3-Dimensional Single Bounce Model

Geometrically based models have been popular aids in determining the statistics of multi-path AOAs in previous studies. They are in particular useful for analyzing the performance of smart antennas beam steering or nulling algorithms, subjected to changes in the channel, often encountered as a result to motion of both the mobile terminals and scatterers. However, indoor environments are quasi-static [35], and such models are

based on idealistic assumptions of real propagation channels, and the shape and size of the scatterer's distribution require the use of field measurements. The validation for these models is therefore subjected to debate [3]. For example, the circular shape for GBCM was originally intended by Jakes and Lee to only analyse correlation between two antenna elements, and to determine effects of beamforming on Doppler spectrum for narrowband signals [3]. Further, GBEM is only applicable to non-sectorized antenna elements or arrays due to the backward propagating rays on the base station antenna, as shown in Fig. 4.8, and assumes that it is relatively close to the ground. Also, even though reflections do occur inside buildings, this can be neglected because mobile users only transmit enough power for the shortest and most direct path, and any wave undergoing a reflection inside the building, then penetrating through the building's wall, will not have sufficient strength to meet the minimum SINR requirements for de-spreading in the base station receiver. In addition, our proposed antenna location is mounted at half the height of the building that it serves. The height is therefore many times than that of a lamppost, where previous micro cell studies have assumed to be the antenna's location. As such, reflections by buildings are more dominant than scatterers on the ground. We propose a modified single bounce model to be incorporated into our multiple cell interference analysis that takes into account of building locations and geometries as introduced in Chapter 3. Following the model shown in Fig. 4.1, and assuming desired users are in building group D, the model considers interference from other users in building groups D, F, C, and E in Sections 4.5.1, 4.5.2, 4.5.3, 4.5.4, and building groups I and J in Sections 4.5.5 and 4.5.6, respectively.

4.5.1 Interference from Building Group D

The mean intra-cell interference from within building group D can be calculated similar to the method used in Eq. 2.31, by substituting the received power and the user PDF from Eqs. 2.28 and 3.10, respectively, into Eq. 4.3 for $I_D(\phi_0,\theta_0)$. The mean interference therefore is

$$\begin{aligned} I_D(\phi_0,\theta_0) &= E\left[\sum_{i=1}^{K-1} P_{r_i}^D\right] \\ &= E\left[\sum_{i=1}^{K-1}\left|f_{\phi_0,\theta_0}(\phi,\theta)\right|^2 P_i^D\right] \\ &= E\left[\sum_{i=1}^{K-1}\left|f_{PA}(\phi,\theta)f'_{\phi_0,\theta_0}(\phi,\theta)\right|^2 \frac{P_c}{\left|f_{PA}(\phi,\theta)\right|^2 M^2}\right] \\ &= P_c(K-1)E\left[F'_{\phi_0,\theta_0}(\phi,\theta)\right] \\ &= P_c(K-1)\int_{X_0}^{X_0+S}\int_{-\phi_{\max 1}(x)}^{\phi_{\max 1}(x)}\int_{\theta_{\max}[c(\phi,X_0)]}^{\pi-\theta_{\max}[c(\phi,X_0)]} u_{building}(x,\phi,\theta)F'_{\phi_0,\theta_0}(\phi,\theta)\,d\theta\,d\phi\,dx \\ &= P_c(K-1)I'_D(\phi_0,\theta_0) \end{aligned} \tag{4.18}$$

where, given the urban model, some of the functions defined in Section 3.3 are reproduced here for the readers' convenience

$$\begin{aligned} c(\phi,x) &= \frac{x}{\cos(\phi)} \\ \phi_{\max 1}(x) &= \tan^{-1}\left(\frac{W_{building}}{2x}\right) \\ \theta_{\max}(p) &= \frac{\pi}{2} - \tan^{-1}\left(\frac{h}{2p}\right). \end{aligned} \tag{4.19}$$

4.5.2 Interference from Building Group F

In addition to signals from the intended users, the antenna array is also subjected to interference from reflection off the building that it serves. As shown in Figs. 4.1 and 4.4,

users from building group D are served by Array 1 mounted in the middle of building group F. Also shown is that building group D acts as a reflector, and interference from users in building group F can be traced from the array in the specific azimuth and vertical angles by reflecting off building group D in the manner shown. In addition, due to the reflection, extra distance is travelled prior to reaching the array, causing an increase in coverage per degree beamwidth, as illustrated in Fig. 4.9.

Because the interferers are in different building groups, served by different arrays, the power controls for the two building groups are also independent from each other and must be taken into account. Referring to Fig. 4.10, Array 1 serves building group D, and Array 2 serves building group F, the effect of power control can be modelled by comparing the total power loss between an interferer and Array 1, with the total power loss between the same interferer and Array 2.

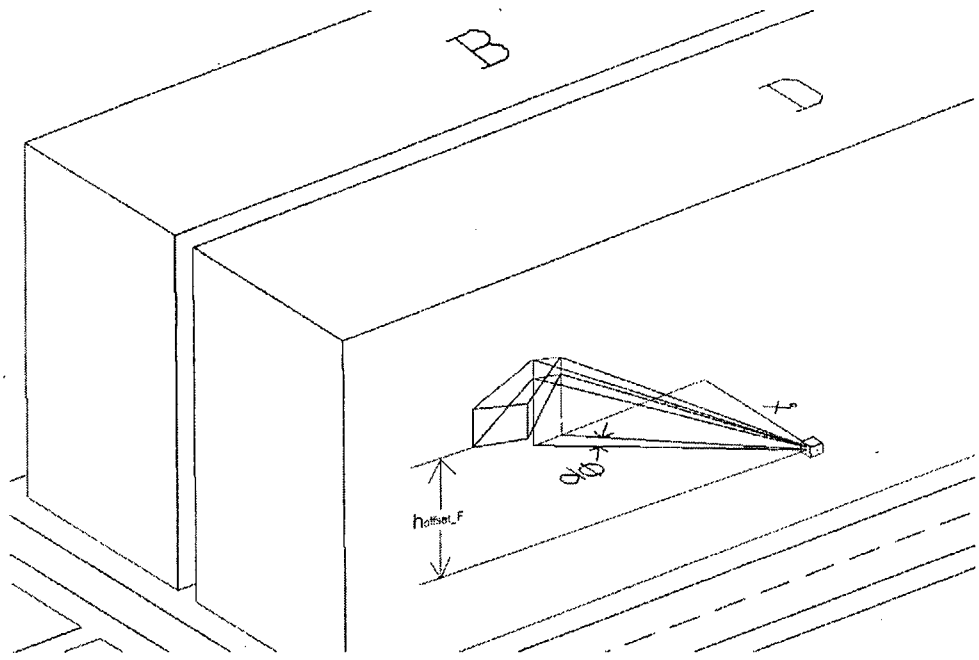

Fig. 4.9 Beam Spot Increase Due to Reflection

In Fig. 4.9, the location of the intra cell interferer is on a floor

$$h_{offset\_F} = \frac{c(\phi, 2X_0)}{\tan(\theta)} \tag{4.20}$$

from where Array 1 is. The vertical angle of arrival from this floor to Array 2 is then

$$\theta_F = \frac{\pi}{2} - \tan^{-1}\left(\frac{h_{offset\_F}}{c(\phi_F, X_0)}\right). \tag{4.21}$$

Referring to Eq. 4.17, the effective gain from the element factor is

$$G^F_{element} = \left|\frac{f_{PA}(\phi,\theta)}{f_{PA}(\phi_F,\theta_F)}\right|^2 \tag{4.22}$$

where the superscript F here signifies gain from the elemental factor is for interferers in building group F.

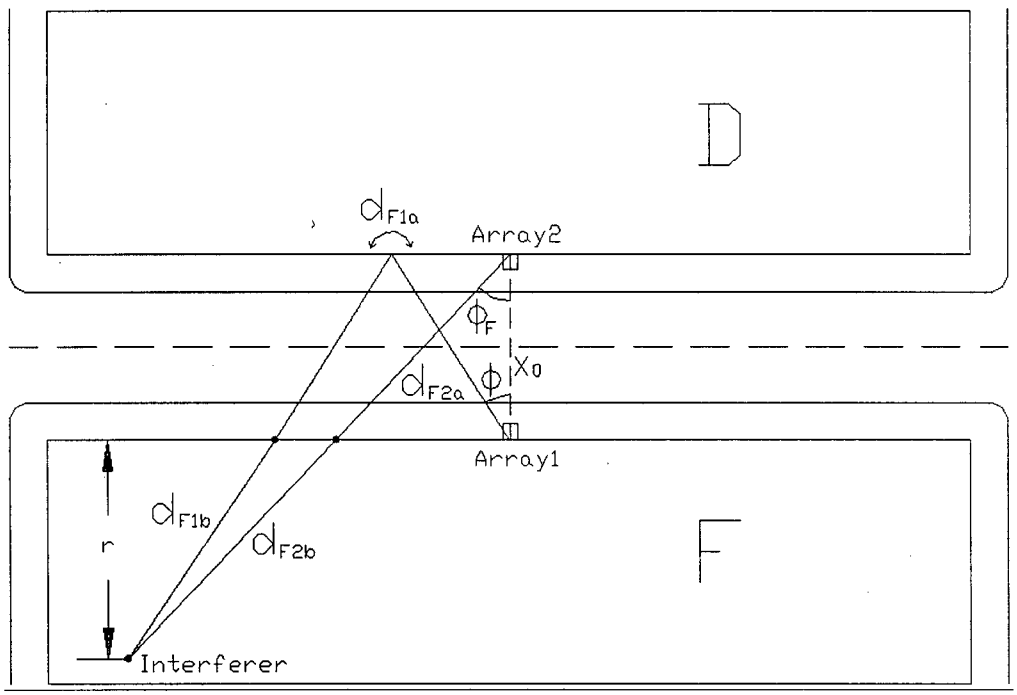

Fig. 4.10 Distance Ratio for Building Groups D and F

The loss due to distance can be broken down into two components

$$\begin{aligned} d_{F1} &= d_{F1a} + d_{F1b} \\ d_{F2} &= d_{F2a} + d_{F2b} \end{aligned} \tag{4.23}$$

where subscript a refers to the distance between the base station array and the exterior wall of building group F, and subscript b refers to the distance between the interferer and the building wall. Because the building is partitioned into different floors, we assume that signals propagate horizontally for the paths d_{F1b} and d_{F2b}. Referring to Fig. 4.10, d_{F1a}, which is the 3-dimensional path as shown on Fig. 4.9, can be expressed as

$$\begin{aligned} d_{F1a} &= \frac{c(\phi, 2X_0)}{\sin(\theta)} \\ d_{F1b} &= c(\phi, x) - c(\phi, 2X_0) \end{aligned} \tag{4.24}$$

and

$$\begin{aligned} d_{F2a} &= \sqrt{c(\phi_F, X_0)^2 + h_{offset\_F}{}^2} \\ d_{F2b} &= c[\phi_F, x - X_0] - c[\phi_F, X_0] \end{aligned} \tag{4.25}$$

where

$$\begin{aligned} \phi_F &= \tan^{-1}\left(\frac{x\tan\phi}{x - X_0}\right) \\ r &= x - 2X_0. \end{aligned} \tag{4.26}$$

Adopting Eq. 4.15 and including the array factor of Array 2, if the power received by Array 2 will be P_c, the transmitted power by the interferer in dB is

$$P_t^F(dB) = 10\log P_c - 20\log\left|f_{\phi_F,\theta_F}(\phi_F, \theta_F)\right| + 32.44 + 20\log d_{F2} + 20\log f + \beta_f \tag{4.27}$$

and the power received in dB by Array 1, after reflecting off building group D is

$$\begin{aligned} P_{r_i}^F(dB) &= 10\log P_t^F - 32.44 - 20\log d_{F1} - 20\log f - \beta_f \\ &\quad - 20\log L_{reflection} + 20\log\left|f_{\phi_0,\theta_0}(\phi,\theta)\right| \\ &= 10\log P_c + 20\log d_{F2} - 20\log d_{F1} - 20\log L_{reflection} + 20\log\left|f_{\phi_0,\theta_0}(\phi,\theta)\right| \\ &\quad - 20\log\left|f_{\phi_F,\theta_F}(\phi_F,\theta_F)\right| \end{aligned} \tag{4.28}$$

where $L_{reflection}$ is as given in Eq. 4.14.

Rewriting the above equation, we have

$$\begin{aligned} P_{r_i}^F &= \frac{P_c {d_{F2}}^2}{{d_{F1}}^2 {L_{reflection}}^2}\left|\frac{f_{\phi_0,\theta_0}(\phi,\theta)}{f_{\phi_F,\theta_F}(\phi_F,\theta_F)}\right|^2 \\ &= \frac{P_c {d_{F2}}^2}{{d_{F1}}^2 {L_{reflection}}^2}\left|\frac{f_{PA}(\phi,\theta) f'_{\phi_0,\theta_0}(\phi,\theta)}{f_{PA}(\phi_F,\theta_F) M}\right|^2 \\ &= \frac{P_c {d_{F2}}^2}{{d_{F1}}^2 {L_{reflection}}^2}\left|\frac{f_{PA}(\phi,\theta)}{f_{PA}(\phi_F,\theta_F)}\right|^2 F'_{\phi_0,\theta_0}(\phi,\theta) \\ &= \frac{P_c {d_{F2}}^2}{{d_{F1}}^2 {L_{reflection}}^2} G^F_{element} F'_{\phi_0,\theta_0}(\phi,\theta) \\ &= P_c G^F_{ch}(\phi_0,\theta_0,\phi,\theta) \end{aligned} \tag{4.29}$$

where

$$G^F_{ch}(\phi_0,\theta_0,\phi,\theta) = \frac{{d_{F2}}^2}{{d_{F1}}^2 {L_{reflection}}^2} G^F_{element} F'_{\phi_0,\theta_0}(\phi,\theta) \tag{4.30}$$

denotes the effective gain of an interferer's signal originated from within building group F, subjected to the various losses in the channel and the specific locations of the interferer and the base station arrays.

From Eq. 4.3, interference from building group F can then be expressed as

$$
\begin{aligned}
I_F(\phi_0,\theta_0) &= E\left[\sum_{i=0}^{K-1} P_{r_i}^F\right] \\
&= E\left[\sum_{i=0}^{K-1} P_c G_{ch}^F(\phi_0,\theta_0,\phi,\theta)\right] \\
&= P_c K E\left[G_{ch}^F(\phi_0,\theta_0,\phi,\theta)\right] \\
&= P_c K \int_{2X_0}^{2X_0+S} \int_{-\phi_{\max 1}(x)}^{\phi_{\max 1}(x)} \int_{\theta_{\max}[c(\phi,2X_0)]}^{\pi-\theta_{\max}[c(\phi,2X_0)]} G_{ch}^F(\phi_0,\theta_0,\phi,\theta) u_{building}^F(x,\phi,\theta)\, d\theta\, d\phi\, dx \\
&= P_c K I'_F(\phi_0,\theta_0) \\
&= P_c\left[(K-1)I'_F(\phi_0,\theta_0) + I'_F(\phi_0,\theta_0)\right]
\end{aligned}
\tag{4.31}
$$

where

$$
u_{building}^F(x,\phi,\theta) = \frac{c(\phi,2X_0)\left[1+\tan^2\left(\frac{\pi}{2}-\theta\right)\right]x\left[1+\tan^2(\phi)\right]}{SW_{building}h}. \tag{4.32}
$$

4.5.3 Interference from Building Group C

As shown in Fig 4.6, direct LOS and diffraction are the propagation mechanisms for interferers originated from within building group C. Coverage per degree angle is also increased due to the increased distance to building group C. Also, Fig. 4.11 shows that building group C can be divided into three zones. Zone C1 is bounded by $\phi_{max13}(X_0)$ and $\phi_{max3}(X_0)$, Zone C2 is bounded by $\phi_{max1}(X_0)$ and $\phi_{max13}(X_0)$, and Zone C3 is bounded by $\phi_{max13}(X_0+S)$ and $\phi_{max1}(X_0)$.

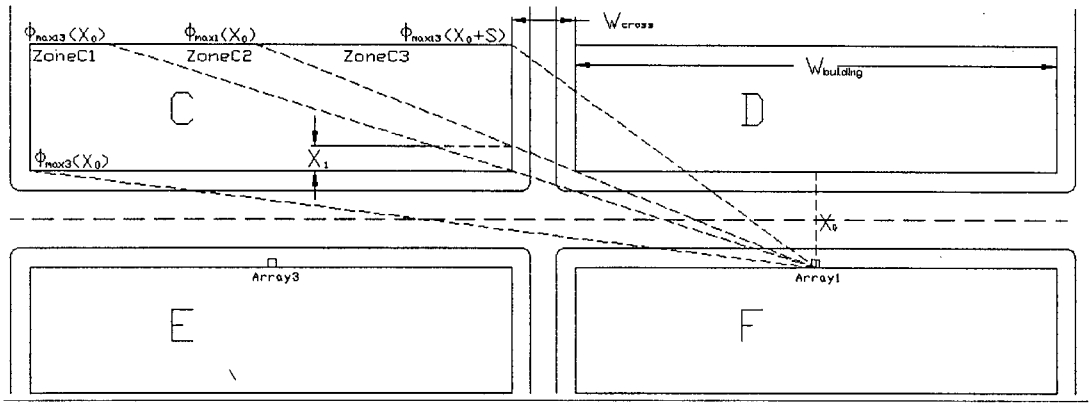

Fig. 4.11 Building Group C Interference Zones

Interference from Zone C1 propagates to Array 1 through the front wall, whereas interference from Zone C2 and C3 propagates through the side wall, with interference from Zone C3 diffracting around the corner of building group D. To model the effects of power control, Fig. 4.12 shows the distances from interferers in the three zones to Array 1 and 3. The effect of power control is modelled similar to the technique used in Section 4.5.2, as

$$\begin{aligned} d_{C11} &= d_{C11a} + d_{C11b} \\ d_{C13} &= d_{C13a} + d_{C13b} \\ d_{C21} &= d_{C21a} + d_{C21b} \\ d_{C23} &= d_{C23a} + d_{C23b} \\ d_{C31} &= d_{C31a} + d_{C31b} + d_{C31c} \\ d_{C33} &= d_{C33a} + d_{C33b} \end{aligned} \tag{4.33}$$

where the first two subscripts distinguishes the origin of the interferers, the third subscript denotes the antenna array, and the alphabet subscript indicates whether the ray is external or internal to the building. For example, d_{C13a}, d_{C23a}, and d_{C33a} represents the distances from Array 3 to the exterior wall of building group C for interferers in Zones C1, C2, and C3, respectively.

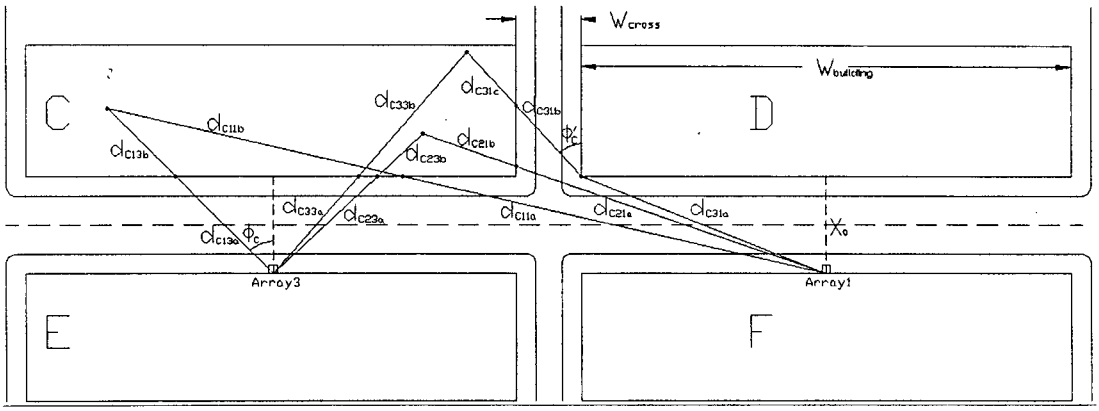

Fig. 4.12 Distance Ratio for Building Groups C and F

From Fig. 4.12, the distance components for Zone C1 can be expressed as

$$\begin{aligned} d_{C11a} &= \frac{c(\phi, X_0)}{\sin(\theta)} \\ d_{C11b} &= c(\phi, x) - c(\phi, X_0) \end{aligned} \tag{4.34}$$

$$\begin{aligned} d_{C13a} &= \sqrt{c(\phi_C, X_0)^2 + h_{offset\_C1}{}^2} \\ d_{C13b} &= c(\phi_C, x) - c(\phi_C, X_0) \end{aligned} \tag{4.35}$$

where

$$\begin{aligned} h_{offset\_C1} &= \frac{c(\phi, X_0)}{\tan(\theta)} \\ \phi_C &= \tan^{-1}\left(\frac{x\tan\phi - W_{building} - W_{cross}}{x}\right) \end{aligned} \tag{4.36}$$

and the vertical angle of arrival to Array 3 is

$$\theta_{C1} = \frac{\pi}{2} - \tan^{-1}\left(\frac{h_{offset\_C1}}{c(\phi_C, X_0)}\right). \tag{4.37}$$

The distance components for Zone C2 are

$$d_{C21a} = \frac{c(\phi,\alpha)}{\sin(\theta)}$$
$$d_{C21b} = c(\phi,x) - c(\phi,\alpha) \tag{4.38}$$

$$d_{C23a} = \sqrt{c(\phi_C, X_0)^2 + h_{offset\_C2}{}^2}$$
$$d_{C23b} = d_{C13b} \tag{4.39}$$

where

$$h_{offset\_C2} = \frac{c(\phi,\alpha)}{\tan(\theta)}$$
$$\alpha = \frac{\frac{W_{building}}{2} + W_{cross}}{\tan(\phi)} \tag{4.40}$$

and the vertical angle of arrival to Array 3 is

$$\theta_{C2} = \frac{\pi}{2} - \tan^{-1}\left(\frac{h_{offset\_C2}}{c(\phi_C, X_0)}\right). \tag{4.41}$$

The distance components for Zone C3 are

$$d_{C31a} = \frac{c[\phi_{\max 1}(X_0), X_0]}{\sin(\theta)}$$
$$d_{C31b} = \frac{W_{cross}}{\sin(\phi_C')\sin(\theta)} \tag{4.42}$$
$$d_{C31c} = c(\phi_C', x - X_0) - \frac{W_{cross}}{\sin(\phi_C')}$$

$$d_{C33a} = \sqrt{c(\phi_C, X_0)^2 + h_{offset\_C3}{}^2}$$
$$d_{C33b} = d_{C13b} \tag{4.43}$$

where

$$h_{offset\_C3} = (d_{C31a} + d_{C31b})\cos(\theta)$$
$$\phi_C^{'} = \tan^{-1}\frac{x\tan(\phi) - \frac{W_{building}}{2}}{x - X_0} \tag{4.44}$$

and the vertical angle of arrival to Array 3 is

$$\theta_{C3} = \frac{\pi}{2} - \tan^{-1}\left(\frac{h_{offset\_C3}}{c(\phi_C, X_0)}\right). \tag{4.45}$$

Adopting Eq. 4.15 and including the array factor of Array 3, if the power received by Array 3 will be P_c, the transmitted power in dB by interferers in Zone C1, C2, and C3 to Array 3 are

$$\begin{aligned}
P_t^{C1}(dB) &= 10\log P_c - 20\log\left|f_{\phi_C,\theta_{C1}}(\phi_C,\theta_{C1})\right| + 32.44 + 20\log d_{C13} + 20\log f + \beta_f \\
P_t^{C2}(dB) &= 10\log P_c - 20\log\left|f_{\phi_C,\theta_{C2}}(\phi_C,\theta_{C2})\right| + 32.44 + 20\log d_{C23} + 20\log f + \beta_f \\
P_t^{C3}(dB) &= 10\log P_c - 20\log\left|f_{\phi_C,\theta_{C3}}(\phi_C,\theta_{C3})\right| + 32.44 + 20\log d_{C33} + 20\log f + \beta_f
\end{aligned} \tag{4.46}$$

and the power received in dB by Array 1, for the three zones are

$$\begin{aligned}
P_{r_i}^{C1}(dB) &= 10\log P_t^{C1} - 32.44 - 20\log d_{C11} - 20\log f - \beta_f + 20\log\left|f_{\phi_0,\theta_0}(\phi,\theta)\right| \\
&= 10\log P_c + 20\log d_{C13} - 20\log d_{C11} + 20\log\left|f_{\phi_0,\theta_0}(\phi,\theta)\right| - 20\log\left|f_{\phi_C,\theta_{C1}}(\phi_C,\theta_{C1})\right| \\
P_{r_i}^{C2}(dB) &= 10\log P_t^{C2} - 32.44 - 20\log d_{C21} - 20\log f - \beta_f + 20\log\left|f_{\phi_0,\theta_0}(\phi,\theta)\right| \\
&= 10\log P_c + 20\log d_{C23} - 20\log d_{C21} + 20\log\left|f_{\phi_0,\theta_0}(\phi,\theta)\right| - 20\log\left|f_{\phi_C,\theta_{C2}}(\phi_C,\theta_{C2})\right| \\
P_{r_i}^{C3}(dB) &= 10\log P_t^{C3} - 32.44 - 20\log d_{C31} - 20\log f - \beta_f - 20\log L_{diffraction} + 20\log\left|f_{\phi_0,\theta_0}(\phi_{\max 1}(X_0),\theta)\right| \\
&= 10\log P_c + 20\log d_{C33} - 20\log d_{C31} - 20\log L_{diffraction} + 20\log\left|f_{\phi_0,\theta_0}(\phi_{\max 1}(X_0),\theta)\right| \\
&\quad - 20\log\left|f_{\phi_C,\theta_{C3}}(\phi_C,\theta_{C3})\right|.
\end{aligned} \tag{4.47}$$

Rewriting Eq. 4.47, we have

$$\begin{aligned} P_{r_i}^{C1} &= \frac{P_c d_{C13}^{\ 2}}{d_{C11}^{\ 2}} G_{element}^{C1} F'_{\phi_0,\theta_0}(\phi,\theta) \\ &= P_c G_{ch}^{C1}(\phi_0,\theta_0,\phi,\theta) \\ P_{r_i}^{C2} &= \frac{P_c d_{C23}^{\ 2}}{d_{C21}^{\ 2}} G_{element}^{C2} F'_{\phi_0,\theta_0}(\phi,\theta) \\ &= P_c G_{ch}^{C2}(\phi_0,\theta_0,\phi,\theta) \\ P_{r_i}^{C3} &= \frac{P_c d_{C33}^{\ 2}}{d_{C31}^{\ 2} L_{diffraction}^{\ 2}} G_{element}^{C3} F'_{\phi_0,\theta_0}(\phi_{\max 1}(X_0),\theta) \\ &= P_c G_{ch}^{C3}(\phi_0,\theta_0,\phi,\theta) \end{aligned} \tag{4.48}$$

where

$$\begin{aligned} G_{element}^{C1} &= \left| \frac{f_{PA}(\phi,\theta)}{f_{PA}(\phi_C,\theta_{C1})} \right|^2 \\ G_{element}^{C2} &= \left| \frac{f_{PA}(\phi,\theta)}{f_{PA}(\phi_C,\theta_{C2})} \right|^2 \\ G_{element}^{C3} &= \left| \frac{f_{PA}(\phi_{\max 1}(X_0),\theta)}{f_{PA}(\phi_C,\theta_{C3})} \right|^2 . \end{aligned} \tag{4.49}$$

The interference from building group C can then be expressed as

$$\begin{aligned} I_C(\phi_0,\theta_0) &= E\left[\sum_{i=0}^{K-1} P_{r_i}^{C1} + P_{r_i}^{C2} + P_{r_i}^{C3}\right] \\ &= P_c K \left\{ \int_{X_0}^{X_0+S} \int_{\phi_{\max 13}(X_0)}^{\phi_{\max 3}(x)} \int_{\theta_{\max}[c(\phi,X_0)]}^{\pi-\theta_{\max}[c(\phi,X_0)]} G_{ch}^{C1}(\phi_0,\theta_0,\phi,\theta) u_{building}^{C1}(x,\phi,\theta) d\theta d\phi dx \right. \\ &\quad + \int_{X_0}^{X_0+X_1} \int_{\phi_{\max 13}(X_0)}^{\phi_{\max 13}(x)} \int_{\theta_{\max}[c(\phi,\alpha)]}^{\pi-\theta_{\max}[c(\phi,\alpha)]} G_{ch}^{C2}(\phi_0,\theta_0,\phi,\theta) u_{building}^{C2}(x,\phi,\theta) d\theta d\phi dx \\ &\quad + \int_{X_0+X_1}^{X_0+S} \int_{\phi_{\max 13}(X_0)}^{\phi_{\max 13}(X_0)} \int_{\theta_{\max}[c(\phi,\alpha)]}^{\pi-\theta_{\max}[c(\phi,\alpha)]} G_{ch}^{C2}(\phi_0,\theta_0,\phi,\theta) u_{building}^{C2}(x,\phi,\theta) d\theta d\phi dx \\ &\quad \left. + \int_{X_0+X_1}^{X_0+S} \int_{\phi_{\max 13}(x)}^{\phi_{\max 1}(X_0)} \int_{\theta_{\max}[\eta_C]}^{\pi-\theta_{\max}[\eta_C]} G_{ch}^{C3}(\phi_0,\theta_0,\phi,\theta) u_{building}^{C3}(x,\phi,\theta) d\theta d\phi dx \right\} \\ &= P_c K I'_C(\phi_0,\theta_0) \\ &= P_c\left[(K-1) I'_C(\phi_0,\theta_0) + I'_C(\phi_0,\theta_0)\right] \end{aligned} \tag{4.50}$$

where

$$u_{building}^{C1}(x,\phi,\theta)=\frac{c(\phi,X_0)\left[1+\tan^2\left(\frac{\pi}{2}-\theta\right)\right]x\left[1+\tan^2(\phi)\right]}{SW_{building}h}$$

$$u_{building}^{C2}(x,\phi,\theta)=\frac{c(\phi,\alpha)\left[1+\tan^2\left(\frac{\pi}{2}-\theta\right)\right]x\left[1+\tan^2(\phi)\right]}{SW_{building}h}$$

$$u_{building}^{C3}(x,\phi,\theta)=\frac{\eta_C\left[1+\tan^2\left(\frac{\pi}{2}-\theta\right)\right]x\left[1+\tan^2(\phi)\right]}{SW_{building}h}$$

$$\eta_C=c\left[\phi_{\max 1}(X_0),X_0\right]+\frac{W_{cross}}{\sin\left(\phi_c'\right)}$$

$$\phi_{\max 13}(x)=\tan^{-1}\left(\frac{\frac{W_{building}}{2}+W_{cross}}{x}\right)$$

$$\phi_{\max 3}(x)=\tan^{-1}\left(\frac{1.5W_{building}+W_{cross}}{x}\right). \qquad (4.51)$$

4.5.4 Interference from Building Group E

From Fig. 4.6, we can see the modes of interference from building group E are reflection from building group D and C, and diffraction around a corner of building group F. Similar to the case for building group C, building group E can also be divided into four zones, as shown in Fig. 4.13, where Zone E1 is bounded by $\phi_{max13}(X_0)$ and $\phi_{max3}(2X_0)$, Zone E2 is bounded by $\phi_{max13}(2X_0)$ and $\phi_{max1}(X_0)$, Zone E3 is bounded by $\phi_{max1}(2X_0)$ and $\phi_{max13}(2X_0)$, and Zone E4 is bounded by $\phi_{max13}(2X_0+S)$ and $\phi_{max1}(2X_0)$.

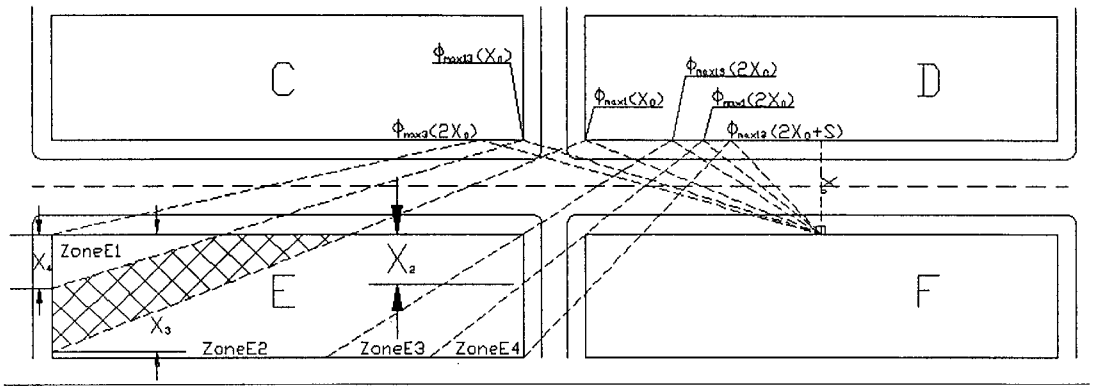

Fig. 4.13 Building Group E Interference Zones

Interference from Zone E1 and E2 exits through the front wall, and interference from Zone E3 and E4 exits through the side wall of building group E with interference from Zone E4 diffracting around a corner of building group F. Also shown is that part of the users in building group E do not contribute interference to Array 1. These users are located between Zones E1 and E2, and their interference are not reflected by building group C or D due to the cross street. To model the effects of power control, Fig. 4.14 shows the distances to the different zones.

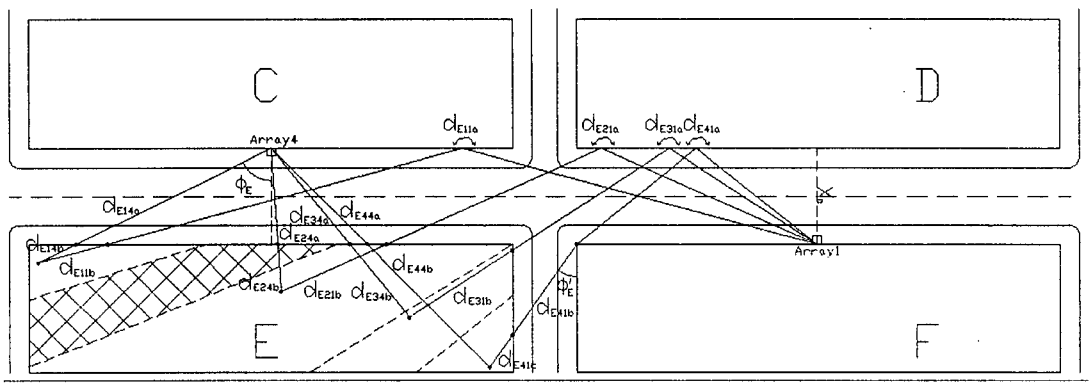

Fig. 4.14 Distance Ratio for Building Groups E and F

Subscripts are assigned similar to those used for building group C, and

$$\begin{aligned} d_{E11} &= d_{E11a} + d_{E11b} \\ d_{E14} &= d_{E14a} + d_{E14b} \\ d_{E21} &= d_{E21a} + d_{E21b} \\ d_{E24} &= d_{E24a} + d_{E24b} \\ d_{E31} &= d_{E31a} + d_{E31b} \\ d_{E34} &= d_{E34a} + d_{E34b} \\ d_{E41} &= d_{E41a} + d_{E41b} + d_{E41c} \\ d_{E44} &= d_{E44a} + d_{E44b}. \end{aligned} \tag{4.52}$$

In Fig. 4.14, the distance components for Zone E1 to Array 1 are

$$\begin{aligned} d_{E11a} &= \frac{c(\phi, 2X_0)}{\sin(\theta)} \\ d_{E11b} &= c(\phi, x) - c(\phi, 2X_0) \end{aligned} \tag{4.53}$$

and the distance components for Zone E1 to Array 4 are

$$\begin{aligned} d_{E14a} &= \sqrt{c(\phi_E, X_0)^2 + h_{offset\_E1}{}^2} \\ d_{E14b} &= c(\phi_E, x - X_0) - c(\phi_E, X_0) \end{aligned} \tag{4.54}$$

where

$$\begin{aligned} h_{offset\_E1} &= \frac{c(\phi, 2X_0)}{\tan(\theta)} \\ \phi_E &= \tan^{-1}\left(\frac{x \tan\phi - W_{building} - W_{cross}}{x - X_0} \right) \end{aligned} \tag{4.55}$$

and the vertical angle of arrival to Array 4 is

$$\theta_{E1} = \frac{\pi}{2} - \tan^{-1}\left[\frac{h_{offset\_E1}}{c(\phi_E, X_0)} \right]. \tag{4.56}$$

The distance components for Zone E2 are

$$\begin{aligned} d_{E21a} &= d_{E11a} \\ d_{E21b} &= d_{E11b} \end{aligned} \tag{4.57}$$

and

$$\begin{aligned} d_{E24a} &= d_{E14a} \\ d_{E24b} &= d_{E14b}. \end{aligned} \tag{4.58}$$

The distance components for Zone E3 to Array 1 are

$$\begin{aligned} d_{E31a} &= \frac{c(\phi,\alpha)}{\sin(\theta)} \\ d_{E31b} &= c(\phi,x) - c(\phi,\alpha) \end{aligned} \tag{4.59}$$

and the distance components for Zone E3 to Array 4 are

$$\begin{aligned} d_{E34a} &= \sqrt{c(\phi_E, X_0)^2 + h_{offset\_E3}{}^2} \\ d_{E34b} &= c(\phi_E, x - X_0) - c(\phi_E, X_0) \end{aligned} \tag{4.60}$$

where

$$h_{offset\_E3} = \frac{c(\phi,\alpha)}{\tan(\theta)} \tag{4.61}$$

and the vertical angle of arrival to Array 4 is

$$\theta_{E3} = \frac{\pi}{2} - \tan^{-1}\left[\frac{h_{offset\_E3}}{c(\phi_E, X_0)}\right]. \tag{4.62}$$

The distance components for Zone E4 are

$$\begin{aligned} d_{E41a} &= \frac{c[\phi_{\max 1}(2X_0), 2X_0]}{\sin(\theta)} \\ d_{E41b} &= \frac{W_{cross}}{\sin(\phi_E')\sin(\theta)} \\ d_{E41c} &= c(\phi_E', x - 2X_0) - \frac{W_{cross}}{\sin(\phi_E')} \end{aligned} \tag{4.63}$$

and

$$\begin{aligned} d_{E44a} &= \sqrt{c(\phi_E, X_0)^2 + h_{offset\_E4}^2} \\ d_{E44b} &= d_{E14b} \end{aligned} \tag{4.64}$$

where

$$\begin{aligned} h_{offset\_E4} &= (d_{E41a} + d_{E41b})\cos(\theta) \\ \phi_E' &= \tan^{-1}\frac{x\tan(\phi) - \frac{W_{building}}{2}}{x - 2X_0} \end{aligned} \tag{4.65}$$

and the vertical angle of arrival to Array 4 is

$$\theta_{E4} = \frac{\pi}{2} - \tan^{-1}\left[\frac{h_{offset\_E4}}{c(\phi_E, X_0)}\right]. \tag{4.66}$$

Adopting Eq. 4.15 and including the array factor of Array 4, if the power received by Array 4 will be P_c, the transmitted power by interferers in Zones E1, E2, E3, and E4 to Array 4 are

$$\begin{aligned} P_t^{E1}(dB) &= 10\log P_c - 20\log\left|f_{\phi_E,\theta_{E1}}(\phi_E, \theta_{E1})\right| + 32.44 + 20\log d_{E14} + 20\log f + \beta_f \\ P_t^{E2}(dB) &= 10\log P_c - 20\log\left|f_{\phi_E,\theta_{E2}}(\phi_E, \theta_{E2})\right| + 32.44 + 20\log d_{E24} + 20\log f + \beta_f \\ P_t^{E3}(dB) &= 10\log P_c - 20\log\left|f_{\phi_E,\theta_{E3}}(\phi_E, \theta_{E3})\right| + 32.44 + 20\log d_{E34} + 20\log f + \beta_f \\ P_t^{E4}(dB) &= 10\log P_c - 20\log\left|f_{\phi_E,\theta_{E4}}(\phi_E, \theta_{E4})\right| + 32.44 + 20\log d_{E44} + 20\log f + \beta_f \end{aligned} \tag{4.67}$$

and the power received by Array 1, for the four zones

$$
\begin{aligned}
P_{r_i}^{E1}(dB) &= 10\log P_t^{E1} - 32.44 - 20\log d_{E11} - 20\log f - \beta_f - 20\log L_{reflection} + 20\log\left|f_{\phi_0,\theta_0}(\phi,\theta)\right| \\
&= 10\log P_c + 20\log d_{E14} - 20\log d_{E11} - 20\log L_{reflection} + 20\log\left|\frac{f_{\phi_0,\theta_0}(\phi,\theta)}{f_{\phi_E,\theta_{E1}}(\phi_E,\theta_{E1})}\right| \\
P_{r_i}^{E2}(dB) &= 10\log P_t^{E2} - 32.44 - 20\log d_{E21} - 20\log f - \beta_f - 20\log L_{reflection} + 20\log\left|f_{\phi_0,\theta_0}(\phi,\theta)\right| \\
&= 10\log P_c + 20\log d_{E24} - 20\log d_{E21} - 20\log L_{reflection} + 20\log\left|\frac{f_{\phi_0,\theta_0}(\phi,\theta)}{f_{\phi_E,\theta_{E2}}(\phi_E,\theta_{E2})}\right| \\
P_{r_i}^{E3}(dB) &= 10\log P_t^{E3} - 32.44 - 20\log d_{E31} - 20\log f - \beta_f - 20\log L_{reflection} + 20\log\left|f_{\phi_0,\theta_0}(\phi,\theta)\right| \\
&= 10\log P_c + 20\log d_{E34} - 20\log d_{E31} - 20\log L_{reflection} + 20\log\left|\frac{f_{\phi_0,\theta_0}(\phi,\theta)}{f_{\phi_E,\theta_{E3}}(\phi_E,\theta_{E3})}\right| \\
P_{r_i}^{E4}(dB) &= 10\log P_t^{E4} - 32.44 - 20\log d_{E41} - 20\log f - \beta_f - 20\log L_{reflection} - 20\log L_{diffraction} \\
&\quad + 20\log\left|f_{\phi_0,\theta_0}(\phi_{\max 1}(2X_0),\theta)\right| \\
&= 10\log P_c + 20\log d_{E44} - 20\log d_{E41} - 20\log L_{reflection} - 20\log L_{diffraction} \\
&\quad + 20\log\left|\frac{f_{\phi_0,\theta_0}(\phi_{\max 1}(2X_0),\theta)}{f_{\phi_E,\theta_{E4}}(\phi_E,\theta_{E4})}\right|.
\end{aligned}
\tag{4.68}
$$

Rewriting Eq. 4.68, we have

$$
\begin{aligned}
P_{r_i}^{E1} &= \frac{P_c d_{E14}^{\,2}}{d_{E11}^{\,2} L_{reflection}^{\,2}} G_{element}^{E1} F'_{\phi_0,\theta_0}(\phi,\theta) \\
&= P_c G_{ch}^{E1}(\phi_0,\theta_0,\phi,\theta) \\
P_{r_i}^{E2} &= \frac{P_c d_{E24}^{\,2}}{d_{E21}^{\,2} L_{reflection}^{\,2}} G_{element}^{E2} F'_{\phi_0,\theta_0}(\phi,\theta) \\
&= P_c G_{ch}^{E2}(\phi_0,\theta_0,\phi,\theta), \\
P_{r_i}^{E3} &= \frac{P_c d_{E34}^{\,2}}{d_{E31}^{\,2} L_{reflection}^{\,2}} G_{element}^{E3} F'_{\phi_0,\theta_0}(\phi,\theta) \\
&= P_c G_{ch}^{E3}(\phi_0,\theta_0,\phi,\theta) \\
P_{r_i}^{E4} &= \frac{P_c d_{E44}^{\,2}}{d_{C41}^{\,2} L_{reflection}^{\,2} L_{diffraction}^{\,2}} G_{element}^{E4} F'_{\phi_0,\theta_0}(\phi_{\max 1}(2X_0),\theta) \\
&= P_c G_{ch}^{E4}(\phi_0,\theta_0,\phi,\theta)
\end{aligned}
\tag{4.69}
$$

where

$$
\begin{aligned}
G_{element}^{E1} &= \left| \frac{f_{PA}(\phi,\theta)}{f_{PA}(\phi_E,\theta_{E1})} \right|^2 \\
G_{element}^{E2} &= \left| \frac{f_{PA}(\phi,\theta)}{f_{PA}(\phi_E,\theta_{E2})} \right|^2 \\
G_{element}^{E3} &= \left| \frac{f_{PA}(\phi,\theta)}{f_{PA}(\phi_E,\theta_{E3})} \right|^2 \\
G_{element}^{E4} &= \left| \frac{f_{PA}(\phi_{\max 1}(2X_0),\theta)}{f_{PA}(\phi_E,\theta_{E4})} \right|^2 .
\end{aligned}
\tag{4.70}
$$

The interference from building group E can then be expressed as

$$
\begin{aligned}
I_E(\phi_0,\theta_0) &= E\left[\sum_{i=0}^{K-1} P_{r_i}^{E1} + P_{r_i}^{E2} + P_{r_i}^{E3} + P_{r_i}^{E4}\right] \\
&= P_c K \left\{ \int_{2X_0}^{2X_0+X_4} \int_{\phi_{\max 13}(X_0)}^{\phi_{\max 3}(x)} \int_{\theta_{\max}[c(\phi,2X_0)]}^{\pi-\theta_{\max}[c(\phi,2X_0)]} G_{ch}^{E1}(\phi_0,\theta_0,\phi,\theta) u_{building}^{E1}(x,\phi,\theta) d\theta d\phi dx \right. \\
&\quad + \int_{2X_0}^{2X_0+X_3} \int_{\phi_{\max 13}(2X_0)}^{\phi_{\max 1}(X_0)} \int_{\theta_{\max}[c(\phi,2X_0)]}^{\pi-\theta_{\max}[c(\phi,2X_0)]} G_{ch}^{E2}(\phi_0,\theta_0,\phi,\theta) u_{building}^{E2}(x,\phi,\theta) d\theta d\phi dx \\
&\quad + \int_{2X_0+X_3}^{2X_0+S} \int_{\phi_{\max 13}(2X_0)}^{\phi_{\max 3}(x)} \int_{\theta_{\max}[c(\phi,2X_0)]}^{\pi-\theta_{\max}[c(\phi,2X_0)]} G_{ch}^{E2}(\phi_0,\theta_0,\phi,\theta) u_{building}^{E2}(x,\phi,\theta) d\theta d\phi dx \\
&\quad + \int_{2X_0}^{2X_0+X_2} \int_{\phi_{\max 13}(x)}^{\phi_{\max 13}(2X_0)} \int_{\theta_{\max}[c(\phi,\alpha)]}^{\pi-\theta_{\max}[c(\phi,\alpha)]} G_{ch}^{E3}(\phi_0,\theta_0,\phi,\theta) u_{building}^{E3}(x,\phi,\theta) d\theta d\phi dx \\
&\quad + \int_{2X_0+X_2}^{2X_0+S} \int_{\phi_{\max 1}(2X_0)}^{\phi_{\max 13}(2X_0)} \int_{\theta_{\max}[c(\phi,\alpha)]}^{\pi-\theta_{\max}[c(\phi,\alpha)]} G_{ch}^{E3}(\phi_0,\theta_0,\phi,\theta) u_{building}^{E3}(x,\phi,\theta) d\theta d\phi dx \\
&\quad \left. + \int_{2X_0+X_2}^{2X_0+S} \int_{\phi_{\max 13}(x)}^{\phi_{\max 1}(2X_0)} \int_{\theta_{\max}[\eta_E]}^{\pi-\theta_{\max}[\eta_E]} G_{ch}^{E4}(\phi_0,\theta_0,\phi,\theta) u_{building}^{E4}(x,\phi,\theta) d\theta d\phi dx \right\} \\
&= P_c K I'_E(\phi_0,\theta_0) \\
&= P_c \left[(K-1) I'_E(\phi_0,\theta_0) + I'_E(\phi_0,\theta_0) \right]
\end{aligned}
\tag{4.71}
$$

where

$$
\begin{aligned}
u_{building}^{E1}(x,\phi,\theta) &= \frac{c(\phi,2X_0)\left[1+\tan^2\left(\frac{\pi}{2}-\theta\right)\right]x\left[1+\tan^2(\phi)\right]}{SW_{building}h} \\
u_{building}^{E2}(x,\phi,\theta) &= u_{building}^{E1}(x,\phi,\theta) \\
u_{building}^{E3}(x,\phi,\theta) &= \frac{c(\phi,\alpha)\left[1+\tan^2\left(\frac{\pi}{2}-\theta\right)\right]x\left[1+\tan^2(\phi)\right]}{SW_{building}h} \\
u_{building}^{E4}(x,\phi,\theta) &= \frac{\eta_E\left[1+\tan^2\left(\frac{\pi}{2}-\theta\right)\right]x\left[1+\tan^2(\phi)\right]}{SW_{building}h} \\
\eta_E &= c\left[\phi_{\max 1}(2X_0),2X_0\right]+\frac{W_{cross}}{\sin\left(\phi_E'\right)}.
\end{aligned}
\tag{4.72}
$$

4.5.5 Total Interference and Capacity

As illustrated in Fig. 4.1, in addition to interference from building groups C and E in the city block on the left side of building group F, just as much interference comes from the city block on the right side. Because of the symmetrical nature, this can be modelled by applying only a negative sign in the azimuth angle of the array factor in the integrands of Eqs. 4.50 and 4.71. Let building groups I and J be on the right city block, the additional interference are

$$
\begin{aligned}
I_I(\phi_0,\theta_0) = P_c K \Bigg\{ & \int_{X_0}^{X_0+S} \int_{\phi_{\max 13}(X_0)}^{\phi_{\max 3}(x)} \int_{\theta_{\max}[c(\phi,X_0)]}^{\pi-\theta_{\max}[c(\phi,X_0)]} G_{ch}^{C1}(\phi_0,\theta_0,-\phi,\theta) u_{building}^{C1}(x,\phi,\theta) d\theta d\phi dx \\
& + \int_{X_0}^{X_0+X_1} \int_{\phi_{\max 13}(x)}^{\phi_{\max 13}(X_0)} \int_{\theta_{\max}[c(\phi,\alpha)]}^{\pi-\theta_{\max}[c(\phi,\alpha)]} G_{ch}^{C2}(\phi_0,\theta_0,-\phi,\theta) u_{building}^{C2}(x,\phi,\theta) d\theta d\phi dx \\
& + \int_{X_0+X_1}^{X_0+S} \int_{\phi_{\max 1}(X_0)}^{\phi_{\max 13}(X_0)} \int_{\theta_{\max}[c(\phi,\alpha)]}^{\pi-\theta_{\max}[c(\phi,\alpha)]} G_{ch}^{C2}(\phi_0,\theta_0,-\phi,\theta) u_{building}^{C2}(x,\phi,\theta) d\theta d\phi dx \\
& + \int_{X_0+X_1}^{X_0+S} \int_{\phi_{\max 13}(x)}^{\phi_{\max 1}(X_0)} \int_{\theta_{\max}[\eta_C]}^{\pi-\theta_{\max}[\eta_C]} G_{ch}^{C3}(\phi_0,\theta_0,-\phi,\theta) u_{building}^{C3}(x,\phi,\theta) d\theta d\phi dx \Bigg\} \\
= & P_c K I_I'(\phi_0,\theta_0) \\
= & P_c \left[(K-1) I_I'(\phi_0,\theta_0) + I_I'(\phi_0,\theta_0) \right]
\end{aligned}
\tag{4.73}
$$

and

$$
\begin{aligned}
I_J(\phi_0,\theta_0) = P_c K \Bigg\{ & \int_{2X_0}^{2X_0+X_4} \int_{\phi_{\max 13}(X_0)}^{\phi_{\max 3}(x)} \int_{\theta_{\max}[c(\phi,2X_0)]}^{\pi-\theta_{\max}[c(\phi,2X_0)]} G_{ch}^{E1}(\phi_0,\theta_0,-\phi,\theta) u_{building}^{E1}(x,\phi,\theta) d\theta d\phi dx \\
= & + \int_{2X_0}^{2X_0+X_3} \int_{\phi_{\max 13}(2X_0)}^{\phi_{\max 1}(X_0)} \int_{\theta_{\max}[c(\phi,2X_0)]}^{\pi-\theta_{\max}[c(\phi,2X_0)]} G_{ch}^{E2}(\phi_0,\theta_0,-\phi,\theta) u_{building}^{E2}(x,\phi,\theta) d\theta d\phi dx \\
& + \int_{2X_0+X_3}^{2X_0+S} \int_{\phi_{\max 13}(2X_0)}^{\phi_{\max 3}(x)} \int_{\theta_{\max}[c(\phi,2X_0)]}^{\pi-\theta_{\max}[c(\phi,2X_0)]} G_{ch}^{E2}(\phi_0,\theta_0,-\phi,\theta) u_{building}^{E2}(x,\phi,\theta) d\theta d\phi dx \\
& + \int_{2X_0}^{2X_0+X_2} \int_{\phi_{\max 13}(x)}^{\phi_{\max 13}(2X_0)} \int_{\theta_{\max}[c(\phi,\alpha)]}^{\pi-\theta_{\max}[c(\phi,\alpha)]} G_{ch}^{E3}(\phi_0,\theta_0,-\phi,\theta) u_{building}^{E3}(x,\phi,\theta) d\theta d\phi dx \\
& + \int_{2X_0+X_2}^{2X_0+S} \int_{\phi_{\max 1}(2X_0)}^{\phi_{\max 13}(2X_0)} \int_{\theta_{\max}[c(\phi,\alpha)]}^{\pi-\theta_{\max}[c(\phi,\alpha)]} G_{ch}^{E3}(\phi_0,\theta_0,-\phi,\theta) u_{building}^{E3}(x,\phi,\theta) d\theta d\phi dx \\
& + \int_{2X_0+X_2}^{2X_0+S} \int_{\phi_{\max 13}(x)}^{\phi_{\max 1}(2X_0)} \int_{\theta_{\max}[\eta_E]}^{\pi-\theta_{\max}[\eta_E]} G_{ch}^{E4}(\phi_0,\theta_0,-\phi,\theta) u_{building}^{E4}(x,\phi,\theta) d\theta d\phi dx \Bigg\} \\
= & P_c K I_J'(\phi_0,\theta_0) \\
= & P_c \left[(K-1) I_J'(\phi_0,\theta_0) + I_J'(\phi_0,\theta_0) \right]
\end{aligned}
\tag{4.74}
$$

The total interference from the six building groups are

$$\begin{aligned} I_{total}(\phi_0,\theta_0) &= I_D(\phi_0,\theta_0)+I_F(\phi_0,\theta_0)+I_C(\phi_0,\theta_0)+I_E(\phi_0,\theta_0)+I_I(\phi_0,\theta_0)+I_J(\phi_0,\theta_0) \\ &= P_c\,[(K-1)I'_D(\phi_0,\theta_0) \\ &\quad +(K-1)I'_F(\phi_0,\theta_0)+I'_F(\phi_0,\theta_0) \\ &\quad +(K-1)I'_C(\phi_0,\theta_0)+I'_C(\phi_0,\theta_0) \\ &\quad +(K-1)I'_E(\phi_0,\theta_0)+I'_E(\phi_0,\theta_0) \\ &\quad +(K-1)I'_I(\phi_0,\theta_0)+I'_I(\phi_0,\theta_0) \\ &\quad +(K-1)I'_J(\phi_0,\theta_0)+I'_J(\phi_0,\theta_0)] \\ &= P_c\,[(K-1)a(\phi_0,\theta_0)+b(\phi_0,\theta_0)] \end{aligned} \tag{4.75}$$

where

$$\begin{aligned} b(\phi_0,\theta_0) &= I'_F(\phi_0,\theta_0)+I'_C(\phi_0,\theta_0)+I'_E(\phi_0,\theta_0)+I'_I(\phi_0,\theta_0)+I'_J(\phi_0,\theta_0) \\ a(\phi_0,\theta_0) &= b+I'_D(\phi_0,\theta_0). \end{aligned} \tag{4.76}$$

Thus, using Eq. 4.1, the SINR can be expressed as

$$\begin{aligned} \text{SINR} &= \frac{P_c}{\frac{\nu}{N}I_{total}(\phi_0,\theta_0)} \\ &= \frac{P_c}{\frac{\nu}{N}P_c[(K-1)a(\phi_0,\theta_0)+b(\phi_0,\theta_0)]} \end{aligned} \tag{4.77}$$

and the mean capacity within building group D when Array 1 steers towards (ϕ_0, θ_0) is

$$K = \frac{1}{\frac{\nu}{N}\text{SINR}a(\phi_0,\theta_0)} - \frac{b(\phi_0,\theta_0)}{a(\phi_0,\theta_0)} + 1. \tag{4.78}$$

4.6 Conclusions

In this chapter, we have presented the modelling and analysis of a multi cell 3-dimensional CDMA system in a downtown environment. The effect on power control

due to reflection, diffraction, building penetration, propagation, and element factor is modelled. A modified single bounce model adapted to our urban model is proposed and coupled with the modified user distribution, an analytical derivation of the interference contributed by neighbouring cells is provided.

Chapter 5 CAPACITY ESTIMATION AND RESULTS

5.1 Introduction

This chapter presents the improvement with the use of our proposed 3-dimensional smart antenna array on the estimated capacity. The use of single element antenna, 1x5 linear array, and 5x5 vertical planar array introduced in Chapter 2 on the model in Fig. 4.1 for both single cell and multicell are compared. In the multicell case, we will illustrate the interference contributed by each of the neighbouring cells on building group D. With a 3-dimensional approach to array and interference analysis, we can show the changes in capacity and interference in surface plots, and therefore provide good insights into the system. The organization of this chapter is as follows. After this introduction, Section 5.2 presents the simulation model and methodology for estimating interference and capacity. Section 5.3 shows the results from the use of single element antenna. Then, improvement with the use of 1x5 linear array is presented in Section 5.4. Section 5.5 shows the results and advantages for using a 5x5 vertical planar array. The change in system capacity due to difference in building's reflectivity is discussed in Section 5.6. Finally in Section 5.7, for comparative purposes, we present the results from a second simulation with the 5x5 vertical planar array to investigate changes in capacity when building dimensions change. Section 5.8 presents the conclusions of this chapter.

5.2 Simulation Model and Methodology

5.2.1 Simulation Model

We have considered the rectangular grid downtown model which consists of a total of 6 building groups facing the same street as illustrated in Fig. 4.1. Each building group is

considered to be a cell of service, and the performance of single element antenna, linear array, and vertical planar array will be compared. Effects of building materials with reflection coefficients tabulated in Table 4.1 on capacity are compared.

The estimation of capacity result from the total interference received from both in cell and out of cell users. Due to the ability of the base station antenna to steer to both azimuth and vertical angles, the total interference is calculated for each (ϕ_0, θ_0) combination, and iterated in 1^0 steps. For Array 1 in Fig. 4.1, the ranges of the steered angles are determined at the beginning from the dimensions of the downtown model as $\phi_0 = [-\phi_{\max 1}(X_0), \phi_{\max 1}(X_0)]$ and $\theta_0 = [\theta_{\max}[c(\phi_0, X_0)], 180^0 - \theta_{\max}[c(\phi_0, X_0)]]$ in order to serve all mobiles in building group D. Because it has been assumed that each base station antenna is mounted at the middle of a building group, we need only to iterate through the angles $\phi_0 = [0, \phi_{\max 1}(X_0))$ and $\theta_0 = [\theta_{\max}[c(\phi, X_0)], 90^0)$ from symmetry.

5.2.2 Simulation Methodology

Fig. 5.1 summarizes the steps for the simulation. First, parameters such as the dimensions and reflection coefficient for the building groups are set, along with the IS-95 parameters. The maximum azimuth angle, $\phi_{\max}(X_0)$, and vertical angle, $\theta_{\max}[c(\phi_0, X_0)]$, are also calculated for possible user locations within building group D to set the bounds within which the antenna array may steer towards.

For each steered angle, (ϕ_0, θ_0), the normalized array factor power response, $F_{\phi_0,\theta_0}(\phi_0, \theta_0)$, is calculated for all angles from which interference may come from. Also at each steered angle, the interference from intra and adjacent cells are computed and the maximum capacity within building group D is found. The simulation then iterates the steered angle to different directions within the bounds set previously in order to find the maximum capacity at each steered angle. Specifically, the simulation first iterates from $[\phi_0 = 0^0, \theta_0 = \theta_{\max}[c(\phi_0, X_0)]]$ to $[\phi_0 = 0^0, \theta_0 = 90^0]$. ϕ_0 is then incremented 1^0 and θ_0 is cycled again from $\theta_{\max}[c(\phi_0, X_0)]$ to 90^0 until $\phi_0 = \phi_{\max}(X_0)$. From this, a capacity surface plot can be generated and the lowest point on the surface indicates the maximum allowable capacity beyond which any increase anywhere within the system will compromise the received SINR. This entire process is repeated for each type of antenna array used, or a change in system parameters, i.e. IS-95 parameters, building sizes, reflection coefficients, etc.

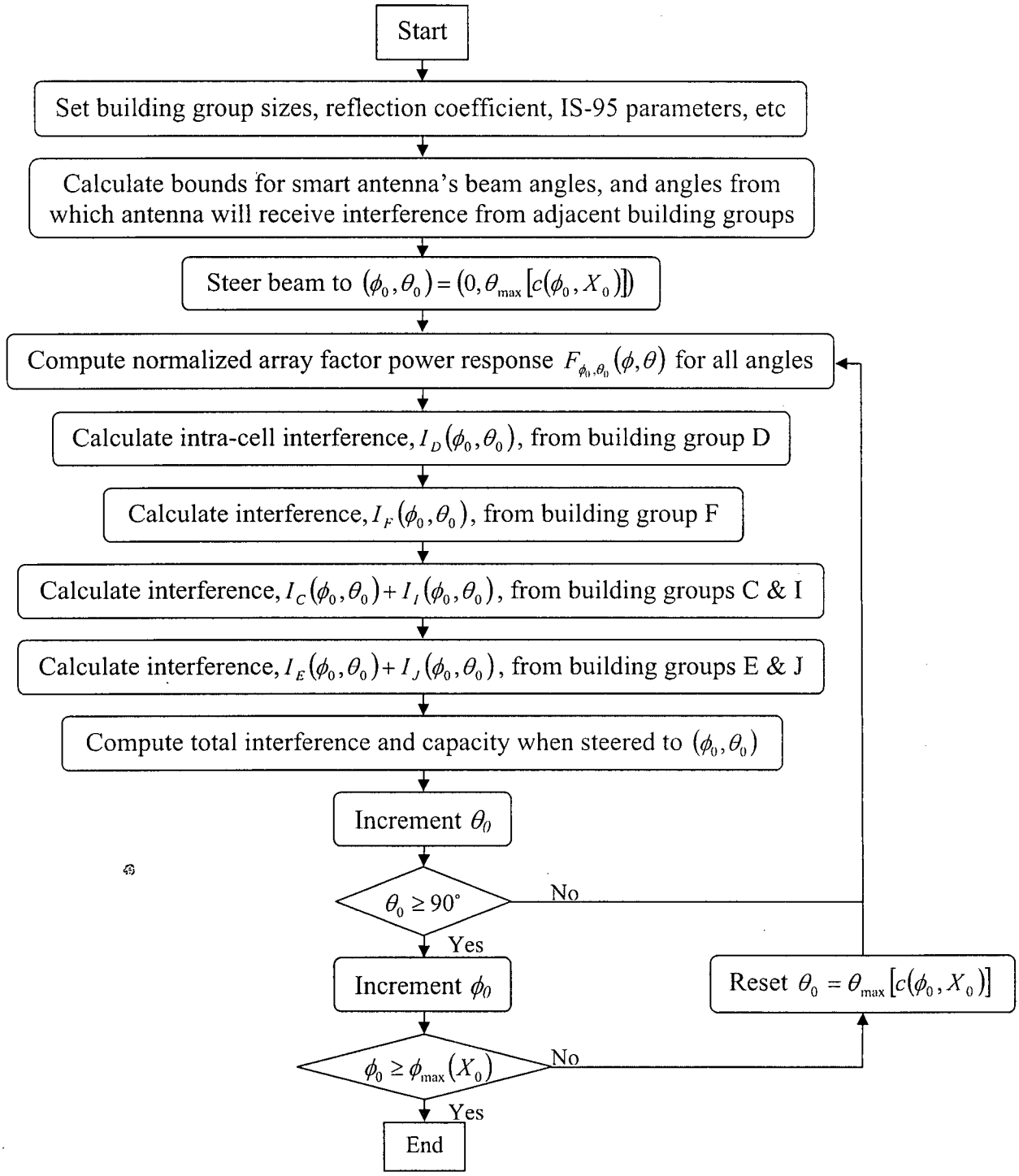

Fig. 5.1 Program Flowchart
(See Fig. 4.1)

5.2.3 Building Group D Intra-cell Interference Simulation

Fig. 5.2 shows the steps for the simulation of intra-cell interference from building group D for Eq. 4.18. Given an interferer's location (x,ϕ,θ), Array 1's normalized array factor, and the user PDF from Eq. 3.10, the weighted interference power is calculated. This is repeated for all interferers' locations within building group D to obtain the mean interference power from building group D. For efficient simulation, interference from (ϕ,θ) and $(-\phi,\theta)$ are computed at the same time to save half of the integration steps.

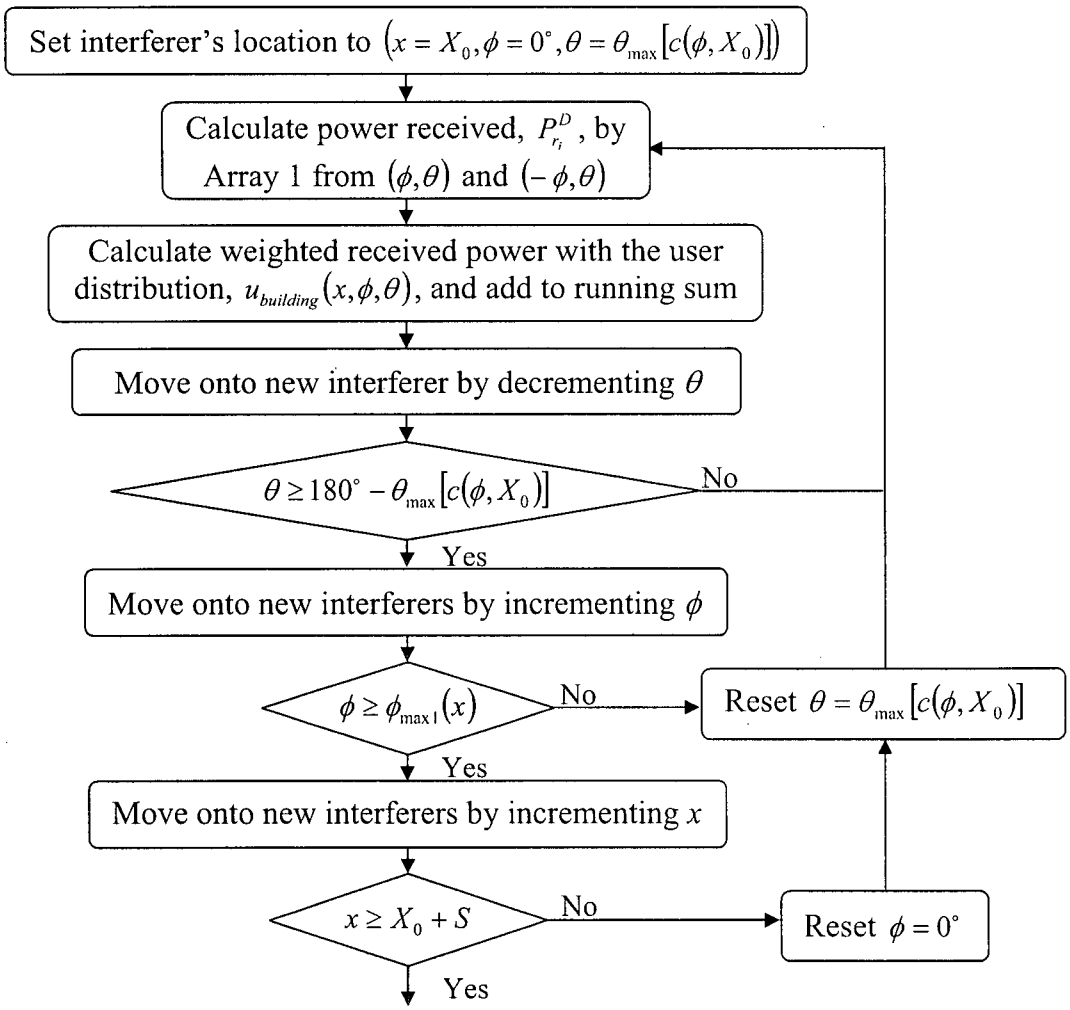

Fig. 5.2 Building Group D Intra-cell Interference Simulation

5.2.4 Building Group F Interference Simulation

Fig. 5.3 describes the steps for simulating interference from building group F for Eq. 4.31. Because interferers in building group F are under the control of Array 2 (see Fig. 4.1), the transmitted power, P_t^F, determined by the interferer-Array 2 distance, AOA to Array 2, and Array 2's normalized array factor, are first calculated using Eqs. 4.20 – 4.27. The power received by Array 1 from this interferer is then calculated with Eqs. 4.28 – 4.30, subjected to the reflection loss, $L_{reflection}$ of Eq. 4.14, off building group D, and the interferer-Array 1 distance-propagation loss. The weighted received power is computed with a user PDF of Eq. 4.32 for building group F. Similar to the simulation for building group D, interference from (ϕ,θ) and $(-\phi,\theta)$ are computed at the same time to save half of the integration steps.

5.2.5 Building Groups C and I Interference Simulation

Figs. 5.4 – 5.6 illustrate the simulation steps for interference from building group C's zones C1 – C3 for Eq. 4.50 and the corresponding zones from building group I for Eq. 4.73. Similar to the power control operation for building group F, the transmitted power, P_t^{C1}, P_t^{C2}, and P_t^{C3} from interferers in the three zones are first determined with Eqs. 4.33 – 4.46. Then the received power by Array 1 are calculated in Eqs. 4.47 – 4.49. The weighted received power can then be determined with user PDFs for the three zones given by Eq. 4.51. Note in Fig. 4.11 that interference from zone C3 comes from $\phi = \phi_{\max 1}(X_0)$ only as interferers in this zone are in the shadow region of building group D. Interferers in building group I at $(-\phi,\theta)$ can be computed concurrently with interferers in building group C from (ϕ,θ).

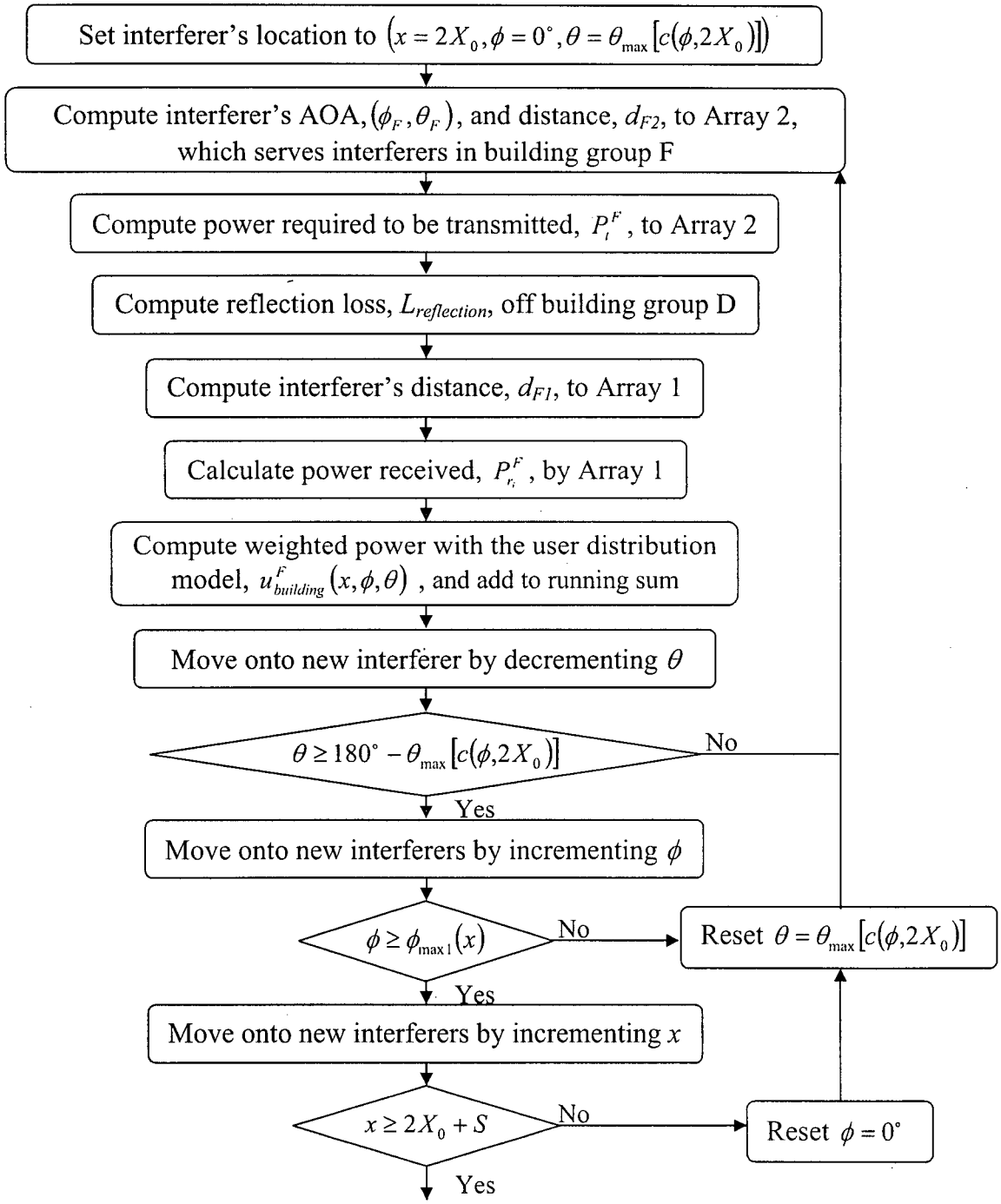

Fig. 5.3 Building Group F Interference Simulation for Fig. 4.10

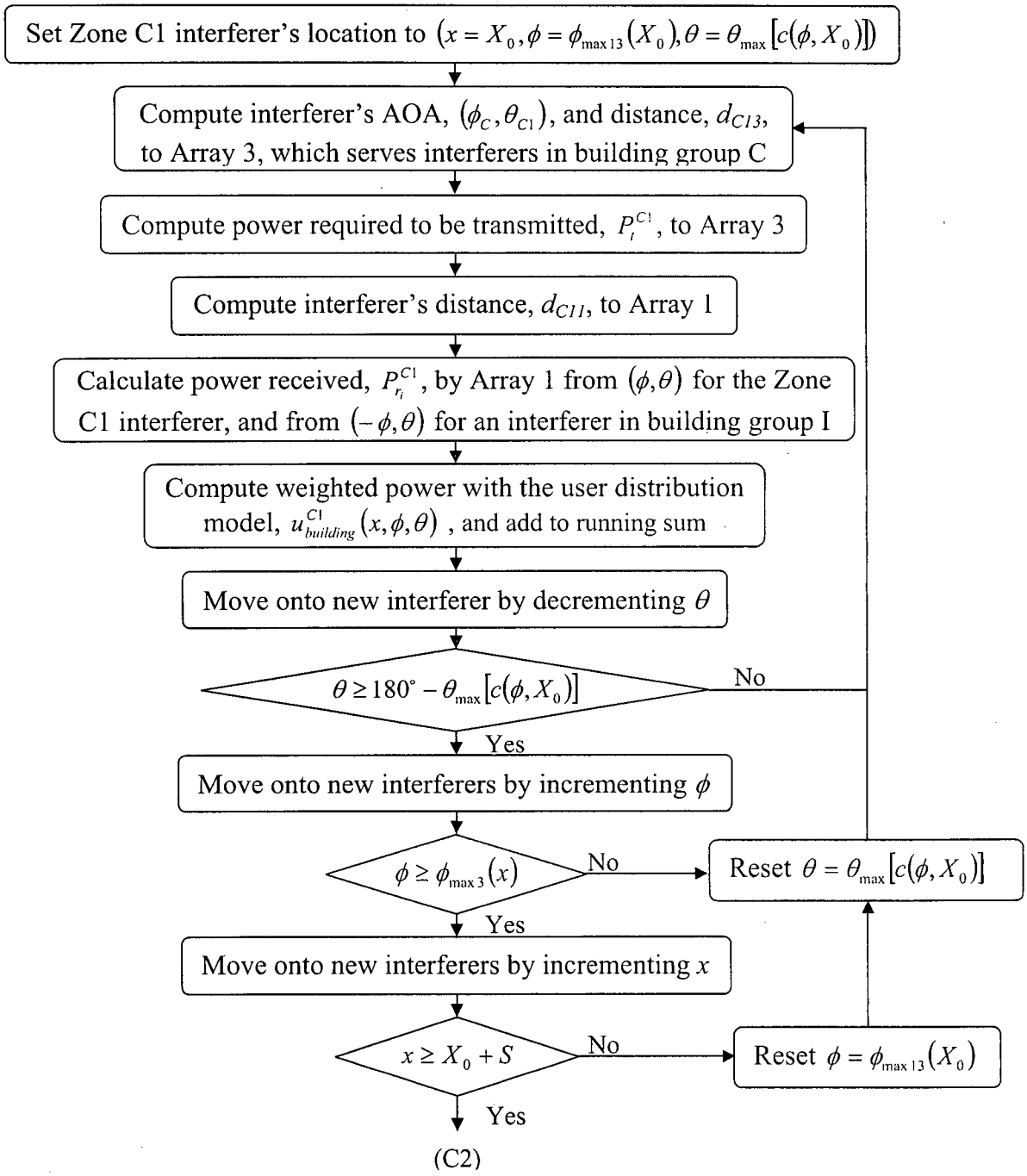

Fig. 5.4 Zones C1 and I1 Interference Simulation for Figs. 4.11 and 4.12

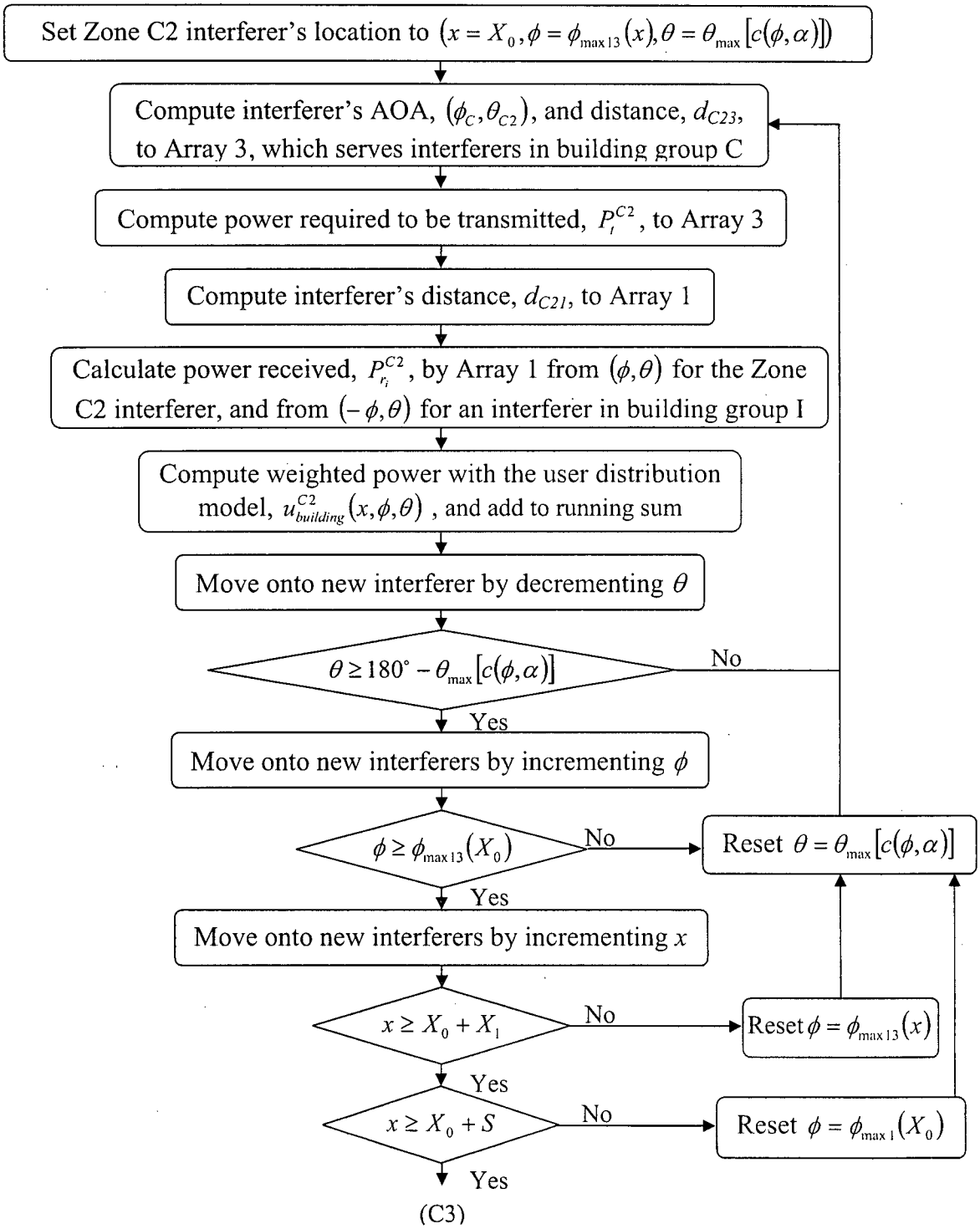

Fig. 5.5 Zones C2 and I2 Interference Simulation for Figs. 4.11 and 4.12

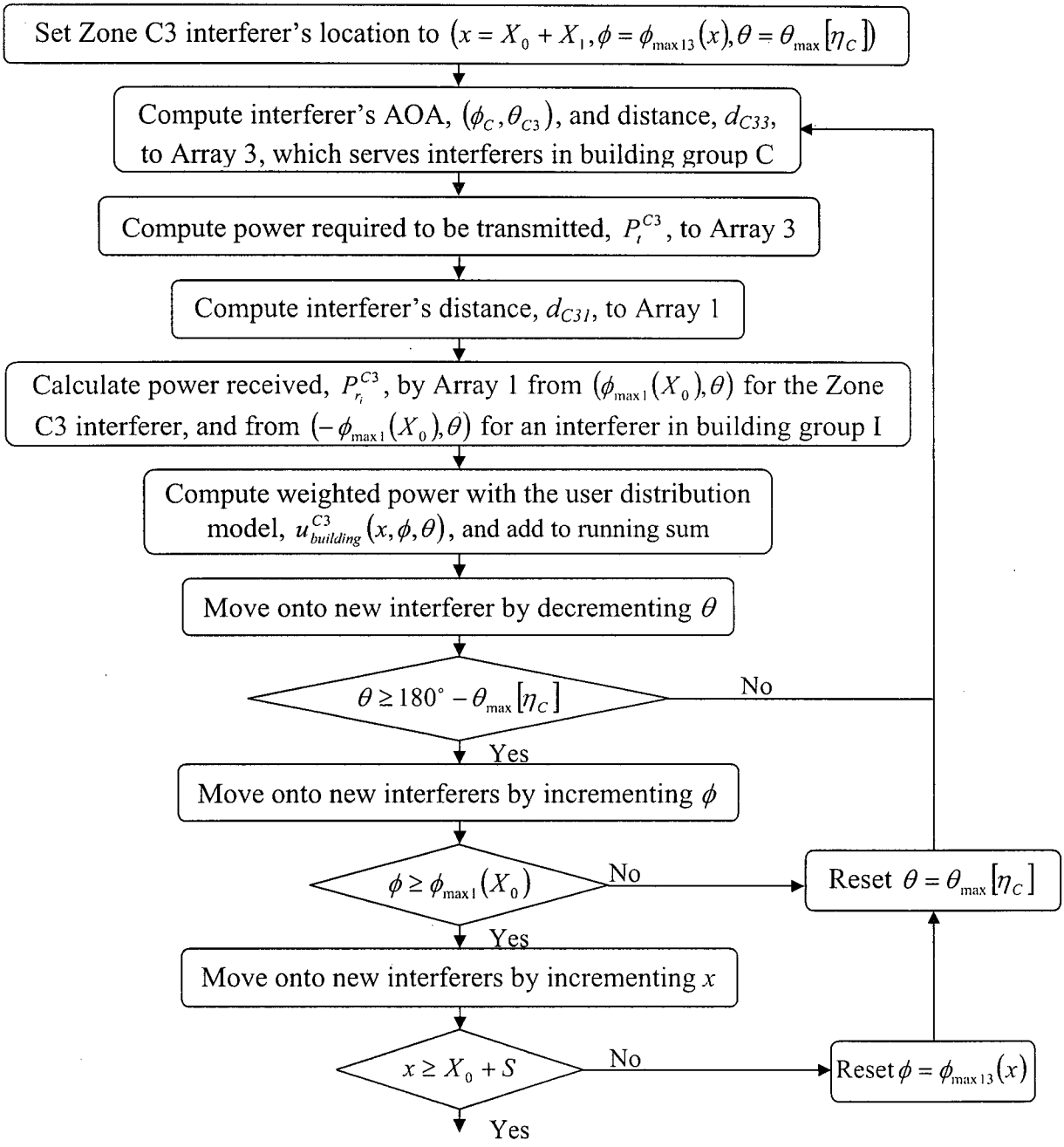

Fig. 5.6 Zones C3 and I3 Interference Simulation for Figs. 4.11 and 4.12

5.2.6 Building Groups E and J Interference Simulation

Fig. 5.7 – 5.10 show the steps for simulating interference from zones E1, E2, E3, and E4 from building group E in Eq. 4.71 and the corresponding zones from building group J in Eq. 4.74. The transmitted power from the four zones P_t^{E1}, P_t^{E2}, P_t^{E3}, and P_t^{E4} are first calculated with Eqs. 4.52 – 4.67. The received power by Array 1 are then computed in Eqs. 4.68 – 4.70. The user PDFs in Eq. 4.72 for the four zones are then used to determine the weighted received power. Similar to building group C's zone C3, zone E4 is in the shadow region of building group F as illustrated in Fig. 4.14. Therefore, interferers from this area comes from $\phi = \phi_{\max 1}(2X_0)$. Also, interferers in building group J from $(-\phi, \theta)$ can be simulated at the same time as interferers in building group E from (ϕ, θ).

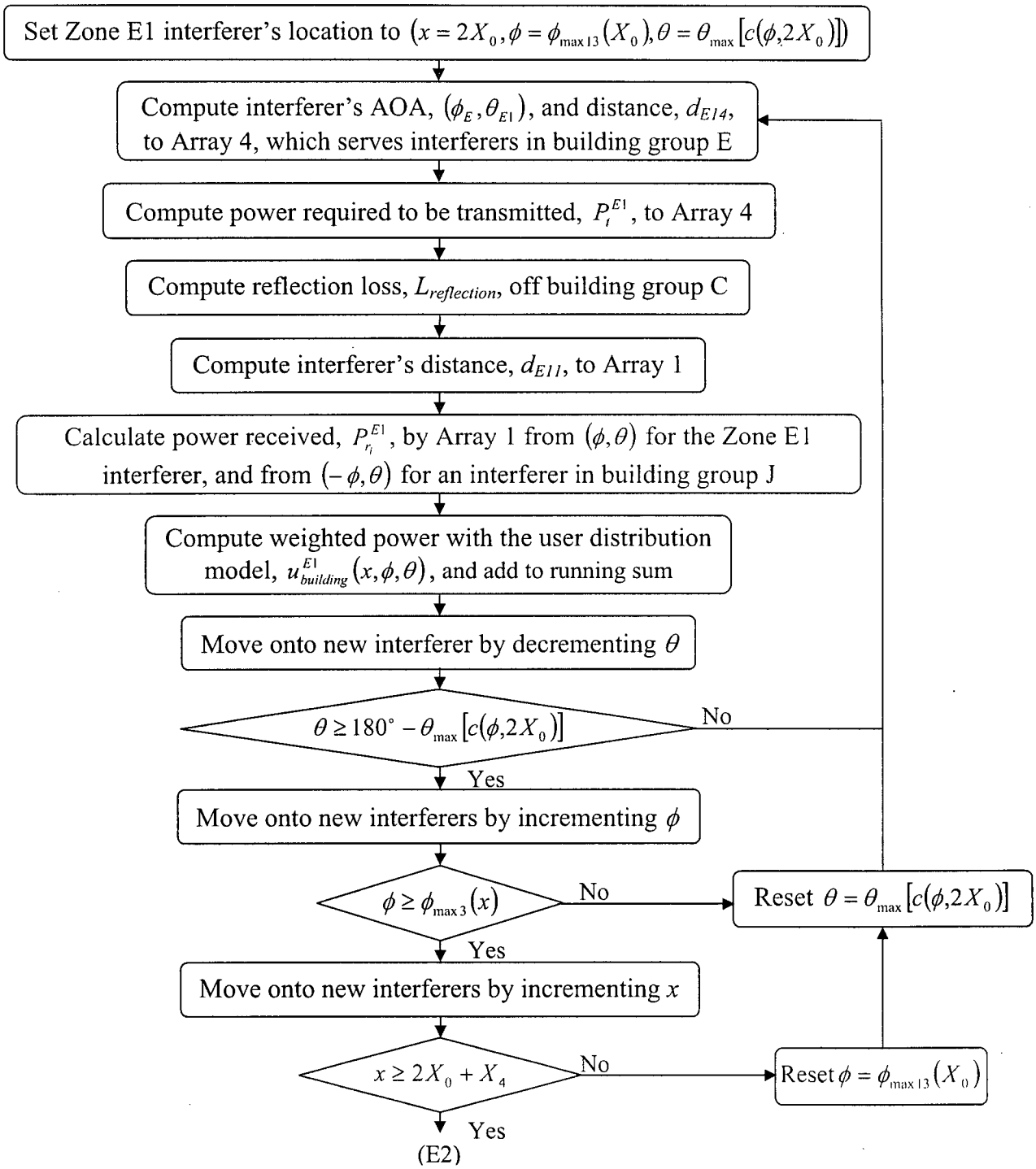

Fig. 5.7 Zones E1 and J1 Interference Simulation for Figs. 4.13 and 4.14

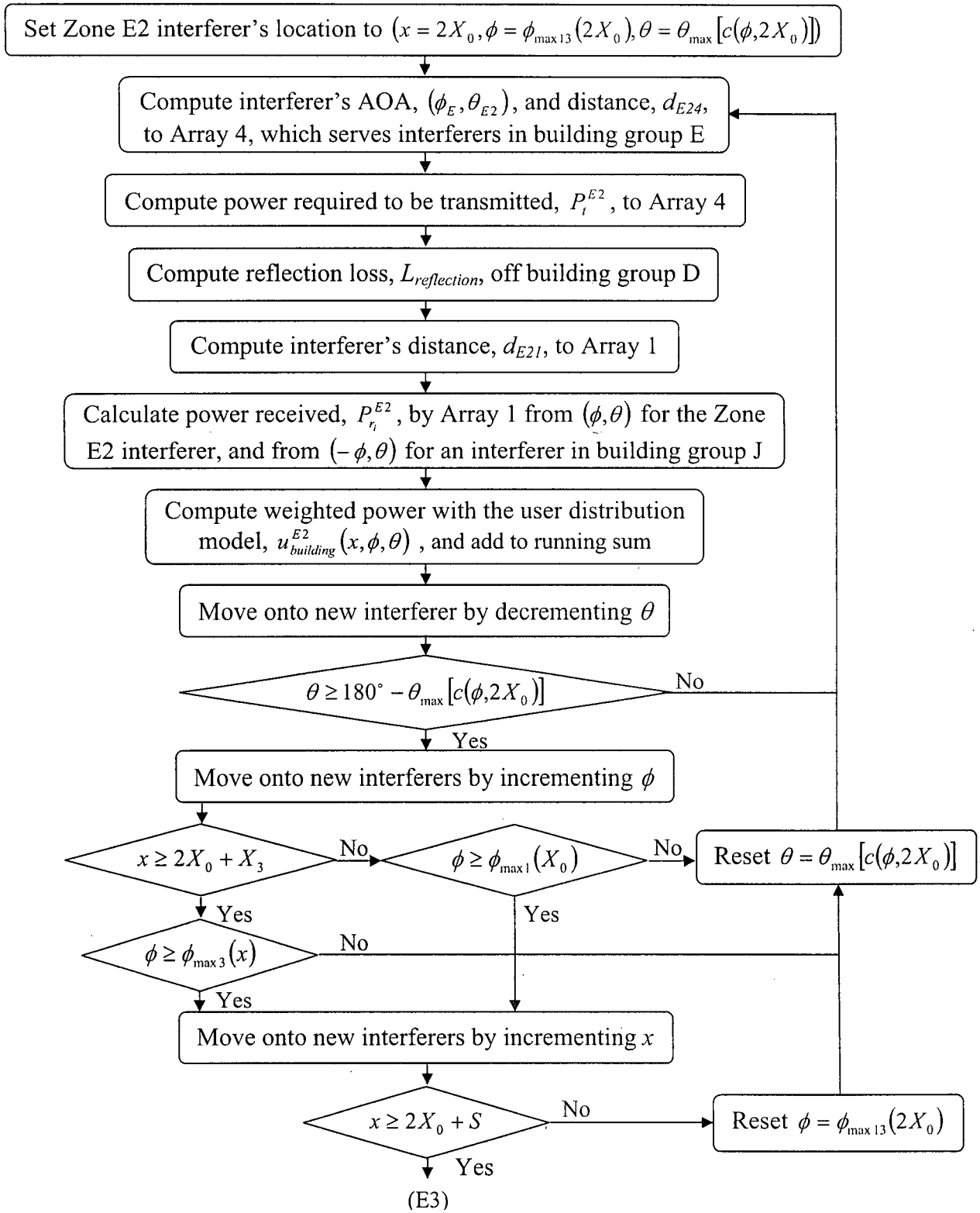

Fig. 5.8 Zones E2 and J2 Interference Simulation for Figs. 4.13 and 4.14

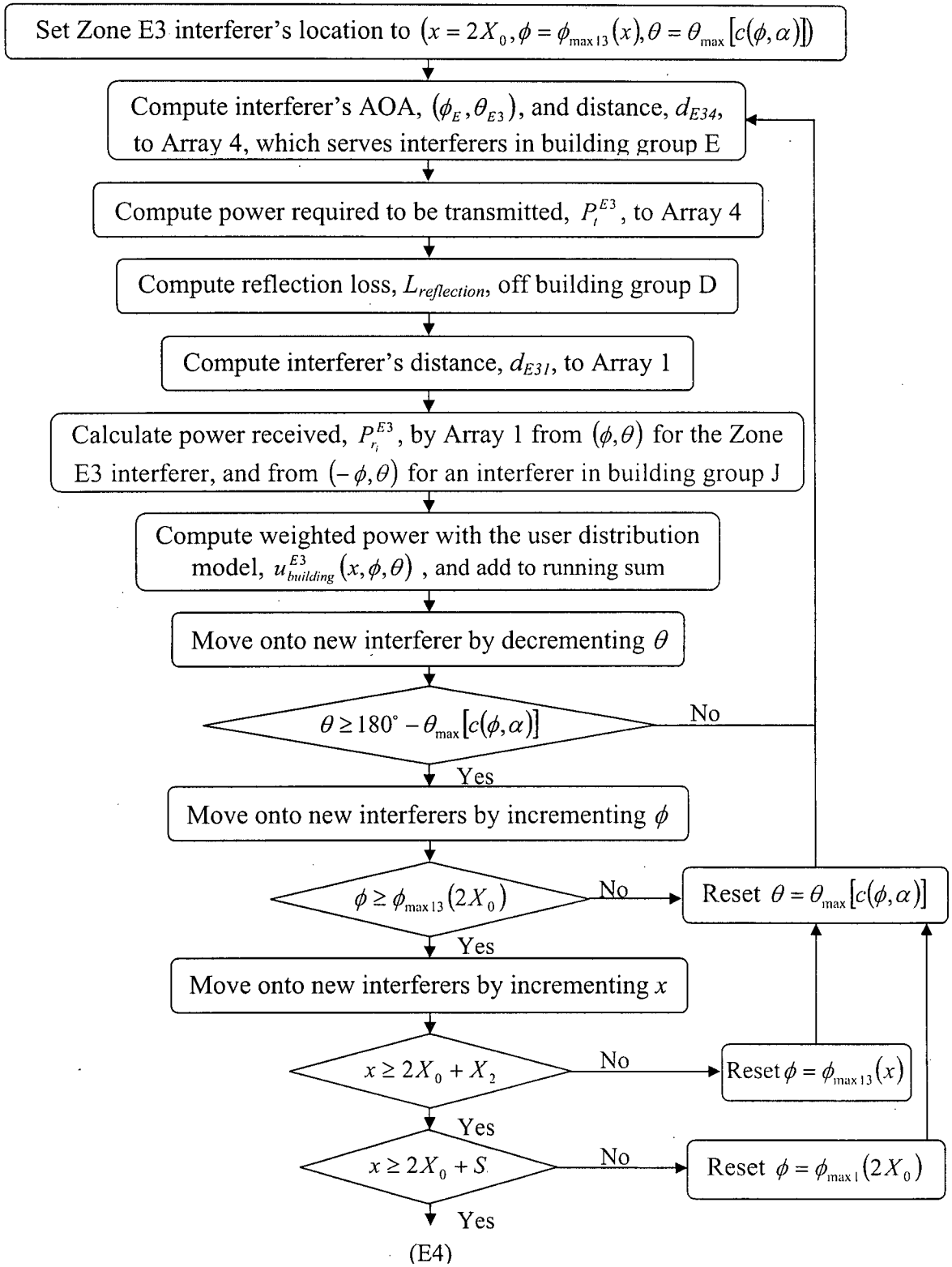

Fig. 5.9 Zones E3 and J3 Interference Simulation for Figs. 4.13 and 4.14

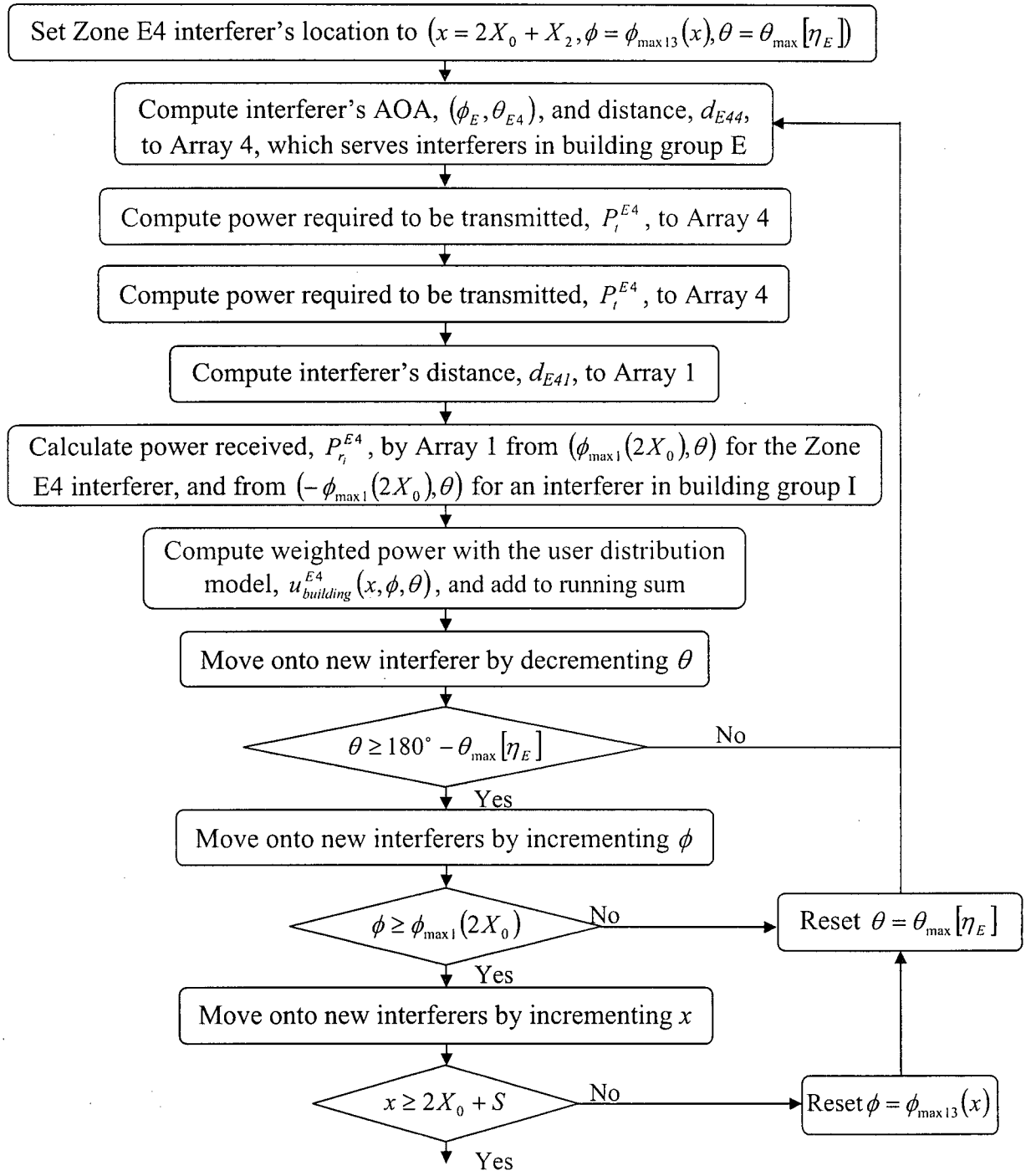

Fig. 5.10 Zones E4 and J4 Interference Simulation for Figs. 4.13 and 4.14

5.3 Single Element Results

We have calculated the capacity surface plot in a multicell situation when only one antenna element is used to serve the cell for buildings constructed primarily with limestone, which has the relative permittivity $\varepsilon_{1r} = 7.51$. Because of the inability to steer, or having a fixed radiation pattern, the single panel antenna is able to support 18 users. Figs. 5.12 – 5.15 show the interference plots from building groups D, F, C and I, and E and J respectively.

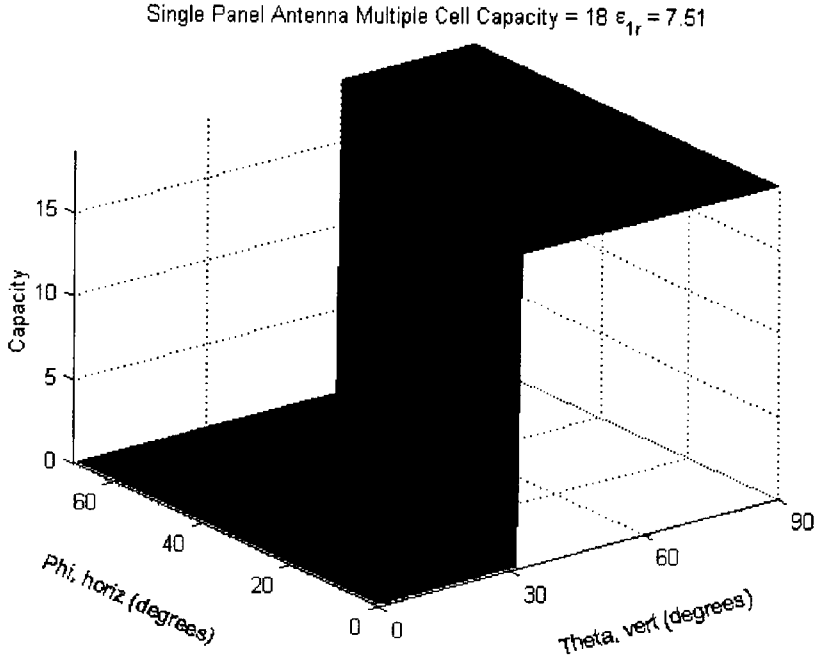

Fig. 5.11 Capacity Plot for Single Panel Antenna

Observe that due to the reflection and propagation loss, interference from building group F is only a fraction of that from the cell of service, or building group D. In Fig. 5.14, interference is yet lower because building group C is even further away. In Fig. 5.15, it may appear contradictory that interference from building group E is higher than that from

building group C, since interference from building group E suffers a longer propagation loss, in addition to a reflection loss. However, this can be explained by observing in Figs. 4.6 and 4.13 that interference from building group E arrive at a smaller azimuth angle, which offers a larger gain given the panel antenna element pattern.

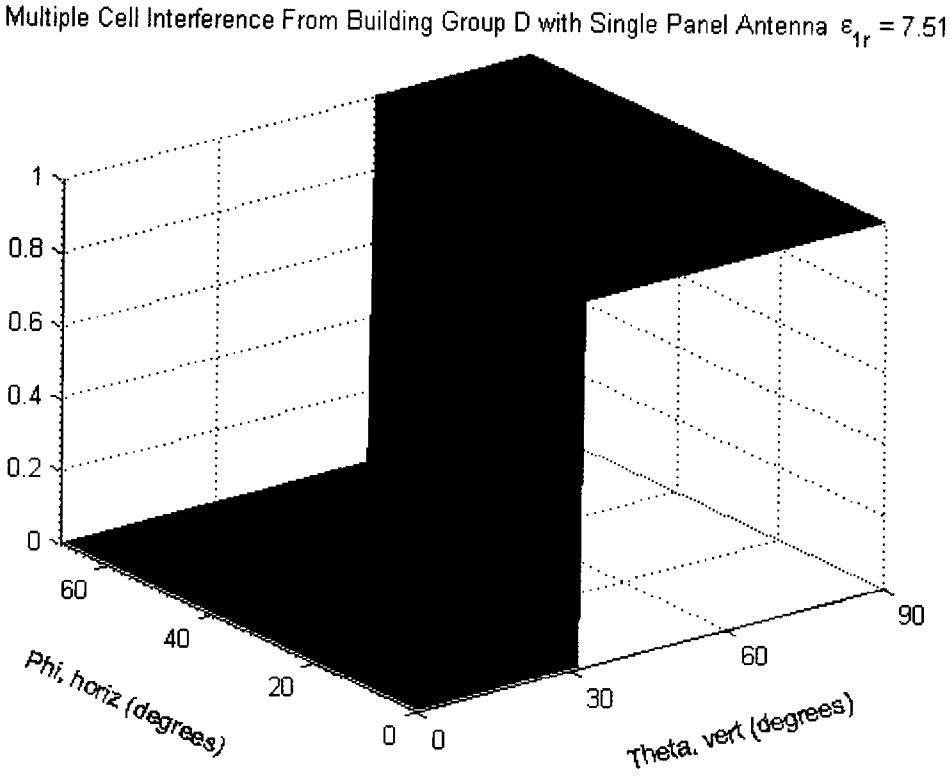

Fig. 5.12 Interference Plot for Single Panel Antenna From Building Group D

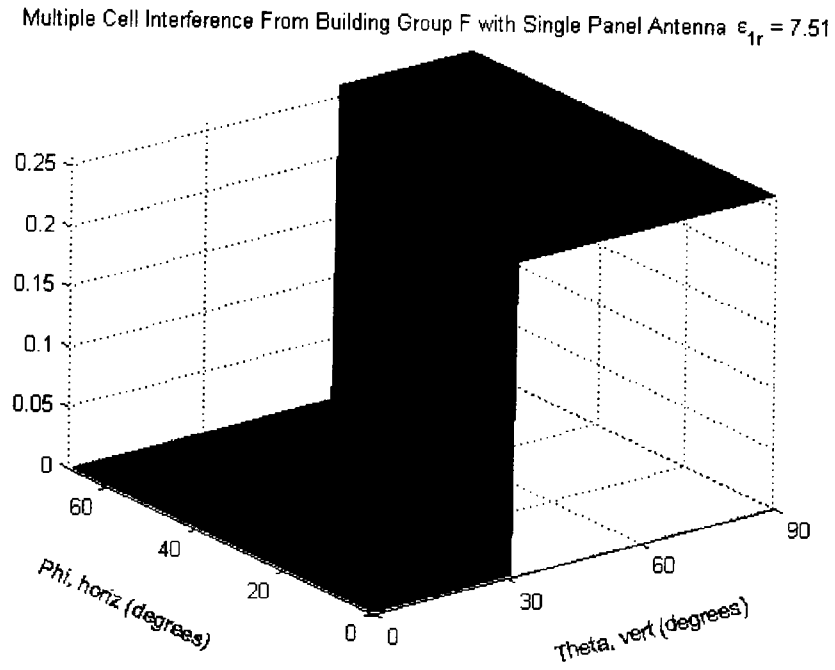

Fig. 5.13 Interference Plot for Single Panel Antenna From Building Group F

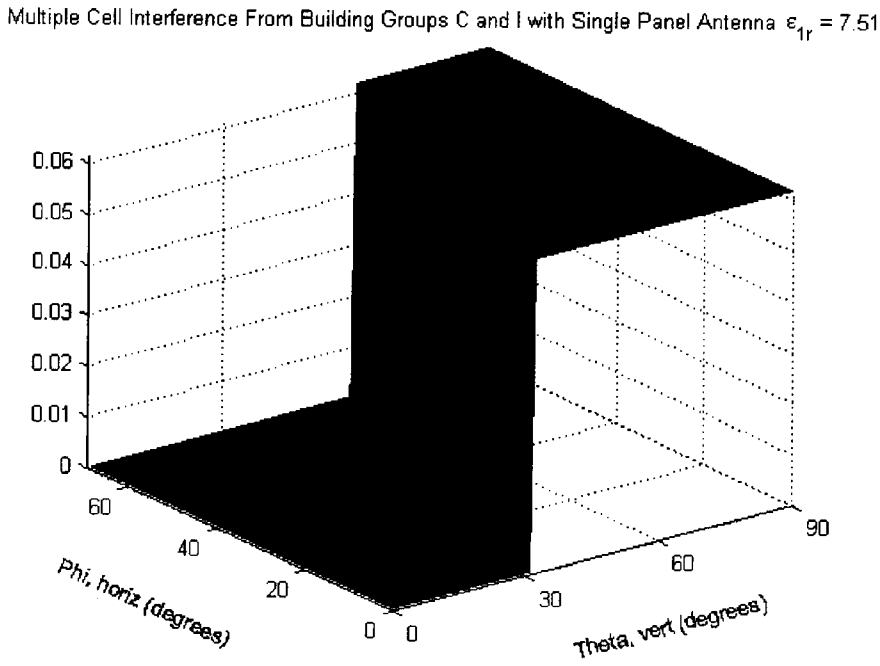

Fig. 5.14 Interference Plot for Single Panel Antenna From Building Groups C and I

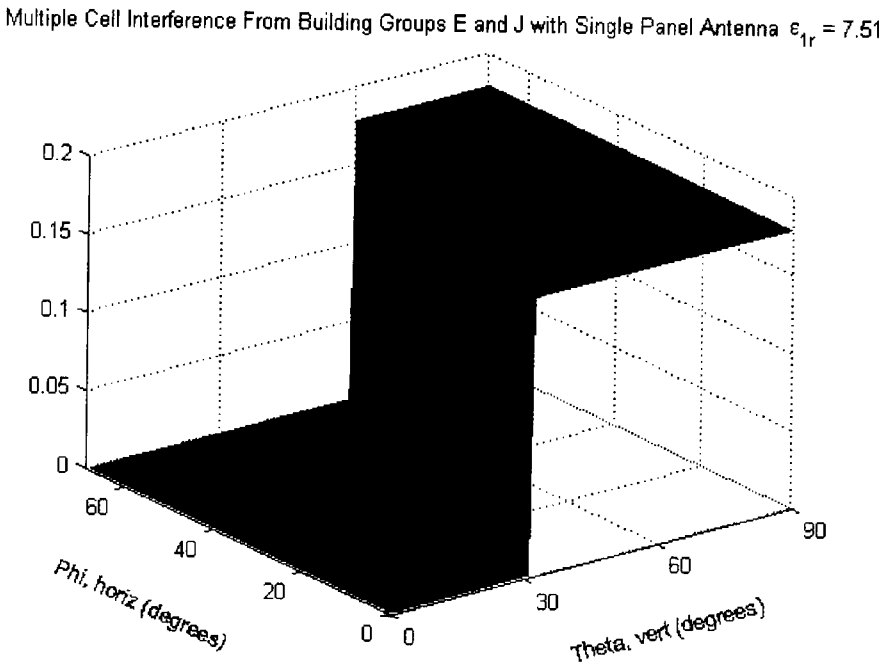

Fig. 5.15 Interference Plot for Single Panel Antenna From Building Groups E and J

5.4 1x5 Linear Array Results

For a 1x5 linear array, the antenna is able to steer to different azimuth directions. Therefore, the capacity surface plot in Fig. 5.16 shows a change in capacity as the array is steered to different AOAs. As anticipated, the capacity supported decreases as the antenna beam is steered to a larger azimuth angle, where it will receive more interference. Also, the capacity does not change at different vertical angles, except at the larger azimuth angles. This is because while a linear array does not have vertical steering ability, it can still sense enough phase difference from different vertical AOAs at a large enough azimuth angle. The capacity with a 1x5 linear array is 74 users.

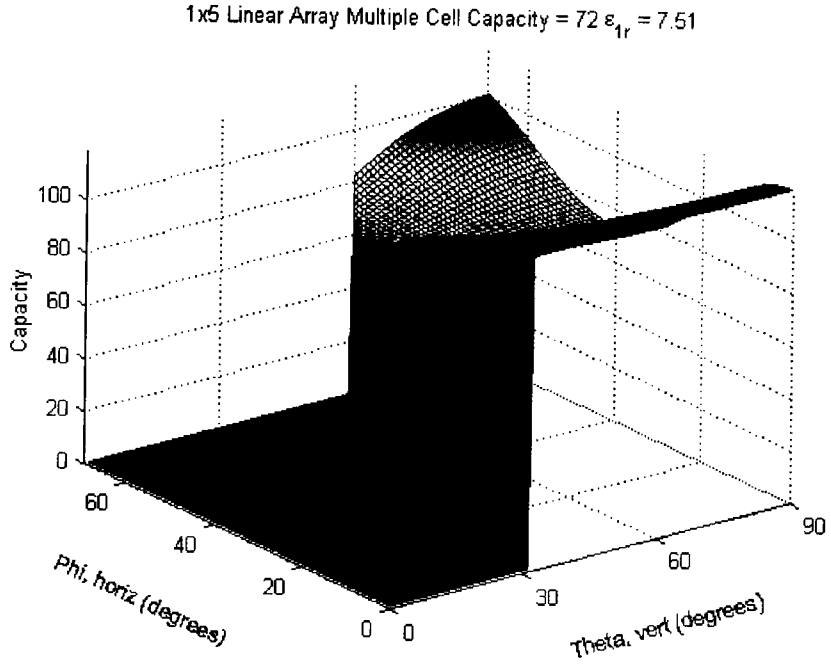

Fig. 5.16 Capacity Plot for 1x5 Linear Array

Fig. 5.17 shows the interference from the building group under service. As indicated, the interference rises as the azimuth angle is increased. However, for angles beyond $\phi_{\max}(X_0 + S)$, where the left side and back walls intersect, the interference tapers off. Fig. 5.18 shows similar result for building group F. In Figs. 5.19 and 5.20, because of the selective azimuth beam steering, interference from building groups C and E doesn't rise until the beam is steered towards the end of building group D. Note that the local minima shown in Fig. 5.20 is indicative of the hashed interference zone in Figs. 4.13 and 4.14. Further, the interference levels are less than that obtained with a single panel antenna element, and that the relative levels can be explained in a similar manner as in the previous section.

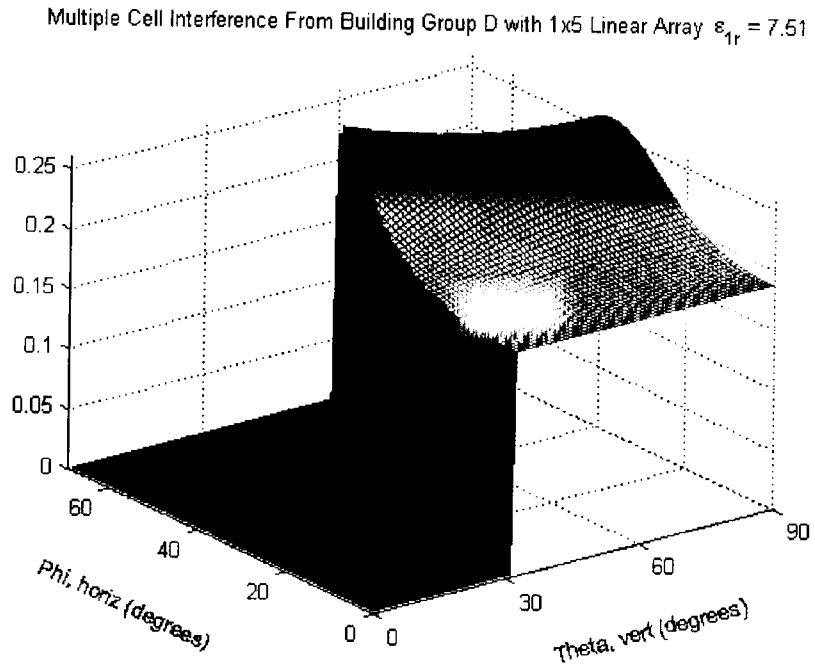

Fig. 5.17 Interference Plot for 1x5 Linear Array From Building Group D

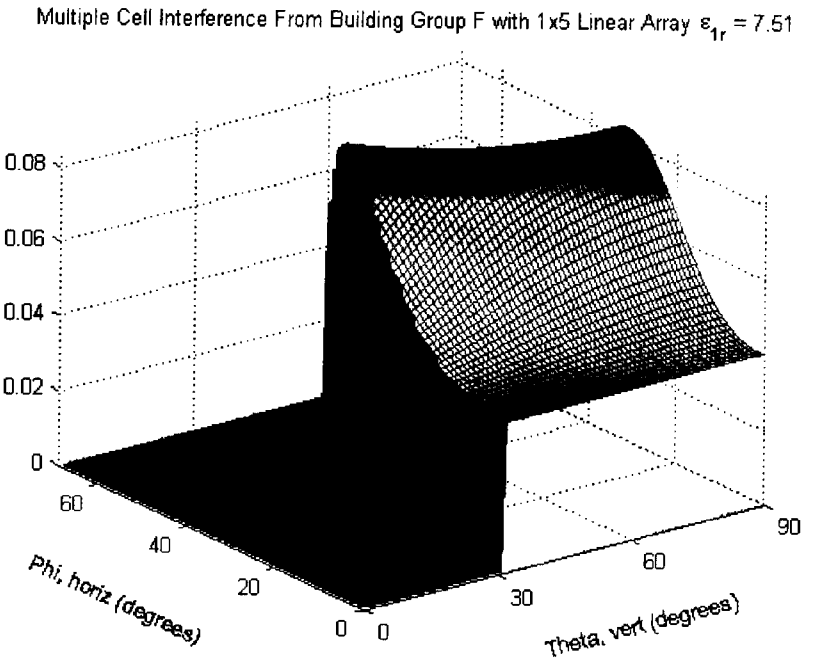

Fig. 5.18 Interference Plot for 1x5 Linear Array From Building Group F

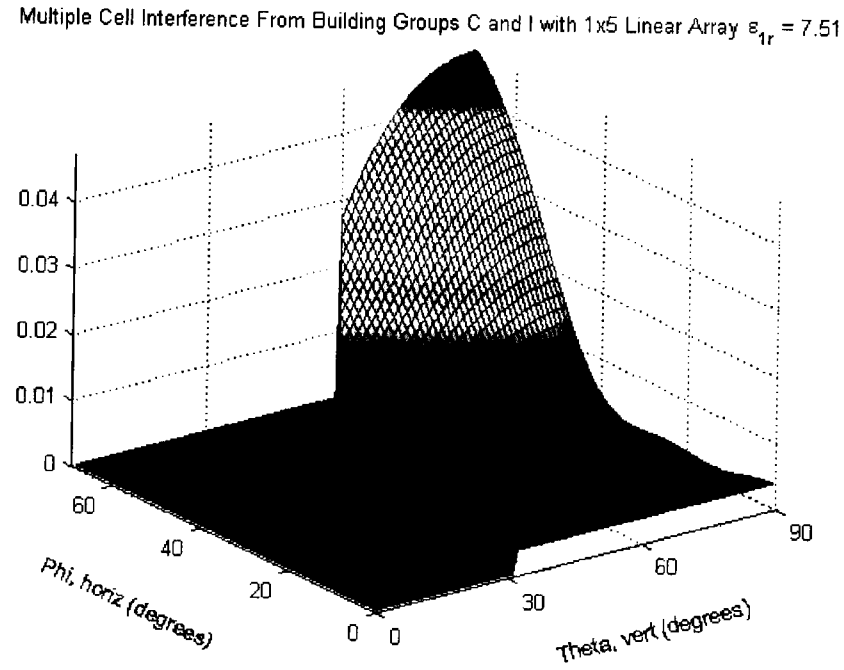

Fig. 5.19 Interference Plot for 1x5 Linear Array From Building Groups C and I

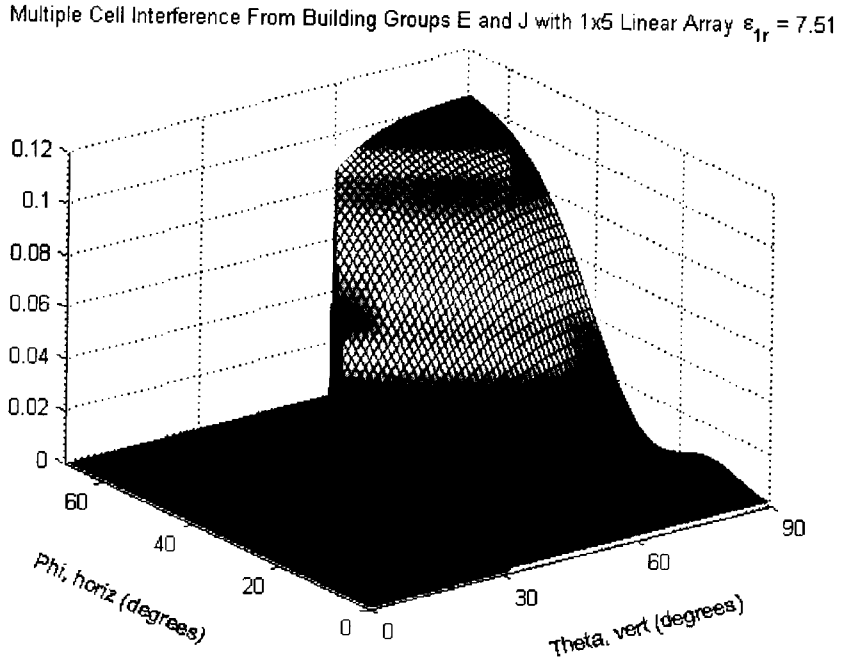

Fig. 5.20 Interference Plot for 1x5 Linear Array From Building Groups E and J

5.5 5x5 Vertical Planar Array Results

Fig. 5.21 illustrates both the vertical and horizontal steering ability of a 5x5 vertical planar array. Because of the narrower vertical beamwidth, the array illuminates the least amount of building space and provides the highest capacity when steered to $(0, \pi/2)$. As the array is steered towards other vertical directions, however, it illuminates more building floors per degree beamwidth and the capacity decreases. Note that when the beam is steered towards the top floors, only the lower portion of the beam is subjected to interference. As such, capacity increases again. The global minima indicates the system capacity, which is 236 users.

Figs. 5.22 – 5.25 show the interference from adjacent building groups. Notice the level is yet lower than that with the use of a 1x5 linear array. The relative levels still follow the same explanation offered with the use of a single panel antenna element, indicating the effect of the element factor in a multiple cell environment.

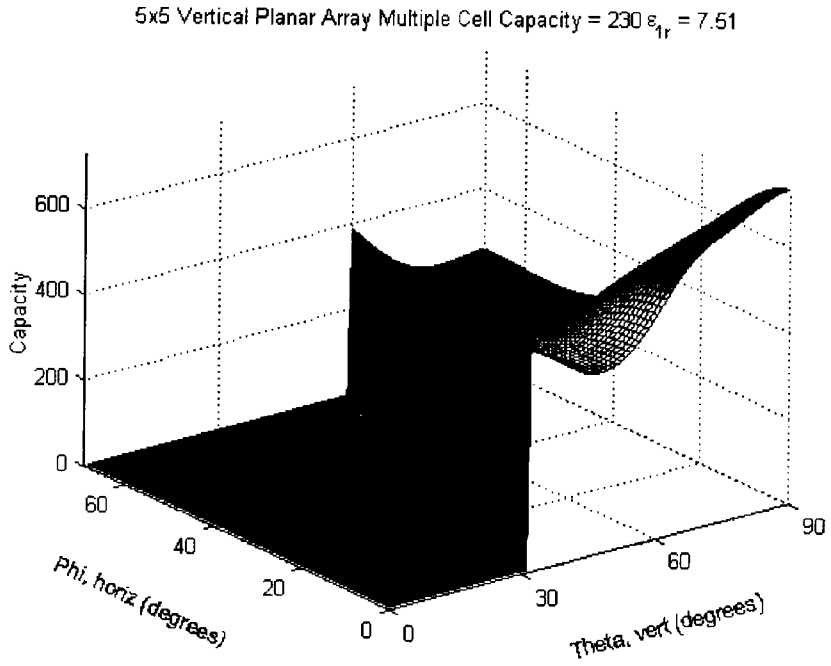

Fig. 5.21 Capacity Plot for 5x5 Vertical Planar Array

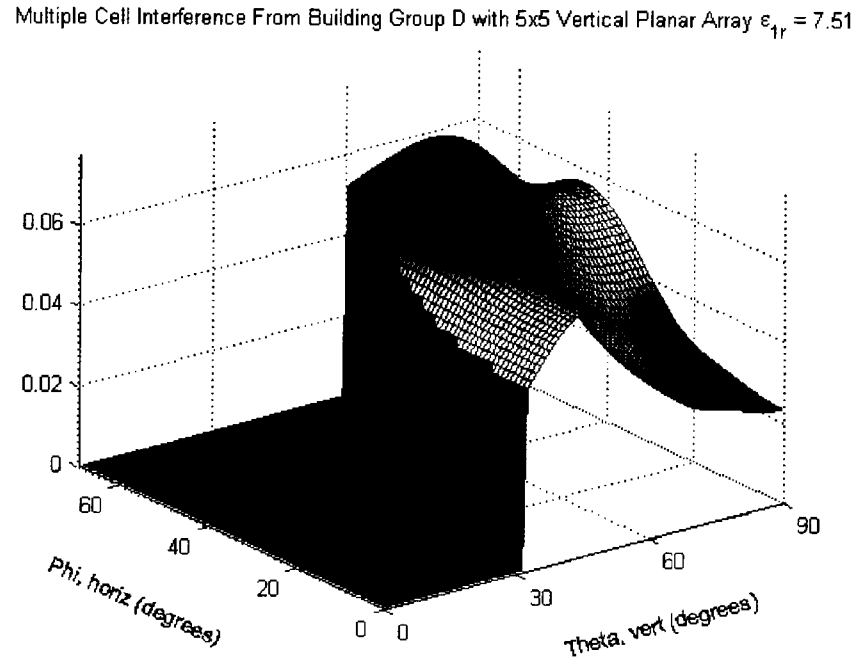

Fig. 5.22 Interference Plot for 5x5 Vertical Planar Array From Building Group D

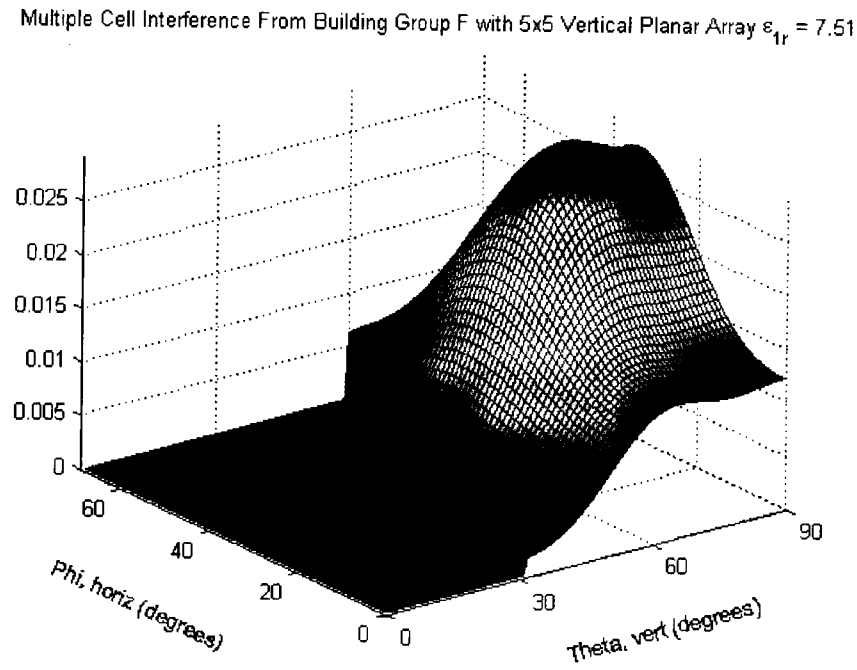

Fig. 5.23 Interference Plot for 5x5 Vertical Planar Array From Building Group F

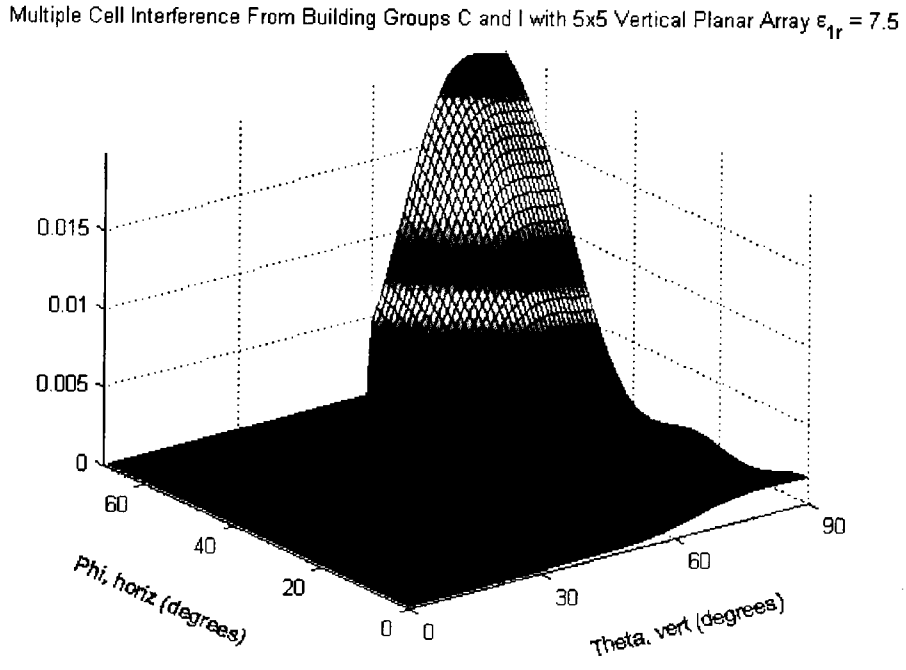

Fig. 5.24 Interference Plot for 5x5 Vertical Planar Array From Building Groups C and I

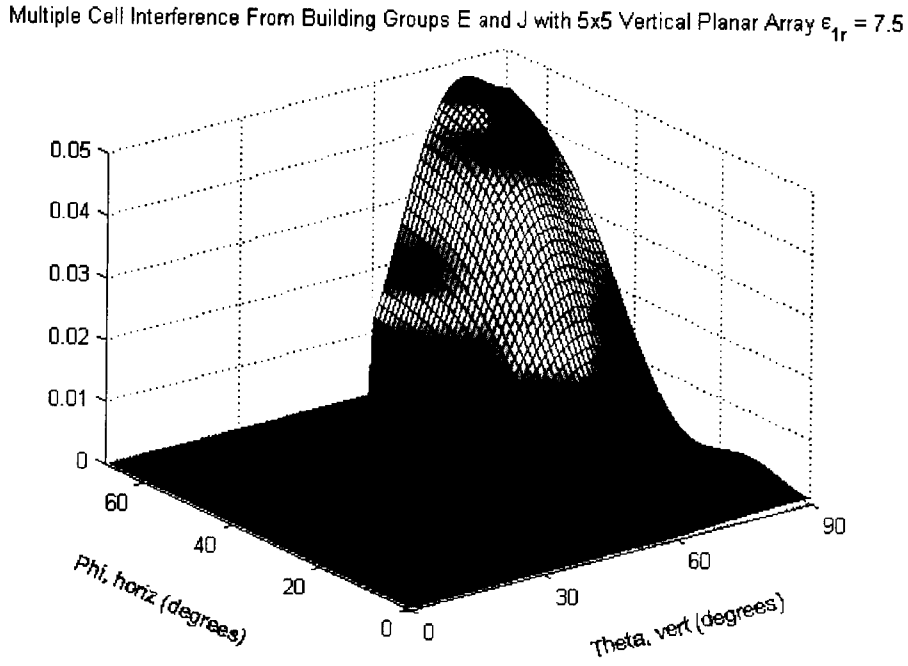

Fig. 5.25 Interference Plot for 5x5 Vertical Planar Array From Building Groups E and J

5.6 Effects of Building Material on System Capacity

As tabulated in Table 4.1, building materials vary greatly in its permittivity. The results shown thus far are for buildings that are made primarily from limestone. To investigate the effects of different materials on the reflection loss, and thus the change in capacity, Plexiglas is assumed to be the primary material and the capacities for the different antenna configurations are listed in Table 5.1, alongside with those obtained assuming a limestone material.

Antenna Type / Material	Single Panel Element	1x5 Linear Array	5x5 Vertical Planar Array
Limestone	18	72	230
Plexiglas	21	81	249

Table 5.1 Capacity Change Relative to Building Materials

As tabulated, the capacity supported is higher for material that has a lower permittivity value.

For comparison purposes, the capacities obtained with a single cell, only building group D, are tabulated in Table 5.2. Because there are no reflections of adjacent cells' interference, the building material does not influence on the capacity results. The values in Table 5.2 shows that a 28% - 33% reduction in capacity is realized in a multi cell environment.

Antenna Type	Single Panel Element	1x5 Linear Array	5x5 Vertical Planar Array
Capacity	27	104	348

Table 5.2 Capacity in Single Cell Environment

5.7 Capacity Dependence on Building Dimensions

To investigate the effect on capacity from changes of building dimensions, a series of simulations were performed on a building with 15 floors (45 meters high) and $W_{building}$, X_0, W_{cross}, and S are 20 meters, 30 meters, 30 meters, and 20 meters respectively. Tables 5.3 – 5.5 tabulate results of changing the parameters X_0, W_{cross}, and S of Fig. 4.1.

X_0	12	15	16	18	30
Capacity	129	131	131	131	101

Table 5.3 Effect on Capacity Due to X_0 in Multi Cell Environment

W_{cross}	5	10	15	20	25	30
Capacity	88	88	96	99	100	101

Table 5.4 Effect on Capacity Due to W_{cross} in Multi Cell Environment

S	15	20	25	30	35
Capacity	105	101	98	95	93

Table 5.5 Effect on Capacity Due to S in Multi Cell Environment

Table 5.3 indicates that there is an optimal distance between the location of the antenna array and the building that it serves. If the antenna array is too close or too far, the capacity supported will drop. This is evident in that if the antenna array is too close to the building, beam spot increases in proportion to the increased steered azimuth and vertical angles needed to reach users located at the edges of the building. On the other hand, if the antenna array is too far away, beam spot increases for all locations in the building.

If adjacent buildings are separated further apart, inter-cell interference also drops. This is shown in Table 5.4 where increases in W_{cross} allows a gradual increase in capacity.

Table 5.5 illustrates capacity decreases if buildings' depth increases. This is because coverage provided deeper into the building is due to the widen of the beam spot. In other words, more interference is received per degree of azimuth and vertical angle, reducing the capacity supported.

Fig. 5.26 shows that a short and narrow building reduces the effectiveness with the use of smart antennas. Note that by comparing Fig. 5.26 with Fig. 5.21, the highest capacity is no longer at $(\phi_0, \theta_0) = (0^0, 90^0)$. This is because given the same beam spot size, the beam now covers a larger proportion of the building, or a higher percentage of interferers. The same local maxima in capacity appears on both figures at the edges of the building, however, as explained Section 5.4.

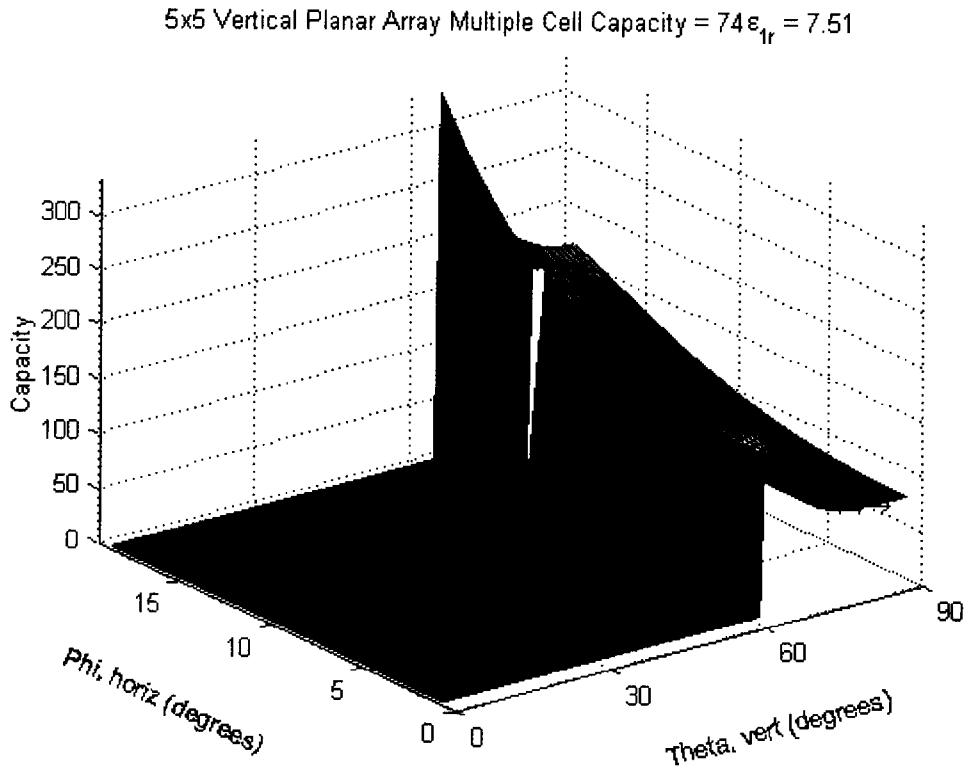

Fig. 5.26 Capacity Plot for 5x5 Vertical Planar Array with $h = 30$m, $W_{building} = 20$m, $W_{cross} = 30$m, $X_0 = 30$m, $S = 20$m

5.8 Conclusions

In this chapter, we have presented results from our simulations of the interference generated by users in building groups in Fig. 4.1 and the resulting supported capacity in building group D. The capacities supported with different antennas, building materials, and building dimensions are provided. The surface plots of both capacities and interference illustrate the steering and interference mitigation abilities of the different antennas used. It is determined that a lower permittivity of building material offers a slight increase in system capacity in a multi cell environment. Also, there is a 28% - 33% decrease in capacity compared to a single cell system. Capacity changes depending on

the specific dimensions of the building served, with a decrease in capacity supported for shorter and narrower buildings. There is also an optimal distance between the antenna array and the building served beyond which capacity will decrease.

Chapter 6 CONCLUSIONS AND SUGGESTIONS FOR FUTURE RESEARCH

6.1 Introduction

In the preceding chapters, we have investigated and compared the performance of using a 3-dimensional array, 1-dimensional linear array, and single antenna element. We then evaluated the capacity supported for a CDMA based system of indoor mobiles. The major contributions of the thesis are as follows:

6.1.1 Antenna Array Design

The complete 3-dimensional radiation pattern of antenna arrays were modelled. To model the arrays accurately, patterns of real antenna elements are used. We model panel antennas by placing a reflector behind a short dipole, and calculate its resulting pattern with both the real and image elements. The vertical pattern of short dipole was also taken into account. This is more accurate than the use of ideal sectorized antenna and isotropic point source. We compared analytically the performance and benefits of using higher dimensional antenna arrays, which provide significant power gains with similar hardware complexities to simpler linear arrays. It was also shown that 3-dimensional arrays have the ability to steer to different vertical angles.

6.1.2 Modified User Distribution

Because of the micro cell model, and the low position of the antenna arrays, the assumption that users are distributed uniformly in all azimuth angles is not valid. For an accurate model of user distribution, a typical downtown geometry with rectangular street

grids was used. The average sizes of buildings and roads were taken from the Vancouver GIS. Then the amount of building space, or interference, were mapped onto each azimuth-vertical degree angle of the antenna array. The user probability distribution function was then derived analytically, based on the average city block dimensions.

6.1.3 Multicell Interference

To evaluate the system capacity accurately, a multicell scenario was assumed and interference from adjacent cells are modelled. Because of power control, the effects of element factor, reflection, diffraction, and propagation loss were included. The power required to be transmitted by an interferer to its serving base station in an adjacent cell is calculated. Then the power arriving to the central array is then found. To ensure that all interferers were accounted for, rays are launched from an array to interferes located in buildings in the same and adjacent city blocks. Rays are allowed to reflect, and diffract in 3-dimension. The reflection takes into account of the building material's permittivity to calculate the effective power loss, while a constant loss was assumed for diffraction based on measured results.

6.1.4 Capacity Results

Surface plots of system capacity when the arrays were steered to different AOAs are provided. It is shown that 3-dimensional arrays can mitigate interference from different vertical directions, and that it provides a gain in capacity over traditional 1-dimensional linear array. Capacities were then tabulated when different building materials were used. The results suggest that building materials do not play a significant role in affecting

system capacity. Single cell capacity was also investigated and the results indicate that there is a 28% - 33% decrease in system capacity when operating in a multicell environment.

6.2 Suggestions for Future Research

6.2.1 Non-Uniform Building Profiles

In this thesis, an assumption was made that all buildings in a city block are of uniform height and form a continuous surface. This allows fast simulation of the effects of city block sizes, building material properties, and different antennas used. However, site specific modelling is needed to investigate the resulting capacity supported in specific environments.

6.2.2 Diffraction Modelling

Although we have modelled the effects of propagation and reflection accurately, we used only a constant diffraction loss for interferers located in shadowed regions. As such, it will be more accurate to include a 3-dimensional diffraction model.

6.2.3 Mutual Coupling

It is well known that mutual coupling effects exist between elements in an antenna array. Because it has been shown that mutual coupling effects, if modelled, suggests a higher supported user capacity, it was not taken into account in this thesis. However, it will be an interesting effect to consider for future works.

6.2.4 Capacity Spot Surge

For uniformity, users were assumed to be distributed evenly inside the buildings. However, the capacity surface plots show that capacities supported can vary greatly, depending on which direction the antenna beam is steered to. In reality, it is quite likely that certain areas of the building will have a higher number of users. It is also likely that certain areas of the building will have a temporary increase in the number of users. It is therefore interesting to consider the effects of a changing user distribution.

Bibliography

[1] P. J. Barry and A. G. Williamson, "Statistical model for UHF radio-wave signals within externally illuminated multistory buildings," *IEE Proceedings-I*, vol. 138, no. 4, pp. 307-318, Aug. 1991.

[2] T. Rappaport and S. Sandhu, "Radio-Wave Propagation for Emerging Wireless Personal-Communication Systems," *IEEE Antennas and Propagation Magazine*, vol. 36, no. 5, pp.14-24, Oct. 1994.

[3] T. S. Rappaport and J. Liberti, *Smart Antennas for Wireless Communications: IS-95 and Third Generation CDMA Applications*, Prentice Hall PTR, 1999.

[4] R. Gahleitner and E. Bonek, "Radio Wave Penetration into Urban Buildings in Small Cells and Microcells," *IEEE Veh. Tech. Conf.*, vol. 2, pp. 887-891, June 1994.

[5] D. Dres, D. Vouyioukas, D. Triantafilidis and P. Constantinou, "Building Penetration Measurements for 2.4 GHz Broadcasting CDMA System," *IEEE Veh. Tech. Conf.*, vol. 4, pp. 1982-1987, Sept. 1999.

[6] H. M. El-Sallabi, "Polarization Consideration in Characterizing Radio Wave Propagation in Urban Microcellular Channels," *IEEE PIMRC*, vol. 1, pp. 441-415, Sept. 2000.

[7] B. S. Lee and A. R. Nix and J. P. McGeehan, "A Spatio-Temporal Ray Launching Propagation Model for UMTS Pico and Microcellular Environments," *IEEE Veh. Tech. Conf.*, vol. 1, pp. 367-371, May 2001.

[8] A. Kavak, "Adaptive Antenna Arrays for Downlink Capacity Increase in Third Generation Wireless CDMA," *IEEE RAWCON*, pp. 77-80, Aug. 2001.

[9] T. S. Rappaport, *Wireless Communication. Principles & Practice*, Prentice Hall PTR, 1996.

[10] L. H. Chan, "Capacity improvements using beamforming antennas in IS-95 cellular CDMA systems," M.A.Sc Thesis, The University of British Columbia, Vancouver, B.C., Canada, Apr 1999.

[11] R. A. Soni, R. M. Buehrer and R. D. Benning, "Transmit Beamforming Combined with Diversity Techniques For CDMA2000 Systems," *IEEE ICASSP*, vol. 2, pp. 1029 -1032, May 2001.

[12] T. Chulajata and H. M. Kwon, "An Adaptive Array Antenna With No Phase Calibration for CDMA2000 Reverse Link," *IEEE MILCOMM*, vol. 2, pp. 816-820, Oct. 2000.

[13] S. M. Chiu, "Capacity Improvements Using Adaptive Nullsteering Antennas in IS-95 Cellular CDMA System," M.A.Sc Thesis. The University of British Columbia, Vancouver, B.C., Canada, March 2002.

[14] Vanmap http://www.city.vancouver.bc.ca/vanmap

[15] T. S. Rappaport and L. B. Milstein, "Effects of Radio Propagation Path Loss on DS-CDMA Cellular Frequency Reuse Efficiency for the Reverse Channel," *IEEE Trans. On Veh. Tech.*, vol. 41, no. 3, pp. 231-242, Aug. 1992.

[16] K. S. Gilhousen, I. M. Jacobs, R. Padovani, A. J. Viterbi, L. A. Weaver, Jr. and C. E. Wheatley III, "On the Capacity of a Cellular CDMA System," *IEEE Veh. Tech. Conf.*, vol. 40, no. 2, pp. 303-312, May 1991.

[17] J. Orriss and S. K Barton, "On the Capacity of Cellular CDMA System Up-links with Multiple Base Station Diversity," *IEEE PIMRC*, vol. 2, pp. 829-832, Sept. 2000.

[18] U. Dersch and R. J. Ruegg, "Simulations of the Time and Frequency Selective Outdoor Mobile Radio Channel," *IEEE Veh. Tech. Conf.*, vol. 42, no. 3, pp. 338-344, Aug. 1993.

[19] H. L. Bertoni, P. Pongsilamanee, C. Cheon and G. Liang, "Sources and Statistics of Multipath Arrival at Elevated Base Station Antenna," *IEEE Veh. Tech. Conf.*, vol. 1, pp. 581-585, Jul. 1999.

[20] J. M. Kim and Y. J. Yoon, "Modeling of the Propagation Characteristics of Smart Antennas in Microcell Environment," *IEEE Antennas and Propagation Society International Symposium*, vol. 4, pp. 2244-2247, June 1998.

[21] Y. L. C. de Jong and M. H. A. J. Herben, "Accurate Identification of Scatterers for Improved Microcell Propagation Modelling," *IEEE PIMRC*, vol. 2, pp. 645-649, Sept. 1997.

[22] K. Cho, K. Nishimori, Y. Takatori and T. Hori, "Adaptive Antennas Employing Vertical Pattern Control for Street Microcell," *IEEE Antennas and Propagation Society International Symposium,* vol. 2, pp. 639-642, June 1998.

[23] G. V. Tsoulos and M. A. Beach, "DS-CDMA Microcellular Networks with Adaptive Antennas," *IEEE GLOBECOMM*, vol. 1, pp. 581-585, Nov. 1996.

[24] J. D. Lim, "Air Interface Capacity and Area Coverage Analyses for cdma2000 Voice and Packet Data Services," *IEEE Veh. Tech. Conf.*, vol. 3, pp. 1770-1774, May 2001.

[25] J. C. Liberti and T. S. Rappaport, "A Geometrically Based Model for Line-of-Sight Multipath Radio Channels," *IEEE Veh. Tech. Conf.*, vol. 2, pp. 844-848, Apr. 1996.

[26] W. L. Stutzman and G. A. Thiele, *Antenna Theory and Design*, John Wiley & Sons, Inc., 1998.

[27] T. Mayer, C. Robertson and T. T. Ha, "Co-channel interference reduction on the forward channel of a wideband CDMA cellular system," *IEEE MILCOMM*, vol. 2, pp. 785-790, Nov. 1999.

[28] F. Niu and H. L. Bertoni, "Path Loss and Cell Coverage of Urban Microcells in High-Rise Building Environments," *IEEE GLOBECOMM*, vol. 1, pp. 266-270, Nov. 1993.

[29] J. Beyer and R. Jakoby, "A Very Fast Ray-Based Field Strength Prediction Tool for Urban Microcells Operating in the UHF-Band," *IEE National Conf. on Antennas and Propagation*, pp. 116-119, Aug. 1999.

[30] G. V. Tsoulos, M. A. Beach and S. C. Swales, "Performance Enhancement of DS-CDMA Microcellular Networks with Adaptive Antennas," *IEEE Veh. Tech. Conf.*, vol. 2, pp. 1086-1090, Apr. 1996.

[31] A. Ranheim and T. Svantesson, "Mutual Coupling Effects on the Capacity of Multielement Antenna Systems," *IEEE ICASSP*, vol. 4, pp. 2485-2488, May 2001.

[32] M. A. Jensen and J. W. Wallace, "The Capacity of MIMO Wireless Systems with Mutual Coupling," *IEEE Veh. Tech. Conf.*, vol. 2, pp. 696-700, Sept. 2002.

[33] J. Fuhl, J.P. Rossi and E. Bonek, "High-Resolution 3-D Direction-of-Arrival Determination for Urban Mobile Radio," *IEEE Trans. On Antenna and Propagation*, vol 45, no. 4, pp. 672-682, Apr. 1997.

[34] S. Y. Tan and H. S. Tan, "Propagation Model for Microcellular Communications Applied to Path Loss Measurements in Ottawa City Streets," *IEEE Trans. Veh. Tech.*, vol. 44, no. 2, pp. 313-317, Aug. 1995.

[35] A. A. M. Saleh and R. A. Valenzula, "A Statistical Model for Indoor Multipath Propagation," *IEEE J. Sel. Areas in Comm.*, vol. 5, no. 2, pp. 128-137, Feb. 1987.

[36] F. Lotse and A. Wejke, "Propagation Measurements for Microcells in Central Stockholm," *IEEE Veh. Tech. Conf.*, pp. 539-541, May 1990.

[37] J. F. Wagen, "Signal Strength Measurements at 881 MHz for Urban Microcells in Downtown Tampa," *IEEE GLOBECOMM*, vol. 2, pp. 1313-1317, Dec. 1991.

[38] A. F. De Toledo, A. M. D. Turkmani and J. D. Parsons, "Estimating Coverage of Radio Transmissions Into and Within Buildings at 900, 1800, and 2300 MHz," *IEEE Personal Communicaions*, vol. 5, issue 2, pp. 40-47, Apr. 1998.

[39] D. J. Cichon and T. Kurner, COST 231 Propagation Prediction Models.

[40] M. Dottling, F. Kuchen and W. Wiesbeck, "Deterministic Modeling of the Street Canyon Effect in Urban Micro and Pico Cells," *Proc. IEEE ICC*, vol 1, pp. 36-40, June 1997.

[41] A. J. Rustako, Jr., N. Amitay, G. J. Owens and R. S. Roman, "Radio Propagation Measurements At Microwave Frequencies for Microcellular Mobile and Personal Communications," *IEEE ICC*, vol 1, pp. 482-486, June 1989.

[42] M. Dottling, T. Zwick and W. Wiesbeck, "Ray Tracing and Imaging Techniques in Urban Pico and Micro Cell Wave Propagation Modelling," *IEE International Conf. on Antennas and Propagation*, vol. 2, pp. 2.311-2.315, Apr. 1997.

[42] K. Mahbobi, "Radio Wave Propagation in Urban Microcellular Environment," *IEEE Veh. Tech. Conf.*, vol. 2, pp. 951-955, May 1992.